Information Self-structuring for Developmental Robotics: Organization, Adaptation, and Integration

Lars Åke Olsson

A thesis submitted in partial fulfilment of the
requirements of the University of Hertfordshire
for the degree of

Doctor of Philosophy

The programme of research was carried out in the School of Computer Science, Faculty of Engineering and Information Sciences, University of Hertfordshire.

April 2006

Acknowledgements

During my PhD studies I have had the great pleasure to work with Professor Chrystopher Nehaniv, my main supervisor, and Dr. Daniel Polani, my second supervisor. Without their knowledge, enthusiasm, and support, my time as a PhD student would have been much harder and less interesting. I am also greatly indebted to Professor Kerstin Dautenhahn, who helped arrange great academic and financial support that has enabled me to visit a number of interesting conferences around the world. I have also had a great time with all the other researchers and PhD students of the Adaptive Systems Research Group, both in the day-to-day life in the lab and St. Albans as well as on various trips around the world. Cheers guys!

I would also like to thank Pierre A.I. Wijkman at Stockholm University, who introduced me to the wonderful world of AI and Artificial Life back in 1996. It was Pierre's great enthusiasm and willingness to share his ideas that inspired me to do research.

On a personal level I want to thank all my friends around the world as well my dear old friends in Sweden, my family, and last but certainly not least, Angela.

Lars Åke Olsson

Abstract

In this thesis we consider how a robot autonomously can find the informational organization of its sensors, adapt its sensors, and how sensors can be integrated into higher level sensors. This enables the robot to develop and adapt its sensory systems depending on its particular embodiment and environment. It also enables the robot to ground its model of its sensors and actuators in its own experiences, rather than being specified by the human designer.

The methods introduced in this thesis are based on information theory. After presenting an overview of information theory and related work from neuroscience and developmental robotics, we introduce the sensory reconstruction method. This method can be used to find the informational relations between sensors, and experiments with an AIBO robot show how the spatial layouts of visual fields can be reconstructed from only raw and unstructured visual sensor data. After showing some examples of how the development of the informational relations between sensors depend on time and the structure of the environment, entropy maximization is proposed as a method for sensor adaptation to find more structure in sensor data. We also introduce a method for computing motion flow based on temporal correlations between sensors, as well as a sensor adaptation method which can be used to adapt sensor fields of different modalities to use classical optical flow algorithms. Finally it is shown how the robot's sensory perceptions can be grounded in its own experiences by motor babbling and sensory reconstruction.

When Gregor Samsa awoke one morning from troubled dreams
he found himself transformed in his bed into a monstrous bug.

Franz Kafka,
Metamorphosis

Contents

List of Figures

Chapter 1

Introduction

Many animals display amazing sensing capabilities and control over their own bodies (e.g., Dusenbery (1992)). They are also often able to predict the way in which certain actions affect the environment around them. To achieve this, many higher animals go through a number of developmental stages, whereby the development of the nervous system completely depends on the particular embodiment and actions of the individual animal, as well as the environment of the animal.

The main aim of this thesis is to study methods that can be used by robots to achieve a similar grounding of their sensory perceptions and actions that are based on the particular body of the robot, its environment, and tasks to perform. To do this the robot, as well as to some the degree the researcher, needs to "understand" the world of the robot – the information available in its sensors, the relations between its sensors and actuators, its embodiment, the statistics of its environment, and possible interaction with other entities. As von Uexküll (1909) wrote almost a

century ago about understanding the world of the animal:

> "Our anthropocentric way of looking at things must retreat further and further, and the standpoint of the animal must be the only decisive one. When this occurs, everything that we hold to be self-evident disappears: all of nature, earth, heaven, stars, indeed, all the objects that surround us. Only those effects remain as factors of the world that, corresponding to [its] construction plan, exert an effect on the animal. Their number and the way they fit together is determined by the construction plan of the animal. Once this correspondence between construction plan and the external factors has been carefully researched, then a new world takes shape around every animal, completely different from our world: its *Umwelt*." -J. von Uexküll (1909)

Traditionally in robotics, though, the possible actions and sensorimotor relations of robots have been specified and built into the robot by the human designer. But, as experienced in many robotic projects, it is extremely hard to design a robotic system to use its sensors in an efficient manner in challenging realistic and changing environments, or with more complex robots. It is also very hard as a human designer to understand the environment in which the robot is acting in from the robot's perspective – its Umwelt. Thus, if the robot learns by itself its possible actions and their effect on its sensors, anthropomorphic bias and human preconceptions of what it is like to be a robot are avoided since

the actions are acquired by self-experienced sensorimotor percepts (Blank et al., 2005). Also, a robot that acquires the skills necessary to act in the world by itself can adapt to changing conditions and embodiment since the learning of relations between actuators and sensors, the *sensorimotor laws*, can adapt over time. By developing autonomous ontogeny by grounding the actions in sensorimotor laws, the robot's repertoire is more open-ended since it is not learning a specific task, and can continue to adapt to changes and new tasks. Finally, studying how autonomous development of sensorimotor skills operates in robots can help validate or extend existing theories in human and animal development.

How can we study autonomous development of sensorimotor capabilities in robots and where and how do we start? A major inspiration to the work presented here is the novel *Metamorphosis* by Franz Kafka (1992). Faced with the bizarre situation of having his brain "plugged in" to the body of a monstrous bug, the main character begins the story with struggling to understand how to control his newly gained body with its numerous legs and new sensory inputs coming from unknown sensory organs. This notion of a brain, or other control system, connected to an unknown body, is in this thesis used as a basis for studying development and grounding of perceptions and actions in autonomous robots.

This is the idea of *information self-structuring* as referred to in the title – the robot should by self-initiated movement and experimentation discover its sensory organization and the affect its actuators have on its sensors, and it can also to some extent shape the statistics of incoming sensory data by active movement (Lungarella et al., 2005). Here

we present a method, *the sensory reconstruction method*, for finding the informational relations of the sensors from unknown and uninterpreted sensor data. By using this method the robot can find the informational relations, or *organization*, of its sensors. This informational organization can, among other things – it turns out – reflect the real spatial organization of the sensors. Experiments are performed where the visual sensors and their spatial organizations are reconstructed from a deluge of sensor data. The incoming sensory data also has statistical structure, and we consider how sensors can be *adapted* for efficient representation and to solve problems which requires sensors with a specific representation of the sensor data. By knowing the informational organization of its sensors the sensors can be combined, or *integrated*, to higher level sensing elements. An example of this, which we will see in later in this thesis, is the integration of sensors of different visual modalities into a coherent visual field which can be used to estimate motion. Equipped with the organization of its sensors, the possibility to adapt its sensors to particular situations, and integration of sensors, the robot can now by experimentation discover the relations between its sensors and actuators.

1.1 Contributions to Knowledge

The central thesis of this dissertation is that information-theoretic methods can be used to ground the ontogeny of sensorimotor systems of embodied robots.

The main contributions of this thesis can be summarized as:

1. We present novel information-theoretic methods in development of sensorimotor control and autonomous sensor organization which can be used in robotics, software agents, etc. Our sensory reconstruction method has also been used and further developed by other researchers – see, e.g., (Kaplan and Hafner, 2005; Hafner and Kaplan, 2005).

2. We have found the temporal scaling of informational correlations of visual data from a robot to follow a power law. To the best of our knowledge, this kind of analysis is novel as it has previously only been performed in the spatial domain and never before on robotic sensor data.

3. We present a method for sensor adaptation in individual sensors to the statistics of sensor data by entropy maximization of the sensor data.

4. We present an empirical comparison of different distance measures used to compute the distances between sensors. These results show how the information metric, by considering the individual as well as joint entropies of the sensors, finds informational relationships not found by the other compared methods.

5. We develop new methods for integration of sensors of different modalities sharing the same information-theoretical properties to higher level sensors. For example, finding and combining red, green, and blue sensors to visual fields used to calculate optical flow, start-

ing from only raw and unstructured data.

6. We present an original algorithm for remapping the data representation of a sensor belonging to larger set of sensors in such a way as to keep the informational relations between the sensors while changing the values of the sensor. This enables a robot to perform traditional optical flow analysis using a sensor field, e.g. visual field, consisting of different modalities such as red, green, and blue sensors.

7. We also present a developmental system implemented on a real robot that learns a model of its own sensory and actuator apparatuses, where the sensorimotor laws are grounded in its own sensorimotor perceptions. The robot has no innate knowledge regarding the modality or representation of the sensoric input and the actuators, and the system exploits generic informational properties of the robot's world.

Most of the work presented in this thesis has been presented to the research community at a number of relevant international conferences and in one journal paper – see appendix A.

1.2 Overview of the Thesis

The rest of this thesis is structured as follows.

Chapter 2 presents the basic concepts of information theory necessary to understand this thesis, and previous work related to our work.

We discuss the statistics of natural environments and how biological neural systems adapt to and develop depending on these statistics. Finally, we give an introduction to embodied artificial intelligence and developmental robotics with a focus on information and grounding of sensorimotor capabilities.

Chapter 3 introduces the sensory reconstruction method, a method for finding structure in raw and uninterpreted sensor data, which is central to this thesis. We start by defining what we mean by a sensor and the information metric which is used to compute the information distance between between pairs of sensors. Then sensoritopic maps are introduced, along with a grouping algorithm. Finally, we introduce a measurement for comparing the spatial organization of reconstructed visual fields and other sensory fields with the physical spatial organization of the sensors.

Chapter 4 introduces the SONY AIBO robot, used in almost all experiments presented in this thesis. Then results from applying the sensory reconstruction method to AIBO sensor data are presented. These results depend on the statistics of the data and we analyse how the information correlatedness scales depending on the spatial as well as temporal distances between visual sensors.

Chapter 5 studies the development of the sensoritopic maps of the previous chapter over time. We also present results from a visual field developing in an environment with only vertical contours and how the informational relations "unfold" as the robot moves to an en-

vironment with natural statistics.

Chapter 6 introduces the concept of entropy maximization which enables a robot or biological organism to adapt its sensors to the statistical structure of its environment. Results are presented that show how entropy maximization enables a robot to find informational relations between sensors not found without entropy maximization, using less resolution of the data.

Chapter 7. Here a number of different methods for computing the value or informational distance between pairs of sensors are presented. Results from robotic experiments show how the information metric performs better than the other presented methods in a sensor reconstruction task.

Chapter 8. Traditional optical flow analysis assumes that the brightness of the images varies more or less smoothly over the images. Here we generalize the concept of optical flow by presenting two methods where it is only required that the informational relations vary smoothly, which does not necessarily entail that they have similar sensor values. The first method is based on temporal-informational correlations, and the second method is based on adapting sensors in such a way as to maintain their informational relationships while making the difference in sensor values smooth between sensors. This method can be used to apply traditional optical flow analysis to sensory fields, e.g., visual fields, of different modalities.

Chapter 9. Here the sensory reconstruction method is used with motor babbling in a robot that develops from no knowledge of its sensors or actuators to being able to perform basic visually guided movement. After finding the organization of the visual field the robot uses body babbling to ground its actions in sensorimotor perceptions.

Chapter 10 summarizes the central contributions and discusses new research questions, possible applications, and future directions.

Appendix A presents our publications published during the work on this thesis and how they relate to the chapters in the thesis.

Chapter 2

Information Theory, Natural Environments, and Developmental Robotics

The overall goal of our work is to build robots that develop and adapt to their particular embodiment and the structure of their experienced world. To discover informational structure we use the framework of information theory which is introduced in section 2.1. We then look at the statistics of natural environments and how animals adapt on the sensoric level to their specific environments in section 2.2. This section also presents measures of integration and complexity from neuroscience that are of interest when studying any kind of sensory system. The final sections contain an overview of embodied artificial intelligence, developmental robotics, and other work related to the work presented in the rest of this thesis.

2.1 Information Theory

Central to the work presented in this thesis is the notion of informational distances between sensors and the information content of the environment, sensors, and actuators. To model this we use the framework of *information theory*, a general theory of communication over a (possibly) noisy communication channel developed by Claude Shannon in the 1940s (Shannon, 1948). While Shannon originally developed the framework as a tool to solve problems in tele communications, the generality of the theory has meant that it has been applied in many different areas as diverse as music, art, psychology, gambling, robotics, and neuroscience – see, e.g., Pierce (1980) and Rieke et al. (1999).

The next section gives a mathematical overview of the basics of information theory used in this thesis – see for example (Shannon, 1948) or (Cover and Thomas, 1991) for more thorough treatment. Much of the generality of Shannon's information theory is due to the fact that it ignores any semantics of the transmitted data, which makes it hard to compute the "relevance" or "meaning" of the information, and section 2.1.2 presents a recent attempt to quantify relevant information.

2.1.1 Mathematical Background

The central concepts of information theory are the *sender*, or *source*, which transmits messages, the *target* of the messages, and the (possibly noisy) *communication channel* over which the messages are transmitted – see figure 2.1. In the mathematical framework channels are modelled

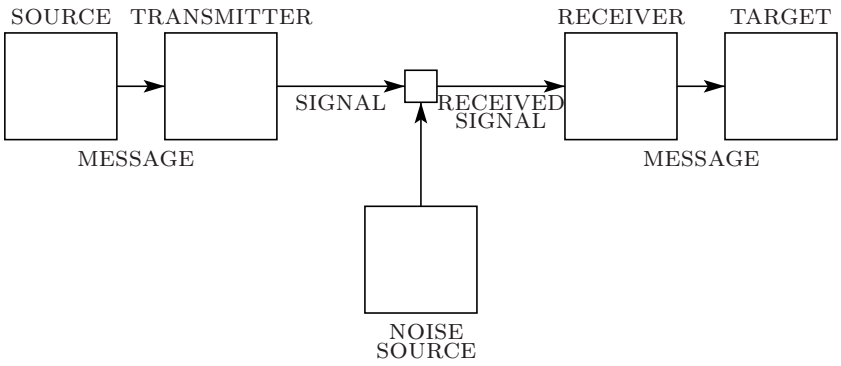

Figure 2.1: The model of communication in information theory. The sender (source) encodes the message with the transmitter, the encoded message is transmitted over a potentially noisy channel, before the receiver decodes the message which is received by the target. [From Nehaniv et al. (2006)]

as random variables, and in this thesis the random variables will always assume a finite number of values, but in general information theory can also be used for continuous channels.

Let $\mathcal{X}$ be the alphabet of values of a discrete random variable (information source) X, where X in the present thesis most often will represent a sensor or actuator. The probability that the random variable X assumes a value $x \in \mathcal{X}$ is denoted $P(X = x)$, or, by simplifying the notation, $p(x)$. Then the *entropy*, or uncertainty associated with X, is

$$H(X) := -\sum_{x \in \mathcal{X}} p(x) \log_2 p(x), \tag{2.1}$$

which specifies in bits the information necessary to determine the value assumed by X. If all possible values of the random variable are equally

likely then the entropy is maximal. If, on the other hand, the random variable always has the same value, then the entropy is zero since there is no uncertainty in the variable. Entropy can also be viewed as a measure of "surprise" – the more surprised one is on average when seeing the next value of a random variable, the more uncertainty, and thus entropy, the random variable contains.

The *joint entropy* of two random variables X and Y is

$$H(X,Y) := -\sum_{x,y\in\mathcal{X},\mathcal{Y}} p(x,y)\log_2 p(x,y). \tag{2.2}$$

The joint entropy can be extended to any number of random variables $H(X_1, X_2, \ldots, H_N)$. If X and Y are independent, the joint entropy is additive:

$$H(X,Y) = H(X) + H(Y) \iff P(x,y) = P(x)P(y). \tag{2.3}$$

If X and Y are not independent, then $H(X) + H(Y) > H(X,Y)$.

The *conditional entropy*,

$$\begin{aligned} H(Y|X) &:= \sum_{x\in\mathcal{X}} p(x)H(Y|X=x) &(2.4)\\ &:= -\sum_{x\in\mathcal{X}} p(x)\sum_{y\in\mathcal{Y}} p(y|x)\log_2 p(y|x) &(2.5)\end{aligned}$$

is the uncertainty associated with the discrete random variable Y if the value of X is known. In other words, how much more information one needs to fully determine Y once X is known. The *mutual information* is

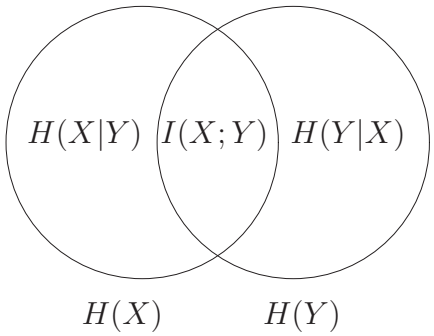

Figure 2.2: Venn diagram showing the relations between mutual information, $I(X;Y)$, entropy, $H(X)$, and conditional entropy, $H(X|Y)$. The joint entropy $H(X,Y)$ is the union of the two circles.

the information shared between the two random variables X and Y and is defined as

$$I(X;Y) := H(X) - H(X|Y) = H(Y) - H(Y|X), \tag{2.6}$$

where $I(X;Y) = I(Y;X)$ and $I(X;Y) \geq 0$. It measures the average reduction in uncertainty about Y when knowing X, or put another way, the average amount of information that Y conveys about X, and X conveys about Y.

Another way to look at the relations between the defined entropies is through a Venn diagram, as shown in figure 2.2. While the mutual information measures what the two random variables have in common, the two conditional entropies contain exactly what the two variables do not have in common. The conditional entropies will be used as a measure of informational distance in this thesis – see section 3.3.

2.1.2 Relevant Information

One important issue when Shannon invented information theory was to ignore the notion of semantics when dealing with transmitted data. This enabled Shannon to introduce entropy as a universal measure of information by focusing only on the probabilities of the transmitted symbols, and not on their meaning or importance. But, almost ever since Shannon introduced his "meaningless" information theory, other researchers have tried to define similar measures that somehow take in to account the semantic meaning of the symbols – see for example (Polani et al., 2001) for an overview.

The notion of relevant information was proposed by Nehaniv (1999) by grounding the meaning of signals in their usefulness for an agent, where the usefulness can be measured in terms of, for example, reproductive fitness or more short-term goals such as homeostasis or achieving a goal. Relevant information was then formalized in relation to utility by Polani et al. (2001) by associating the relevance of information with the utility to an agent to perform a certain action.

In the approach of Polani et al. (2001), let $\hat{X}$ be a sensor that measures the state of the universe X for an agent. Most of the information in X is of no relevance to the agent, and $\hat{X}$ can be viewed as a compressed version of the relevant information in X, since the alphabet of the sensor $\hat{X}$ is much smaller than all the possible states of the universe X. The relevance of the information in $\hat{X}$ depends on the utility of that information for the agent to maximize some goal, and the sensor $\hat{X}$ can also be viewed as a *bottleneck* that "squeezes" relevant information from the world, without

compressing information that is of no use to the agent. Polani et al. (2001) use the information bottleneck method of Tishby et al. (1999) to "squeeze" relevant aspects of an information source by information-theoretic means. In this approach a *relevance indicator variable*, Y, is used, where Y represents everything that is relevant in X for the agent to perform an optimal action.

Given that the relevance indicator Y is known, $I(X;Y)$ now measures the total amount of relevant information available in the world to perform an optimal action given a certain state of the world. However, the agent perceives its information about the world through the sensor $\hat{X}$, and while the total information available to the agent is $I(X;\hat{X})$, the relevant information available to the agent is $I(Y;\hat{X})$, where $I(X;Y) \geq I(Y;\hat{X})$.

2.2 Natural Statistics and Neural Information Processing

All embodied agents, whether they are biological organisms or robots, act and are embedded in an environment. In the last 50 years or so, neuroscientists have started to hypothesize about and study how organisms adapt and develop depending on their environment. As a natural consequence of this, there has also been a number of studies attempting to quantify the statistics of natural environments, quite often using the framework of information theory.

In this thesis are we interested in applying information theory to build robots that adapt their sensory systems to their particular embodiment,

environment, tasks to perform, and to ground the perceptions in the experiences of the robot itself. Thus, it is of interest to understand more about the statistics of natural environments, and how biological organisms might adapt to these statistical structures.

2.2.1 Statistics of Natural Environments

The sensory world of an organism – its Umwelt – depends, broadly speaking, on three different things: 1) the organization and physical design of the organisms sensors and body (the embodiment), 2) the actions of the agent, and 3) the statistical structure of the organism's environment, i.e., the structure of the signals of different possible sensor modalities such as vision, olfaction, and acoustic waveforms. From an evolutionary point of view, it must be the case that the organization of the sensoric system and the actions performed are adapted to the particular statistics of the world, and not the other way around, even though organisms to some extent can change the statistics of incoming sensory signals by performing particular actions. Consequently, understanding the statistics of natural environments is important for understanding how sensory systems, as well as maybe also higher level cognition, actually works (Barlow, 2001).

The study of the statistics of natural signals is still in an early exploratory phase (Rieke et al., 1999), and most examples in this section come from the study of visual environments, which is the most studied sensory modality (Ruderman, 1994; Field, 1994; Simoncelli, 2003). But reasoning about, for example, sensory states spaces and efficient coding, is also relevant for all other possible sensory modalities.

To make the statistics of sensory input more concrete, consider a hypothetical organism or agent equipped with a 100 by 100 pixels grey scale camera. Each pixel measures the light intensity in the range $\{0, 1, \ldots, 255\}$, where 0 is black and 255 white. Thus, each possible image can be considered as a point in 10,000-dimensional state space, where each axis specifies the intensity of one pixel. This state space of all possible images is mind-boggingly huge – $256^{10,000}$ possible different images.

An important question is how natural signals in different environments are distributed in this space of all possible signals, or in other words, what is the probability density $p(x)$ of natural images like? First consider the two images in figure 2.3(a) and figure 2.3(b) that were randomly drawn from a uniform distribution of the possible image state space. These images contain no redundancy and hence no structure that can be exploited – see figure 2.4.

Now compare the two random images to the two natural images in figure 2.3(c) and 2.3(d). The two natural images are very different to the random images and it is believed that the natural images occupy a small fraction of the possible state space of images (Ruderman, 1994) – something that is reflected in the redundancy in the images. This means that one part of the image can be used to predict another part of the image, and that the sensory system of the agent or organism can exploit the redundancy to represent the input in a more efficient way, see figure 2.4.

Given that natural images are highly non-random, what kind of properties do natural images share? Maybe the most obvious one is that

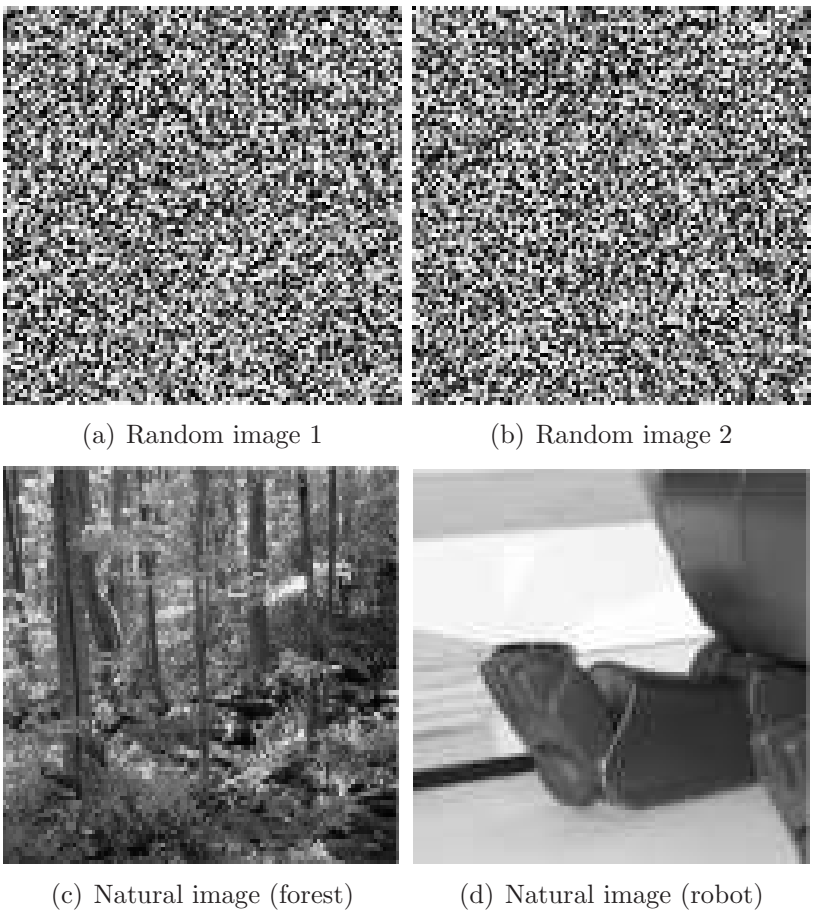

(a) Random image 1 (b) Random image 2

(c) Natural image (forest) (d) Natural image (robot)

Figure 2.3: Example of random and natural images. Figure 2.3(a) and 2.3(b) were randomly drawn from a uniform distribution of the image state space, and figure 2.3(c) and figure 2.3(d) are two examples of natural images.

natural images often contain contours, something that is lacking in the random images in figure 2.3. Studies of the orientation of contours in natural images have found that natural images from man-made environments, as well as more natural forest environments, contain more horizontal and vertical contours than contours of other angles (Coppola et al.,

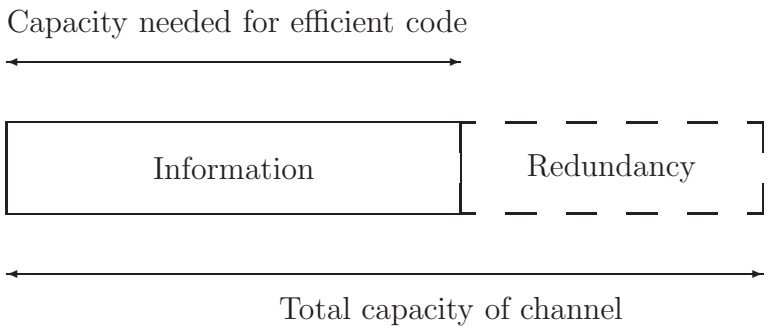

Figure 2.4: Signal representing an image with redundancy. Natural images contain structure, meaning that the image contains redundancy. The image can be compressed by finding a more efficient encoding of the image. In a random image the total capacity of the channel is equal to the capacity needed for an efficient code.

1998). Other typical properties of natural images are spatial and temporal coherence. Consider, for example, nearby photoreceptors, which usually sample regions of visual space close to each other. Thus, nearby photoreceptors often sample the same object in natural scenes, which usually is coherent in respect to colour, orientation, and other parameters. Temporal coherence means that visual scenes are redundant over time, where the value of one pixel in one time frame usually is highly correlated with the same pixel in the next frame. It has also been found that other modalities, e.g., odour concentrations and acoustic waveforms, share some of these properties with natural images. For instance, in general the local contrast in natural images has the same exponential form of the probability distribution as sound pressure in musical pieces (Rieke

et al., 1999).

One other interesting property of natural images is that they often are scale invariant in regards to the correlations just described (Ruderman, 1994). Scale invariance indicates that the statistical structure of natural images does not change when observations are made at different scales, where scale here can mean different resolutions, size of the images, or point of observation (Simoncelli and Olshausen, 2001). This was also found for the robotic visual data used in this thesis – see section 4.4.

2.2.2 Neural Development and Adaptation

Natural signals have, as we saw above, a certain structure, and some interesting questions to ask are: To what extent are biological organisms evolutionary adapted to the structure of their environments? How does evolution find new sensory channels to exploit? Do sensory systems develop differently depending on the conditions of the environment when they form? Can sensoric systems adapt to changing conditions during the lifetime of an individual or even within seconds? How important are self-initiated movements? How can robots be developed to do the same?

These are all some of the questions pondered in the area of *sensor evolution* – see, e.g., Dautenhahn et al. (2001). This thesis attempts to provide a couple of suggestions regarding the final question; how robots can exploit the statistical structure of their environments – see for example chapter 6. To answer some of the other questions, we need to turn to biology and neuroscience.

In the late 1950s and early 1960s H. B. Barlow and others (Barlow,

1961) suggested that the visual system of animals "knows" about the structure of natural signals and uses this knowledge to represent visual signals. At that time the suggestions were mostly based on pure speculation and inspiration from information theory – neither the tools necessary for the measurements, nor the exact ideas about what to measure were available (Barlow, 2001).

In a seminal study, Laughlin (1981) recorded the distribution of contrasts as seen through a lens with the aperture the size of a fly photoreceptor while moving in a forest. A single cell in the fly encodes contrast variations with a graded voltage response. The distribution of contrasts has some shape, and Laughlin was interested in whether the voltage response conveyed the maximal amount of information, given the specific distribution of contrasts by maximizing the entropy of the voltage distribution. This can be viewed as single neuron cell version of Linsker's Infomax principle (Linsker, 1988). Laughlin compared the computed ideal conversion of contrast to voltage given his collected data from the forest and found the match to be very good with the measured response of the second order neurons in the fly visual system. This result suggests that the early visual system of the fly is adapted to the statistical structure of natural scenes in its environment. Since Laughlin's work focused on global statistics, the adaptation must have taken place over evolutionary time. Recent results indicate that the fly visual system also adapts to the current conditions in much shorter timescales, on the order of seconds or minutes (Brenner et al., 2000). This means that individual neurons adapt their input/out relations depending on the structure of

incoming signals. There is also evidence that the coding of the signals adapts to the input distributions in the vertebrate retina (Bialek and de Ruyter van Steveninck, 2004). In chapter 6 of this thesis we implement and experiment with a similar system using the visual sensors of a robot.

It has also been found that ferrets have more neurons selective for vertical and horizontal contours than other angles (Chapman et al., 1996). This might be an adaptation to the statistics of their natural visual environment, as many natural environments have more vertical and horizontal contours than oblique contours – see section 2.2.1 above and Coppola et al. (1998).

Another question is how organisms over evolutionary time discover new sensory channels to exploit and how machines can be created that can do the same. This is, indeed, a very interesting question, but will not be addressed by us in this thesis. Maybe the first real implementation of this was Gordon Pask's work in the 1950s (Pask, 1959; Cariani, 1993). Pask experimented with electrochemical control systems where current was passed through liquid solutions containing metallic salts. The systems evolved their own sensors, sensitive to sound and magnetical fields, and, according to Pask, their own relationships between their internal states and the outside world. More recently, Bird and Layzell (2002) attempted to evolve an oscillator in hardware. When analysing the resulting correctly working circuit, they found – to their surprise – that the evolved circuit "cheated" by picking up external signals, working more like a radio receiver than an oscillator. This device, according to

Bird and Layzell (2002), is the second example of unconstrained sensor evolution following Pask (1959). There has also been some work evolving circuits using non-standard electronic components, e.g., Harding and Miller (2004) that evolved a tone discriminator in liquid crystal, thereby avoiding the predictable nature of standard electronic circuits.

A better studied issue is how biological sensory systems develop after birth and how this development depends on the particular environment and actions of the organism. Here, as is common in neuroscience, the visual system is the most studied. Many experiments have been performed with animals where their visual field somehow has been restricted to contours of a certain orientation, e.g., Blakemore and Cooper (1970); Wiesel (1982); Callaway (1998). The results of these experiments are not completely conclusive but many experiments indicate that animals that have been reared in an environment with only vertical contours have more neurons selective for vertical contours. This might be explained from a purely informational point of view – see section 5.3 of this thesis where we perform a similar study using a robot. Held and Hein (1963) showed how normal visual development not only depends on the visual environment itself, but also on self-initiated movement. Here two kittens were held in a highly structured visual environment where the actions of an active kitten (who could move almost freely) were transmitted to a passive kitten sitting in a box. Thus, both kittens received the same visual input, but only the active one received it connected to self-initiated movement. The results showed how only the active kittens developed normal behaviour in visually guided tasks. Recently, Suzuki et al. (2005)

have performed experiments similar in essence to Held and Hein (1963), with robots using Hebbian learning rules showing similar results.

Finally it should be noted that it is hard to say where the exploitation of statistical structure ends and learning begins, since the statistical structure also is used in learning.

2.2.3 Neural Integration and Complexity

It has been argued – see for example Tononi et al. (1998) and Tononi and Sporns (2003) – that there are at least two major challenges facing all higher nervous systems. 1) Information about stimuli needs to be extracted and represented in an efficient way and mapped to *functionally specialized* neurons in the brain. 2) The information then needs to be *functionally integrated* to allow coherent states of the brain to emerge which can guide behaviour. These two principles are, at least in some sense, conflicting, since efficient representation of signals means reducing redundancy, while integration generates mutual information(which essentially is redundancy). Tononi et al. (1998) further hypothesize that the combination of specialization and integration is central to how well a control system is adapted to a particular environment, where localized and specialized sub-systems interact on a global scale. Evidence for this has been found in real cortical connections (Sporns et al., 2000).

To study functional specialization and integration they have developed measures of integration and complexity of neural systems using information theory, which also are useful when studying sensory systems of robots (Lungarella et al., 2005).

Let $\mathcal{X}$ be a system composed of a set of elements $\{X_1, X_2, \ldots, X_N\}$, where each element X_i is a random variable that can assume a discrete number of states. The *integration*, which measures the total entropy loss (Tononi et al., 1998), is defined as:

$$IN(\mathcal{X}) = \sum_{i=1}^{N} H(X_i) - H(\mathcal{X}), \tag{2.7}$$

where $H(\mathcal{X})$ here denotes the joint entropy of all the elements in $\mathcal{X}$. $IN(\mathcal{X})$ is zero only if the elements of the system are independent, and is positive when there are statistical dependencies among the elements. Essentially, this definition of integration is a multivariate generalization of mutual information. If the system $\mathcal{X}$ only contains two random variables then the integration is equivalent to the mutual information of the two variables.

The *complexity* of a system is defined as

$$C(\mathcal{X}) = H(\mathcal{X}) - \sum_{i=1}^{N} H(X_i|\mathcal{X} - X_i), \tag{2.8}$$

where $H(X_i|\mathcal{X} - X_i)$ is the conditional entropy of one element X_i given the complementary set $\mathcal{X} - X_i$. The complexity is high for systems that combine functional segregation and integration, while it is low for random systems and systems that are highly uniform (Tononi et al., 1998).

2.3 Embodied Artificial Intelligence

The central idea of embodied artificial intelligence (Brooks, 1991; Thelen and Smith, 1994; Pfeifer and Scheier, 1999; Sporns, 2003) is that cognitive and behavioural processes emerge from the coupling between brain, body, and environment. This can be contrasted with the *mind-as-computer* metaphor of early artificial intelligence and cognitive science – see for instance Newell and Simon (1976), Fodor (1981), or almost any older textbook on artificial intelligence and/or cognitive science. In the mind-as-computer approach to artificial intelligence and cognition there is a strong separation between the cognitive structures (symbols and representation), the brain (software), and body(hardware). Perception is merely viewed as a means of creating internal representations rich enough to allow for symbolic manipulation. Embodied artificial intelligence, on the other hand, places more emphasis on the embodiment of the agent. The brain, body, and environment are reciprocally coupled, and cognitive processes arise from having a body with specific sensory and actuator capabilities interacting with, and moving in, the world.

Embodied artificial intelligence also puts a stronger emphasis on the relation between perception and actions. For instance, in *active vision* (Ballard, 1991), the view is that visual processes can be simplified if the sensing is appropriately connected to the actions of the agent in the world. This has also been studied in many psychological and physiological experiments that have found clear indications that perception needs to be grounded in actions – see, for example, O'Regan and Noe (2001) for

an overview. In essence, organisms are not – and artificial systems should not, according to embodied artificial intelligence, be – passively exposed to sensory input, but rather interact actively with the environment.

From this embodied perspective the idea of letting the robot learn and develop by exploring its embodiment, possible actions, and environment, is a conceptually small step. This step is taken in the field of developmental robotics. In the coming sections we introduce developmental robotics and focus more in detail on some areas particularly relevant for this thesis: motor babbling, sensorimotor laws, and studies of the informational relationships between embodiment, actions, and the environment.

2.3.1 Developmental Robotics

Developmental robotics (Lungarella et al., 2004) and autonomous mental development (Weng et al., 2001), can be viewed as embodied artificial intelligence with a special interest in how a robot, or infant, can develop new skills or perceptual or cognitive capabilities. These fields have two major driving forces. One is to build more adaptable, autonomous, and sociable robots by drawing inspiration from developmental psychology and neuroscience. The other major driving force is to use robots as embodied tools to help the investigation of the development of neural systems and cognitive abilities.

From methodological and philosophical points of view, developmental robotics can also be viewed as a part of *biorobotics*. Biorobotics – or constructive biology – tries to answer biological questions by building

physical models of animals, and also advance engineering by drawing inspiration from biological systems (Beer et al., 1998).

2.3.2 Aspects of Development

What, then, is development, and how does it work in biological organisms? And how is development different from learning?

Ontogenetic development – development in an individual during its lifetime – is different from learning in that it involves species-specific growth at the cell, body, and brain level, while learning is more a pure "software" problem. Development also involves changes in, for instance, motor control, but it is usually connected to the development of the physical body as well, or new sensory channels made available.

Piaget (1953), maybe the most well known developmental psychologist, viewed development as an incremental process. According to Piaget, later stages of development build on earlier stages. Reaching, for instance, builds on the subskills of a stable gaze and head and trunk control (von Hofsten, 1993). While Piaget suggested that human development is a stable and well-ordered process, Thelen and Smith (1994) have found quite the opposite. In their view, development is messy and chaotic, unstable, and contrary to Piaget's ideas, a developed skill might sometimes even regress.

Development can also be viewed as a set of constraints in the neural and sensory systems (Lungarella et al., 2004). While a lower resolution in a sensory system, or less neural processing power, might at first seem as a handicap, it can, in fact, scaffold development. Limited resolution of, for

instance, vision, may actually improve the perceptual efficiency by reducing the complexity of the environment – basically it helps the neonate to avoid "information overload" (Slater and Johnson, 1997). When a skill is learned or some other condition has been met, more resolution or processing power can be "released". Similarly, the acquisition of motor activity seems to go through similar stages of development where more degrees of freedom are released with time (Bernstein, 1967; Thelen and Smith, 1994).

One other important aspect of development is categorization. Categorization is the ability to make distinctions, e.g., to identify and discriminate between sensory stimulations, emotions, and motor actions (Thelen and Smith, 1994). In general, organisms can discriminate between an enormous range of different stimuli (Edelman, 1987). While some categorizations are innate in higher animals, and even more so in less complicated organisms, categorization is dependent on active exploration of the environment and the capabilities of the organism. Starting from the raw sensory data coming from the sensors, the organism develops through interaction with the development ways of structuring the data in to higher level categorizes (Edelman, 1987). In the rest of this thesis we investigate how a robot can find structure in the raw incoming sensory data and relate it to its own actions.

One way an organism, or robot, can learn to categorize is through *self-exploration*, also known as *body babbling*. Related to self-exploration is *anticipation*, or *prediction*, which can be viewed as *internal forward models* (Jordan and Rumelhart, 1992). Forward models allow prediction

of the future state of a system given the current state and some input. For instance, how infants learn to predict how to catch a ball which is moving in front of the baby (von Hofsten, 1993).

The next two sections will discuss self-exploration, the more philosophical ideas of sensorimotor laws as the basis for visual perception, and related work in developmental robotics.

2.3.3 Body Babbling

In the process of learning a *sense of bodily self* in human infants, systematic exploration of the sensory and perceptual consequences of their actions plays a major role (Rochat, 1998). For example, young infants perform the same actions over and over again (Piaget, 1953), and it has been observed that newborn infants spend up to 20% of their time while awake touching their face with their hands (Korner and Kraemer, 1972). This phenomenon, in analogy with the vocal babbling in the early process of language learning, is also called *body babbling* (Meltzoff and Moore, 1997). It has also been found in experiments with kittens, that visually guided behaviour only develops when changes in visual stimulation are related to self-initiated movements performed by the kitten itself (Held and Hein, 1963).

Body babbling has been investigated by a number of researchers in robotics to explore the possible sensorimotor space of a specific embodiment. For example, Berthouze et al. (1998) developed a system performing basic visuo-motor behaviours which were categorized by a neural network. In (Kuniyoshi et al., 2003) body babbling was used to develop

a system capable of imitation. Berthouze and Kuniyoshi (1998) also developed a system capable of performing unsupervised learning of visual sensorimotor patterns, where the classification used Kohonen maps. The resulting self-organized Kohonen maps showed four different categories of movement: vertical, 'in-depth motions', horizontal, and a fourth, not clearly defined, intermediate category between the horizontal and 'in-depth motions' categories. Related work by Kuperstein (1988) studied adaptive hand-eye coordination for reaching. Here a neural network model was developed that learnt to reach a cylinder arbitrarily placed in space. Self-produced motor signals were used to explore many different arm positions with the cylinder in the hand and topographic sensory information stored in maps. These topographic mappings allowed the system to learn to reach only from sensory receptors and motor feedback, without a priori knowledge about object features. Learning of associations between vision and arm movements has also been studied by Andry et al. (2004). This work is similar to Kuperstein's in many respects via its use of visuo-motor maps and neural network control, but also raised the idea of co-development between sensorimotor and imitative capabilities.

One common feature of the methods just presented is that they all assume that the agent knows about the structure of its sensors, and that all the sensors are visual sensors or have similar properties of continuity to visual sensors. In the methods presented in the following chapters of this thesis, especially in chapter 9, the focus is different since it is the agent itself that must learn the informational structure of its sensors before it can develop sensory guided movement.

2.3.4 Sensorimotor Laws

The work in this thesis is also inspired by the more philosophical ideas described by O'Regan and Noe (2001), where the authors propose a new theory that tries to answer the major question of what visual experience is and where it occurs. Many traditional theories rest on the idea that the brain somehow produces an internal image of the world. Instead, O'Regan and Noe (2001) propose that seeing is a way of acting to explore the world mediated by the agent's mastery of the laws of sensorimotor contingencies, which are a set of rules of interdependence between movement and stimulation of the sensors. Some of these ideas have been translated into algorithms by Philipona et al. (2003), and extended in (Philipona et al., 2004). There the authors consider the question of whether it is possible for a robot with an unknown body to learn that its body is located in a three dimensional world. They are able to give this question a positive answer by presenting an algorithm that can deduce the dimensionality of the world by analyzing the laws that link motor outputs to sensor inputs. Results from simulation show how a robot with multimodal sensors discovers the Euclidean space structure implicit in the equations describing the physical world of the simulation. This is different from the work presented in this thesis in that the present work does not require continuity for the individual sensors, and, moreover, has also been validated on a real physical robot.

2.3.5 Information, Embodiment, and Environment

Part of the title of this thesis is the word "structuring", which here refers to the statistical dependencies, or relationships, between the sensing elements and actions of the robot. The sensing elements, apart from potentially innate knowledge of the robot, solely determine what the robot can know about the world. Consequently, the statistical structure of the environment is all the robot can use to find its way around the world.

The statistical structure available to a robot or organism can be exploited on many levels – from adaptation of the motion sensitive neurons of the fly as we saw in section 2.2.2 – to object recognition in computer vision, a human discussing the latest Seinfeld episode, or a robot avoiding obstacles of a certain colour. The differences between these four examples are that the last three examples are on a higher level than the first one. While the adaptation in the fly is on a purely information theoretical and statistical level, the last three examples are on a semantic level. That is, in the final three examples the sensory data of the agent is assigned meaning (semantics), while in the first example only the probabilities of the symbols are considered.

How are the symbols assigned meaning? This is a deep philosophical as well as technological problem known as the *symbol grounding problem* (Harnad, 1990). Traditionally in robotics and artificial intelligence the meaning of sensor data has been assigned by hand, based on the domain knowledge and technical skills of the programmer. In this thesis much of the focus is on the lower, purely statistical, level of sensor structure, and we make no claim to solve the symbol grounding problem. But we

aim at building robots where the meaning of the sensor data is subjectively grounded by the robot itself by finding the informational relations between its sensors and its performed actions. This can, for example, be done in body babbling as described above in section 2.3.3.

What affects the lower level informational relations between sensors in robots, how can it be studied, and how can it be useful? These questions have been studied by a number of authors in the last years, quite often using the framework of information theory. In general, there are three aspects that affect the informational relationships between sensors (Sporns and Pegors, 2004):

- **The embodiment of the robot**. This includes the particular sensors used; their modalities, resolution, but also their positions on the robot and the relative positions of pairs of sensors. For instance, as we will show in chapter 4 the mutual information between visual sensors is dependent on the spatial distance between the sensors.

- **The environment of the robot.** This includes the statistics of the environment – see section 2.2.1, and the actions of other agents in the environment.

- **The actions of the robot.** The movements that the robot performs can also affect the informational relationships between the sensors of the robot (Lungarella et al., 2005).

Quick et al. (1999) defines the degree of embodiment as the degree to which an agent is structurally coupled to its environment. More recent

work by Quick et al. attempts to quantify the embodiment by information theoretic analysis of the sensor and actuator channels of robots. As far as we are aware, have there not been many studies of how the statistics of sensor data depends on the particular embodiment of a robot or organism. In neuroscience, some recent studies of the statistics of natural videos have connected cameras to the head of a cat that roams freely around – see for instance (Betsch et al., 2004) – and their results regarding contours and statistics are similar to those found in earlier studies of natural statistics presented in section 2.2.1.

Pierce and Kuipers (1997) introduced a method, here called the sensory reconstruction method, where the spatial layout of the sensors of a robot can be found from unstructured and raw sensor data. The method was evaluated in simulation only by Pierce and Kuipers (1997) for a visual field and a simulated robot equipped with distance sensors. The sensory reconstruction method is central to this thesis and is here extended by us to consider all possible relations between the sensors by the use of information theory. It is also evaluated by us using a real physical robot. For a detailed overview of the sensory reconstruction method – see chapter 3.

Inspired by the idea of informational maps of sensors presented in this thesis and by us in (Olsson et al., 2004a,c), Hafner and Kaplan (2005) extended the maps to also include the sensors and actuators of other robots. This enables the robot to map its own sensors and actuators to the observed body structure, which, according to Hafner and Kaplan (2005), can help elucidate the body schema and the correspondence prob-

lem (Alissandrakis, 2003). One problem with this approach is how, in general, the robot would get access to the raw sensory streams of other robots in the environment. Information-theoretic measures have also been used to classify behaviour and interactions with the environment using raw and uninterpreted sensor data from the agent. In (Tarapore et al., 2004) the statistical structure of the sensoric input was used to fingerprint interactions and environments. Mirza et al. (2005b) considered how the informational relationships between its sensors, as well as actuators, can be used to build histories of interaction by classifying trajectories in the sensorimotor phase space. In (Kaplan and Hafner, 2005) the authors also considered clustering behaviours by the informational distances between sensors by considering configurations of matrices of information distances between all pairs of sensors.

One other aspect of the information available in an agent's sensors is that the particular actions of the agent can have an impact on the nature and statistical structure of its sensoric input. This has been studied in a number of papers since (Lungarella and Pfeifer, 2001); see for instance (Sporns and Pegors, 2003, 2004; Lungarella et al., 2005). The experimental setup in these papers have all been quite similar, with a camera mounted on a two degree-of-freedom pan-tilt platform positioned in front of a screen, where the screen showed either natural or random images. In the experiments the camera has performed random movements or saliency-based tracking (foveation) of images on the screen. The results show how the visually guided movement decreases the entropy of the input while increasing the statistical dependencies between the sensors.

Lungarella et al. (2005) also computed the integration and complexity described in section 2.2.3. The results showed that both the integration and complexity were much larger for five by five patches in the centre of the visual field while foveating. These results are consistent with the hypothesis that coordinated sensorimotor movement, in this case foveation, can induce changes in global informational measures.

The flow of information in the perception-action loop of agents has also been studied from a purely information-theoretic perspective in a number of papers by Klyubin et al. (2004, 2005a,b). The main idea of their work is *empowerment*, which, basically, is the *potential* capacity of information flow from the actions of the agent that can be retrieved at a later time from the agent's sensors. Essentially, empowerment measures how much information an agent can "inject" into the environment through its actions and then later recover. Empowerment can be used as a measure to guide the development of efficient perception-action loops, to study the information flow in biological and artificial agents, or as a heuristic for an agent to seek situations which are more interesting and relevant. While the presented methods in (Klyubin et al., 2004, 2005a,b) so far only have been implemented and tested in small and abstract simulations, it would be very interesting to see how it would scale to larger, real robotic systems.

2.4 Conclusion

In this chapter we have presented the mathematical framework of information theory, the statistics of natural signals, how biological organisms exploit these statistics, measures of neural integration and complexity, developmental robotics, and related work to this thesis studying the informational structure in sensors and actuators of embodied robots.

As discussed above, there are indications from neuroscience of how the sensoric systems of animals adapt, both over evolutionary time, as well as within seconds, to the statistics of the environment of the organism. The aim of developmental robotics is to create robotic systems that adapt and develop to their specific embodiment, environment, and tasks to perform. Information theory provides a general framework for studying the informational relationships between sensors, actuators, and actions performed by the agent.

One thing, in our opinion, missing from much of the previous work using information theory to study the low level informational organization in sensors and actuators, is how to actually exploit the discovered structure. While it is of interest in itself to find, e.g., how foveation of objects leads to increased correlations between sensors in the centre of the visual field, it would also be interesting to study how these regularities can be exploited by the robot. This is something which is partly addressed in this thesis. Here we present a method for sensor adaptation which exploits the statistical structure of the sensor data, as well as showing how the informational relations between sensors can be grounded in

the actions of the robot. It is also important to point out that all the presented methods in this thesis have been tried on a real robot, as well as sometimes in simulation, to get more realistic sensor data.

Chapter 3

The Sensory Reconstruction Method

The sensory reconstruction method is a method for finding structure in raw and uninterpreted sensor data, meaning that there are no built-in assumptions about the modalities or representation of the data in the sensors. The idea is that the robot should learn how different sensors are related and how different actions and environments affect the data it receives through its sensors. This enables the robot to develop and adapt in different ways depending on its particular embodiment and environment.

In the method, first introduced by Pierce and Kuipers (1997), and extended by us during the work of this thesis by using information-theoretic methods, sensoritopic maps are created that show the informational relationships between sensors, where sensors that are informationally related are close to each other in the maps. The sensoritopic maps might also reflect the real physical relations and positions of sensors. For exam-

ple, if each pixel of a camera is considered a sensor, it is possible to reconstruct the organization of these sensors even though initially their spatial positions are not known and the only input is a number of normalized sensor data streams – see for example the experiments in chapter 4. These maps can be used for different applications as we will show in the following chapters.

The sensory reconstruction method consists of a number of steps that will be described in this chapter after some background is given. We start by giving a formal definition of what we mean by a sensor in section 3.1, and section 3.2 presents how we view a sensor as a compressed representation of a measured property of the world of the robot and how probabilities can be estimated from the sensor data. Central to the sensory reconstruction method is computing the informational distance between all pairs of sensors which results in a distance matrix. We use the information metric (Crutchfield, 1990), which is described in section 3.3. Given this distance matrix a sensoritopic map can be created which is presented in section 3.4. How groups of similar sensors can be found and what the best dimension is to represent these sensors is presented in section 3.5. We then introduce a measurement for comparing the spatial organization of reconstructed visual fields with the physical spatial organization of the sensors in section 3.6.

3.1 What is a Sensor?

In this thesis a sensor is defined as a device that quantifies some property of the world or some property internal to the agent, such as a pixel of a digital camera or battery level, that the agent has access to. The sensor does not represent the real value of the property, but rather a compressed and estimated value – see section 3.2. An actuator is a value that the agent can change and that has some physical effect in the world. In other words, a sensor is a read-only variable, while an actuator is a read-and-write variable.

A sensor S_x, where $1 \leq x \leq N$, can assume one of a discrete number of values $S_x^t \in \mathcal{X}$ at each time step t, $1 \leq t \leq T$, where $\mathcal{X}$ is the alphabet of S_x. Thus, each sensor can be viewed as a time-series of data $\{S_x^1, S_x^2, \ldots, S_x^T\}$ with T elements. Each sensor S_x can also be viewed as a random variable X drawn from a particular probability density function $p_x(x)$, where $p_x(x)$ is estimated from the time series of data. Similarly the joint probability distribution $p_{x,y}(x, y)$ is estimated from the time-series of sensors S_x and S_y.

3.2 Probability Estimation and Binning

In the work presented here each sensor or actuator variable can, as mentioned above, be modelled as a discrete random variable X that can assume values from a finite alphabet $\mathcal{X}$. In general the measured property can assume a larger range of values than the resolution of the sensor. The sensor S_x is a compressed representation of a particular quantity in

the world, which we denote as X_{raw}, that the sensor registers. Thus, a sensor can be viewed as a mapping from a larger alphabet $\mathcal{X}_{raw}$, where $|\mathcal{X}| < |\mathcal{X}_{raw}|$, to the smaller alphabet $\mathcal{X}$, where the number of elements in $\mathcal{X}$ is $C = |\mathcal{X}|$. Perhaps the most common method to do this is by *uniform binning*, where the possible values of $\mathcal{X}_{raw}$ are divided into the bins B_i, $\mathcal{X}_{raw} = B_1 \cup \cdots \cup B_C$, where each bin contains the same number of values from $\mathcal{X}_{raw}$. That is, $\forall B_i,\ |B_i| = \frac{|\mathcal{X}_{raw}|}{C}$. Now let each bin B_i correspond to one symbol in the alphabet $\mathcal{X} = \{1, 2, \ldots, C\}$ and the probability mass function $p(x)$ can then be estimated from the frequency distribution of the bins.

This method, although commonly used, is associated with a number of problems – see for example (Lungarella et al., 2005). One problem is that the size and placement of the bins might affect whether an important feature of the data is captured or not. For example, imagine a sensor reading raw values in the range $\mathcal{X}_{raw} = \{1, 2, \ldots, 100\}$ with two bins, one corresponding to $B_1 = \{1, 2, \ldots, 50\}$, and the other $B_2 = \{51, 52, \ldots, 100\}$. For instance, if the raw values alternate between 5 and 22, the value of the sensor is always symbol 1, meaning that the entropy of the sensor will be 0.0, even though there really is entropy in the sensor. Related to this is the problem of deciding on how many bins to use; if too few bins are used important features of the data might be missed, and if too many are used it is hard to estimate the underlying probability distribution given a small set of data due to undersampling (Lungarella et al., 2005). In general, there is no method of computing how many bins are best for a certain application without making

assumptions about the underlying data source.

Despite these problems we have used uniform binning in the experiments presented in some of the chapters of this thesis, for example chapter 4 and 7, using 10 bins unless we state otherwise . The reason for this is simplicity and that we wanted to find out how much can be achieved without any assumptions about the underlying sensor data from a certain source. In chapter 6 we present an alternative binning method which constantly adapts to the statistical structure of the sensor input. This enables the sensor to arrange the bins in such a way as to add more resolution where it is needed, given the statistical structure of the current sensor data.

3.3 The Information Metric

Central to the sensory reconstruction method is the computation of the informational distance between pairs of sensors. Pierce and Kuipers (1997) used the 1-norm Euclidean distance, defined as

$$d_{1n}(S_x, S_y) = \frac{1}{T}\sum_{t=1}^{T} |S_x^t - S_y^t|, \tag{3.1}$$

which computes the absolute difference between the sensor values of sensor S_x and S_y for each time step. After using this distance measure we found that it does not always capture all functional relationships between sensors, due to its linear nature. This means that only the values of the sensors are compared, which limits the use of the method to sensors of

the same modality. But, since we were interested in sensors of potentially different modalities, we wanted to use a metric that operates on probabilistic relations between the sensors and that could also find non-linear correlations. One such distance measure is the information metric (Crutchfield, 1990). The information metric is defined as

$$d_{im}(S_x, S_y) := H(X|Y) + H(Y|X), \tag{3.2}$$

where $H(X|Y)$ is the conditional entropy of X given Y defined in section 2.1.1. It can also be viewed as the opposite of mutual information – see the Venn diagram in figure 2.2. While mutual information, $I(X;Y)$, measures the shared information between two random variables, the information metric determines the information they do not have in common.

To compute the information metric distances for a set of sensors, one needs to compute the joint entropies for all pairs of sensors. This means that the computational complexity is $O(N^2C^2)$, where N is the number of sensors and C the number of bins used.

To get a normalized metric in the range $[0.0, 1.0]$ one can divide by the maximal distance,

$$d_{im}(S_x, S_y) = \frac{H(X|Y) + H(Y|X)}{\log_2 |\mathcal{X}| + \log_2 |\mathcal{Y}|}, \tag{3.3}$$

which is equivalent to the maximal entropy of the two sensors.

The information metric is, just like the 1-norm distance, a metric not just by name but also in the formal mathematical sense. A mathematical

metric, $d(X, Y)$, is a distance function on a set of points, mapping pairs of points (X, Y) to non-negative real numbers. A distance metric in the mathematical sense also needs to satisfy the three following properties:

1. $d(X, Y) = d(Y, X)$ (Symmetry).
2. $d(X, Y) = 0 \quad \text{iff} \quad Y = X$ (Equivalence).
3. $d(X, Z) \leq d(X, Y) + d(Y, Z)$. (Triangle Inequality).

If the second fails but the first and third hold, then we have a pseudo-metric, from which one canonically obtains a metric by identifying points at distance zero from each other. This is done here and in (Crutchfield, 1990).

Why can it be useful to use a distance measure which is a metric in the mathematical sense? If a space of information sources has a metric, it is possible to use some of the tools and terminology of geometry. It might also be useful to be able to talk about sensors in terms of spatial relationships. This might be of special importance if the computations are used to actually discover some physical structure or spatial relationships of the sensors, for example as in the experiments of chapter 4, where the spatial layout of visual sensors as well as some physical symmetry of a robot was found by information-theoretic means. There is also a technical reason which is related to how the appropriate dimensionality that is required to represent the sensors in a sensoritopic map is computed, which is presented in sections 3.4 and 3.5. Basically, if a distance matrix is computed using a non-metric, it might be the case that some calculated eigenvalues in metric scaling may become negative, possibly

resulting in some imaginary coordinates (Krzanowski, 1988). Finally, using a symmetric distance measure is useful since it is possible to halve the number of distance calculations by noting that $d(X, Y)$ always is equal to $d(Y, X)$.

3.4 Creating Sensoritopic Maps

To create a sensoritopic map the information distance is first computed between all pairs of sensors as described above using the information metric, equation 3.2. If there are N sensors, this requires $\frac{N^2-N}{2}$ distance computations when using a symmetric distance measure and by noting that $d(X, X)$ always is zero.

The resulting distance matrix specifies the informational distance between all pairs of sensors. To create a sensoritopic map from the distance matrix, the N sensors are projected to a plane. In general, a perfect mapping given a N by N distance matrix requires $N-1$ dimensions, but often a lower dimensionality is the most appropriate to reflect the nature of the sensors and the data. For example, a rectangular visual field is best represented in two dimensions, and that this is the case can actually be shown algorithmically using only the sensor data – see section 3.5 and the experiments in chapter 4.

To project the sensors of the distance matrix to a lower dimension is a constraint-solving problem that can be solved by a number of different methods such as metric scaling and Sammon mapping (Krzanowski, 1988), self-organizing maps (Kohonen, 2001; Polani, 2002), elastic nets

(Goodhill et al., 1995), and relaxation (Pierce and Kuipers, 1997). Metric scaling and Sammon mapping are eigenvalued-based methods, where the only difference is that Sammon mapping emphasizes small distances since the errors of the mapping are normalized with the distances in the normal space. Self-organizing maps are an unsupervised neural networks based method, where artificial neurons are placed in a grid, and elastic nets are a probabilistic extension to self-organizing maps using a different learning rule. Here it was decided after some experimentation to use the relaxation method presented in (Pierce and Kuipers, 1997), primarily because of its speed and qualitatively better results found by visual inspection of reconstruction of known visual layouts. It is also possible to use the coordinates found by metric-scaling as starting coordinates for the relaxation method explained below, but in our experience this step is not necessary for good results. When metric-scaling is used to compute the dimensionality, as explained in section 3.5, the coordinates from metric scaling can be re-used as the starting coordinates for the relaxation method.

In the relaxation method each sensor $S_i, 1 \leq i \leq N$, is assigned a random position $\mathbf{p_i}$ on a plane. The force $\mathbf{f_i}$ on each point $\mathbf{p_i}$ is

$$\mathbf{f_i} = \sum_{j=1, j!=i}^{N} \frac{(||\mathbf{p_i} - \mathbf{p_j}|| - d(X_i, X_j))(\mathbf{p_j} - \mathbf{p_i})}{||\mathbf{p_j} - \mathbf{p_i}||}. \tag{3.4}$$

Each point $\mathbf{p_i}$ is moved according to the force $\mathbf{f_i}$ acting on that point:

$$\mathbf{p_i} = \mathbf{p_i} + \frac{\mathbf{f_i}}{N} \tag{3.5}$$

The algorithm is iterated for a number of steps moving each point according to equation 3.5 until only very small movements occur – we stopped when the average movement was less than $\frac{1}{1000}$ of the longest distance between two sensors. This usually takes between 500 to 1000 steps for 100 sensors, depending on the sensory data and distance matrix. The computational complexity of this algorithm is $O(N^2)$, since we for each time step have to iterate over all pairs of sensors.

Figure 3.1 shows an example of sensoritopic maps for 100 visual sensors from a SONY AIBO[1] robot developing from zero to 800 iterations, where the real spatial organization has been more or less captured (reconstructed) in the sensoritopic map. For more examples see chapter 4.

One problem with the relaxation method, as with many other dimension reduction methods, is the so called "Horseshoe effect" (Krzanowski, 1988). Objects that are further apart in terms of distance in the distance matrix end up being closer in the computed map. This can be seen in figure 3.1 where the right side of the map, sensors $1, 11, \ldots, 92$ etc, is slightly bent as a horseshoe rather than a straight line, which is the case in the real visual field the sensor data was captured from.

3.5 Grouping and Dimensionality

Given the sensoritopic map, sensors that are close can be grouped together. To begin with, groups of sensors that are similar are found,

[1] AIBO is a registered trademark of SONY Corporation.

1	2	3	4	5	6	7	8	9	10
11	12	13	14	15	16	17	18	19	20
21	22	23	24	25	26	27	28	29	30
31	32	33	34	35	36	37	38	39	40
41	42	43	44	45	46	47	48	49	50
51	52	53	54	55	56	57	58	59	60
61	62	63	64	65	66	67	68	69	70
71	72	73	74	75	76	77	78	79	80
81	82	83	84	85	86	87	88	89	90
91	92	93	94	95	96	97	98	99	10

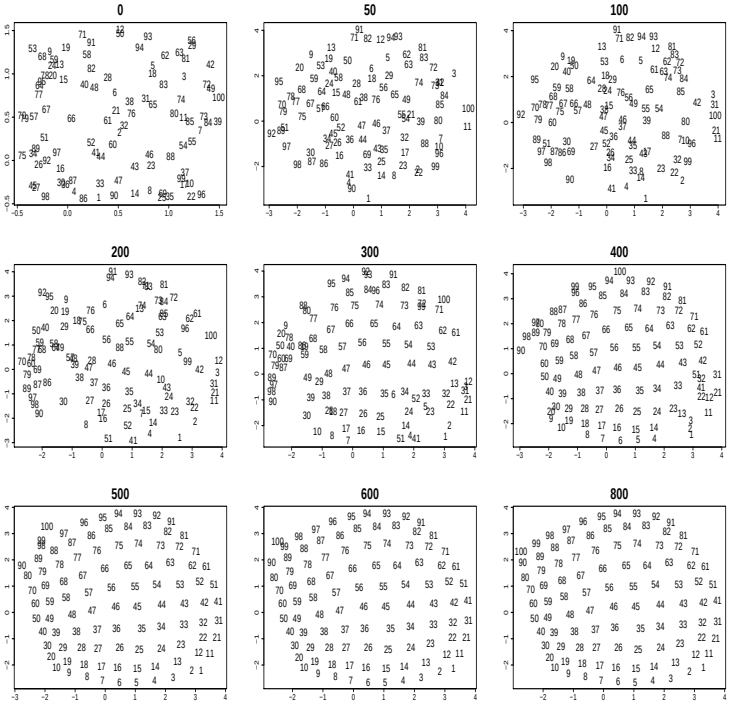

Figure 3.1: The layout of the visual sensors numbered 1 to 100 and sensoritopic maps starting with random coordinates for the 100 sensors from 0 iterations to 800 iterations of the relaxation algorithm. After 800 iterations the real layout has been reconstructed, albeit mirrored with 1 in the lower right corner and 100 in the upper left.

where two sensors, S_x and S_y, are similar,

$$S_x \approx S_y \quad \text{if} \quad d(S_x, S_y) \leq \min\{\epsilon_x, \epsilon_y\}, \tag{3.6}$$

where the ϵ_x is calculated from the minimum distance, $\epsilon_x = 2\min\{d(S_x, S_y)\}$, to any of its neighbours. To form equivalence classes, Pierce and Kuipers (1997) use the *related-to* relation which is the transitive closure of the $\approx$ relation. This is computed recursively via

$$S_x \sim S_y \quad \text{iff} \quad S_x \approx S_y \vee \exists S_z : (S_x \sim S_z) \wedge (S_z \sim S_y). \tag{3.7}$$

Given such an equivalence class the appropriate number of dimensions to represent the data can be computed using several methods. It should be noted that, in general, no formally objective method exists for deciding on the number of dimensions to use (Krzanowski, 1988), and the results will always to some extent be subjective. But, the scree method based on eigenvalues (Cattell, 1966) presented here, which also is one of the most commonly used methods for this problem, was verified by us to give reasonable results on typical data obtained by us in simulations as well as with real robots.

The scree method of Cattell (1966) works in the following way. Given the distance matrix D of the information distances between all pairs of sensors, find the n first principal components – see for example (Krzanowski, 1988). Let λ_p be the eigenvalue associated with the pth principal component of D. Then $\lambda_1 > \lambda_2 > \ldots > \lambda_{n-1} > \lambda_n$ and maximizing $\lambda_p - \lambda_{p+1}$ gives us p as the correct dimension to represent the distance matrix D. One possible limitation of the scree method is if there are two or more dimensions that maximize $\lambda_p - \lambda_{p+1}$. In the experiments presented in this thesis this never happened. An example of eigenvalues for different

two-dimensional as well as one-dimensional visual fields can be found in section 4.3.2.

3.6 Measuring Reconstruction

Up until now the term "reconstructed" has been used in an informal way, where, for example, a visual field is reconstructed if the sensoritopic map and the real layout of the sensors look similar – see for example figure 3.1. Here the sensoritopic map after 800 relaxation iterations looks similar to the (discrete) layout of sensors from which the sensor data was acquired. If the sensors are of various different modalities, e.g., infrared distance sensors, joint positions, audio, and touch sensors, this is not as easy to formalize and a higher level interpretation of the maps is more dependent on the particular sensors and their modalities. In the next chapter we will present some interpretation of sensoritopic maps consisting of a number of a different modalities, but most results presented in this thesis are of visual sensors, although sometimes of different visual modalities.

One way to quantify the similarity between a number of visual sensors and their physical position is by computing the relative distances between pairs of sensors in the reconstructed visual field and the real layout of the sensors. Let $r_{i,j}$ be the Euclidean distance between two sensors i and j in the reconstructed map, and $\ell_{i,j}$ the distance between the same two sensors in the real layout, where the x and y coordinates in both cases have been normalized into the range $[0.0, 1.0]$. Now the average distance

between all pairs of sensors can be compared,

$$d(r,\ell) = \frac{2}{N^2 - N} \sum_{i}^{N} \sum_{j=i+1}^{N} |r_{i,j} - \ell_{i,j}|, \tag{3.8}$$

where N is the number of sensors. Since the distances always are symmetric, $d(\ell, r) = d(r, \ell)$, and the distance between a sensor and itself always is zero, are there only $\frac{N^2-N}{2}$ pairs of sensors to compare, and not N^2. This measure is hereafter called *average reconstruction distance*.

Equation 3.8 compares the relative positions of the sensors and not the physical positions, and $d(r, \ell)$ will have a value in the range $[0.0, 1.0]$. A distance of zero means that the relative positions are exactly the same, and sensors placed at completely random positions will have an average distance of approximately 0.52. This was estimated by simulation.

3.7 Conclusion

We have in this chapter presented the sensory reconstruction method, which is method for finding structure in raw and uninterpreted sensor data. After defining what we mean by a sensor it was described how a sensor is a compressed representation of the measured property, and how the probability distribution of a sensor can be estimated.

Central to the method is the informational distance between sensors. We proposed the information metric (Crutchfield, 1990) as an appropriate metric since it captures both linear and nonlinear dependencies between sensors – see for example (Tononi et al., 1998). This should be

contrasted with the 1-norm metric used by Pierce and Kuipers (1997) which only captures linear dependencies. Why capturing nonlinear dependencies is useful for sensor integration is discussed in chapter 6, and chapter 7 compares the information metric in more detail with a number of other distance measures.

From the distance matrix of the informational distances between all pairs of sensors, sensoritopic maps are created using the relaxation algorithm. To find the appropriate dimension in which to represent the map the scree method can be used (Cattell, 1966).

Chapter 4

Reconstruction of Sensory Organization

In this chapter we investigate how the sensory reconstruction method, presented in the previous chapter, can be used by an autonomous robot to find informational relations between sensors from raw and uninterpreted sensor data. One way to view this problem is to imagine having your brain connected to an unknown machine, with various sensors and actuators, and your goal is to find out about the structure of this machine. For instance, what wires connected to your brain correspond to the camera on the machine, and also how these wires should be connected to "see" what the camera records. This problem can also be viewed in terms of development where the robot bootstraps its sensory processing organization and grounds its perceptions in the informational structure actually found in the sensors, rather than the structure being hard wired in to the robot.

Here we present sensoritopic maps of all the sensors of an autonomous robot, and find that some symmetry of the physical body of the robot can be found in the sensoritopic maps. In the sensoritopic maps it turns out that the sensors that come from the camera are grouped together and the spatial relations of the sensors in the map correspond to their spatial layout in the robot. We also look at how visual fields of different shapes and different modalities can be reconstructed.

What the robot can learn and know about the world and how well a visual field can be reconstructed, depends on the statistics of the incoming sensory data. In neuroscience statistical analysis of natural environments is used to understand how neural systems develop and are adapted to their particular environment – see section 2.2.1. Ruderman (1994) found that the spatial coherence of natural scenes scales as a power law. Here we look at the collected visual sensor data from the robot and find that the spatial coherence of the robot data, just as the collected natural scenes collected by Ruderman (1994), scales as a power law. A similar analysis is also performed for the temporal coherence, i.e., how the visual data is related over time. Again, the results show that the collected AIBO data scales as a power law in the time domain.

The rest of this chapter is structured as follows. To begin with the SONY AIBO robot – the robot used in all our robotic experiments – is introduced, and an overview of all its sensor possibilities is given. Then results from reconstruction of all AIBO sensors are given before we focus on only the visual sensors. After presenting results of reconstruction of visual fields of various shapes and different modalities we also show how

a "scrambled" visual field can be "de-scrambled" using the sensory reconstruction method. Then the statistics of the visual data are analyzed in more detail.

4.1 Introducing the SONY AIBO Robot

In almost all the experiments presented in this thesis a SONY AIBO[1] robot model ERS-210 was used – see figure 4.1. The AIBO is a commercial four-legged dog-like autonomous robot equipped with a wireless ethernet card for communication with other robots and computers. The AIBO is the size of a small puppy, length 289 mm, width 152 mm, and height 278 mm. To program the AIBO we used the Tekkotsu[2] framework.

The AIBO is equipped with a number of sensors including one infrared distance sensor, colour camera, paw sensors, and gravitational sensors. These are all listed and described below including the sensor name abbreviations used in sensoritopic maps.

Sensors of different modalities can assume values of different ranges, e.g., $\{0, 1, \ldots, 255\}$ for visual sensors and degrees in the range $[-11, 89]$ for the leg elevation sensors. To create the raw and uninterpreted sensor data with no explicit information of the modality of a sensor, the sensor data from each sensor was normalized in the range $[0, 1]$.

For a much more complete overview of the AIBO including drawings, operational limits, etc, see (Sony, 2002).

[1] AIBO is a registered trademark of SONY Corporation.
[2] http://www.tekkotsu.org

(a) SONY AIBO Robot

0	1	2	3	4	5	6	7	8	9
10	11	12	13	14	15	16	17	18	19
20	21	22	23	24	25	26	27	28	29
30	31	32	33	34	35	36	37	38	39
40	41	42	43	44	45	46	47	48	49
50	51	52	53	54	55	56	57	58	59
60	61	62	63	64	65	66	67	68	69
70	71	72	73	74	75	76	77	78	79
80	81	82	83	84	85	86	87	88	89
90	91	92	93	94	95	96	97	98	99

(b) Visual sensor layout

Figure 4.1: The SONY AIBO robot. Figure 4.1(a) shows the SONY AIBO robot sitting in the lab. Figure 4.1(b) shows the downsampled layout of the visual sensors of the camera.

4.1.1 Vision

The AIBO is equipped with a CCD camera located inside the head to capture image frames. The camera has a field view of 57.6 degrees wide and 47.8 degrees tall. In our experiments we used the camera in the 88 by 72 pixels mode, with eight bits for each channel (red, blue, green). In most experiments – see the descriptions of the experiments – the image was downsampled to 10 by 10 or eight by eight pixels by averaging, where each pixel was the average value over seven by seven pixel squares of the whole image for the 10 by 10 image and nine by nine pixels for the eight by eight image. The pixels (sensors) of the camera are numbered with sensor 0 in the upper left corner and sensor 99 (or 63) in the lower right corner of the camera – see figure 4.1(b). A letter, $\{R, G, B, I\}$, is used to signify whether the sensor represents the (R)ed, (G)reen, (B)lue, or (I)intensity of the pixel, where the intensity for a sensor in position N is

Sensor	Range	Note
BLP	0 or 1	Back left paw (1 means touch)
BRP	0 or 1	Back right paw
FLP	0 or 1	Front left paw
FRP	0 or 1	Front right paw
Ch	0 or 1	Under the mouth
B	0 or 1	Back Button
HF	$[0, 1]$	Head front (1 max pressure, 0 minimum)
HB	$[0, 1]$	Head back (1 max pressure, 0 minimum)

Table 4.1: Pressure sensors of the Sony AIBO ERS-210.

$I_N = \frac{R_N+G_N+B_N}{3}$. For instance, $G61$ is the green channel of pixel 61. If no letter is given, the sensor implicitly represents the intensity.

4.1.2 Pressure Sensors

There are eight pressure sensors, listed in Table 4.1. These are all binary, apart from the head sensors that have a wider range.

4.1.3 Joint Positions and Duties

Each leg on the AIBO has three degrees of freedom, knee, rotation (back or forward along body), and toward or away from body (elevation). The head can be moved in three ways, tilt (elevation), pan (heading), and roll. The tail can be tilted and panned. The jaw can be moved up down. This comprises a total of 18 degrees of freedom. Each one of these joints has two values: the current force of the motor, called the duty, and the current position of the joint. Table 4.2 lists these sensors. Here lower case names denote duties and upper case positions.

Sensor	Unit	Range	Note
BLE, BRE, FLE, FRE	Degrees	$[-11, 89]$	Leg elevation
BLK, BRK, FLK, FRK	Degrees	$[-27, 147]$	Knee position
BLR, BRR, FLR, FRR	Degrees	$[-27, 147]$	Leg rotation
ble, bre, fle, fle	-	$[-1, 1]$	Elevation motor power
blk, brk, flk, frk	-	$[-1, 1]$	Rotation motor power
blr, brr, flr, frr	-	$[-1, 1]$	Knee motor power
JAW	Degrees	$[-47, -3]$	Jaw position
jaw	-	$[-1, 1]$	Jaw motor power
NP	Degrees	$[-89.6, 89.6]$	Neck pan position
NT	Degrees	$[-82, 43]$	Neck tilt position
NR	Degrees	$[-29, 29]$	Neck roll position
np	-	$[-1, 1]$	Neck pan motor power
nt	-	$[-1, 1]$	Neck tilt motor power
nr	-	$[-1, 1]$	Neck roll motor power
TP	Degrees	$[-22, 22]$	Tail pan position
TT	Degrees	$[-22, 22]$	Tail tilt position
tp	-	$[-1, 1]$	Tail pan motor power
tt	-	$[-1, 1]$	Tail tilt motor power

Table 4.2: Positions and duties of the Sony AIBO ERS-210. Here B and b signifies back, F and f forward, L and l left, R and r right, where lower case signifies duties and upper case positions.

4.1.4 Other Sensors

The AIBO also has an infrared distance sensor placed on its nose, gravitational sensors, temperature, and power-remaining sensors. These are listed in table 4.3.

Sensor	Unit	Range	Note
Ir	mm	$[100, 900]$	Distance to target
Ba	m/s^2	$[-19.6133, 19.6133]$	Y-axis. Front positive
La	m/s^2	$[-19.6133, 19.6133]$	X-axis. Right positive
Da	m/s^2	$[-19.6133, 19.6133]$	Z-axis. Up positive
Te	Celsius	$[-20, 50]$	Temperature
P	Fraction	$[0, 1]$	Power left (0.0 no power)

Table 4.3: Other sensors of the Sony AIBO ERS-210.

4.1.5 Sound

There are two microphones, located on the right and left side of the head, giving the AIBO stereo hearing (two channels). The sampling frequency is 16 kHz and the quantitized bit length 16 bits Linear PCM. Sound was not used in any of the experiments in this thesis.

4.2 Reconstruction of all AIBO Sensors

Here we present results from exploratory experiments applying the sensory reconstruction method to all the AIBO sensors.

4.2.1 Experimental Setup

In this first experiment, looking at all the sensors as well as duties of the AIBO, a basic exploratory behaviour from the Tekkotsu framework was used. The AIBO was walking around in the office avoiding obstacles and otherwise walking straight. We also tried different behaviours such as ball following and kicking behaviours with similar results. The sensor data

was collected over the wireless network and for the presented sensoritopic maps the fram-rate was 10 frames per second, but we also tried different frame-rates up to 25 frames per second with similar results. All the joint positions, duties, pressure, and various sensors described in section 4.1 were collected along with 100 visual sensors, resulting in a total of 150 sensors. In this experiment the visual field was a 10 by 10 rectangle of the pixels from the upper left corner of the camera, but averaged pixels as described in 4.1.1 were tested and produced similar results.

4.2.2 Results

Figure 4.2 shows an example of a sensoritopic map constructed after 1000 time steps of collected data of all the 150 sensors and duties. The first thing to notice is the symmetry and organization. To the right in the map we find the visual sensors, labeled 0-99. Even without knowing that sensors 0-99 are vision sensors, one could guess that they are sensors positioned in a square formation that measure some kind of piecewise smoothly varying phenomena. Looking closer at the organization of these sensors we find that the positions of these sensors in the map roughly corresponds to their position in the visual field of the robot. For instance, visual sensor 99 is closest to visual sensors 98, 88, and 89, which corresponds to the layout of 4.1(b). How, why, and when the sensory reconstruction method manages to reconstruct the visual field will be studied in more detail in the following sections.

In the center of the map we find the paw sensors and some sensors that never change value, such as the temperature and power sensors.

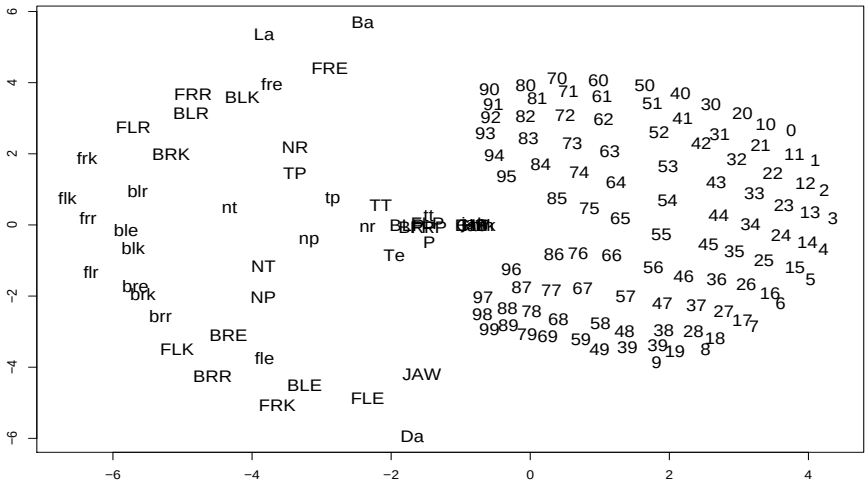

Figure 4.2: Sensoritopic map of all AIBO sensors. For a legend to all the abbreviations of sensors – see section 4.1.

To the left we find the neck positions and duties sensors and all the leg positions and joints. By focusing only on the leg sensors and duties we find that the symmetry of the body of the robot reflected in the map. Consider for example figure 4.3, which shows the same data without the visual sensors.

The back left leg positions *BLE*, *BLK*, and *BLR* are close together and more or less mirrored by the back right leg positions *BRE*, *BRK*, and *BRR*. Since the robot used a gait optimized for robotic soccer the front legs have different relative positions than the back legs due to the forward leaning gait. The motor duties of the back left (*ble*, *blk*, *blr*) and right (*bre*, *brk*, *brr*) legs are also grouped together. We also find that the paws, *BLP*, *BRP*, *FLP*, and *FRP*, are closely grouped together in the map. This indicates that these sensors are closely informationally

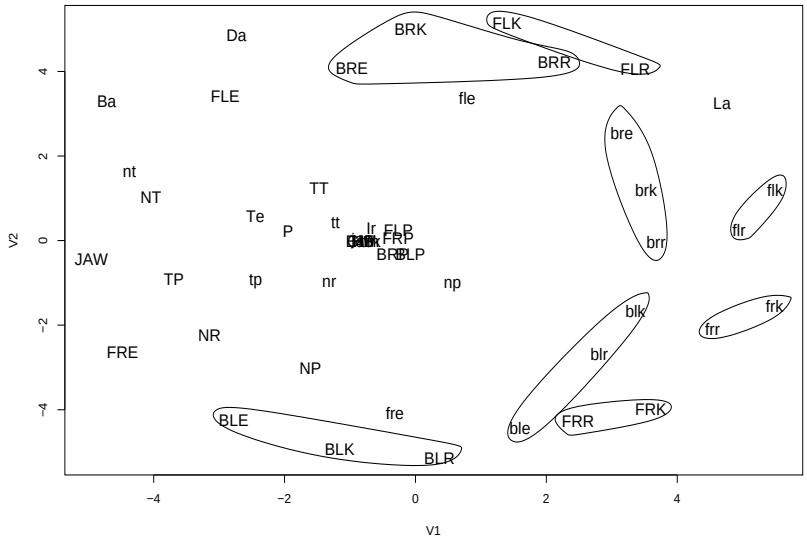

Figure 4.3: Sensoritopic map of all sensors excluding the visual sensors. The groupings were made by hand to highlight the symmetry of the sensors in the map – see discussion in section 4.2.2.

related, and that the current status of one paw can be used to predict the states of the other paws. This is due to the AIBO using a predictable gait.

The sensor maps of figure 4.2 and figure 4.3 can be seen as the first steps toward "AIBO-unculus" maps, in a sense similar to homunculus maps of humans where each region of the body is represented by corresponding regions both in the somatic sensory cortex and primary motor cortex (Kandel et al., 2000).

There are also sensors that do not seem to be related at all that are close together in the maps, e.g., the tail and the temperature sensors. In this experiment temperature was roughly constant, and the tail was never used, so its position and motor values were static and thus the information distance is very close to zero. By performing active probing

we expect it to be possible to separate, or *unfold*, sensors that have been closely grouped together. This is shown in section 5.3 where the AIBO moves between two environments with different visual statistics.

4.3 Reconstruction of Visual Sensory Organization

After looking at sensoritopic maps of all the sensors of the AIBO we here focus on the visual sensors.

4.3.1 Experimental Setup

In the experiments presented below the AIBO was placed in a sitting position on a desk in our robotics laboratory – see figure 4.1(a). The robot only moved its head with uniform speed using the pan and tilt motors in eight directions; up, down, left, right, and four diagonal directions. We also collected visual data while the AIBO was walking around in the office with similar results to the results presented in this chapter. Five sequences of 6000 frames each of visual data were collected from the camera at a resolution of 88 by 72 pixels with eight bits for each channel (red, green, blue) at an average rate of 20 frames per second while the robot was moving. The five sequences of visual data were for some experiments described below divided in to 30 sequences of 1000 time steps of data – see details in the individual sections below. The collected images were downsampled to 10 by 10 pixels using averaging.

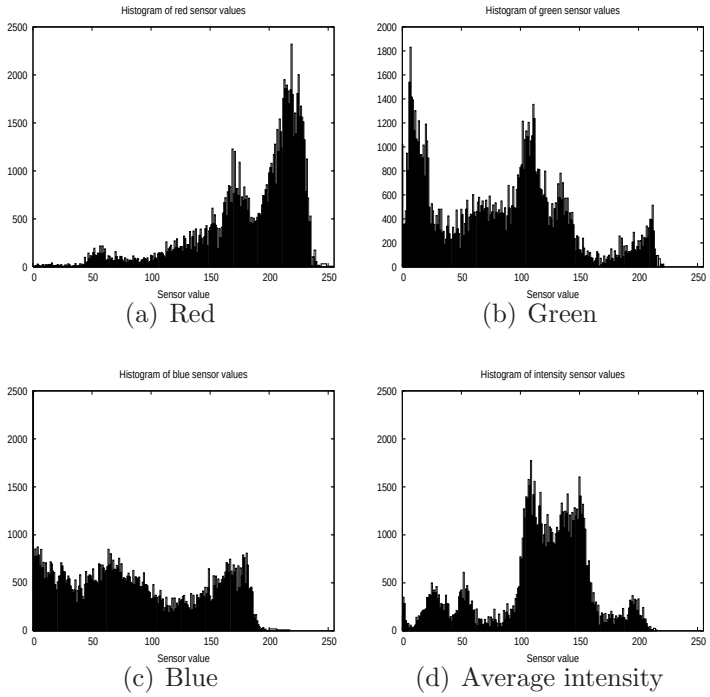

(a) Red (b) Green

(c) Blue (d) Average intensity

Figure 4.4: Histograms of vision sensor intensities where the vertical axis shows number of occurences of the value in the data.

Figure 4.4 shows the histograms for a typical sequence of 1000 time steps of the downsampled images for the red, green, blue, and intensity data. As shown the characteristics of the different sensor modalities are quite different. While the red values were often high, with most sensor readings higher than 150, the green sensor were mostly below 100. The blue sensors were more uniformly distributed between 0 and 180. Since the intensity is defined as the average, most of the intensity readings end up being located between the peaks of the red and green sensors.

It is also possible to look at the relationships between sensors of dif-

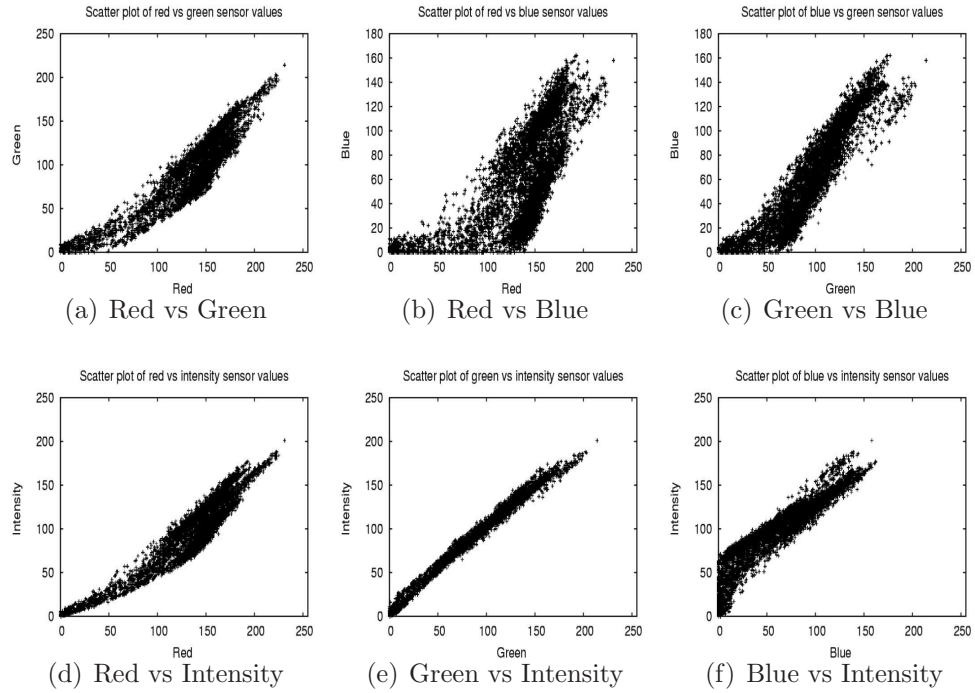

(a) Red vs Green (b) Red vs Blue (c) Green vs Blue

(d) Red vs Intensity (e) Green vs Intensity (f) Blue vs Intensity

Figure 4.5: Scatter plots of sensor values from sensors of different modalities in the same position.

ferent modalities. Figure 4.5 shows scatter plots with the state space of the sensor values from pairs of sensors of different modalities from the same position, where, for instance, one point are the values read from sensors $B5$ and $R5$ at time step t. While all pairs of sensor modalities were more or less correlated, as indicated by the linear relationships in the scatter plots, there are a few things to notice. How much a sensor modality is correlated with another is determined by the spread of the values from the straight line of linear regression. Looking at the scatter plot for the red and blue sensors we see that the spread is much greater

than for, e.g., the red and green sensors. This means that the correlation between the red and blue sensors is lower than for the red and green sensors. In other words, knowing the value of a red sensor means, on average, that we will know less about the corresponding blue sensor than the corresponding green sensor. In section 4.3.3 we will examine how informational relations of sensors of different modalities (red, green, blue) from the same pixel and nearby pixels can be recovered by extensions of our methods.

4.3.2 Visual Fields of Different Shapes

In this section we consider how the sensory reconstruction method can reconstruct sensor fields arranged in different shapes, such as a triangular and circular shapes. In the previous sections it was implicitly assumed that the best representation of the sensor field was in two dimensions. To verify the method for finding the appropriate number of dimensions of section 3.5, we calculated the best dimension to represent sensor fields of various shapes of known dimensions. The seven different shapes used were a one-dimensional top row of 10 sensors (sensor 0 to 9 in figure 4.1(b)), and the six shapes of figure 4.7(a) to 4.7(c) and figure 4.8(a) to 4.8(c). The expected result would be for reconstruction for the row of sensors to be one-dimensional while for all the other sensor fields it should be two-dimensional. The presented sensoritopic maps are examples of typical maps, and all of the 30 sequences of data produced very similar results – see table 4.4 below.

Figure 4.6 shows the normalized eigenvalues from metric-scaling us-

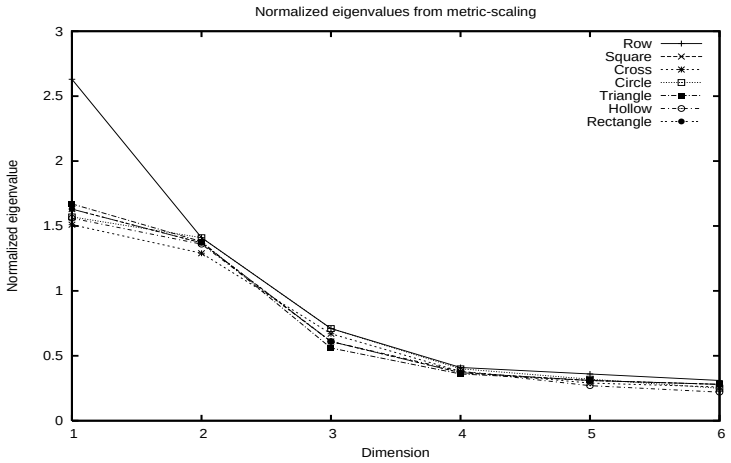

Figure 4.6: Figure shows the eigenvalues, which correspond to the variance, per dimension from metric-scaling. The eigenvalues are normalized by dividing by the number of sensors for each layout.

ing the method of section 3.5. The figure shows the eigenvalues for a typical map generated after 1000 time steps for the red sensors, but all modalities and 30 sequences of data resulted in similar results – see also table 4.4 below. Remember that the appropriate dimension to represent a sensoritopic map is found by maximizing $\lambda_p - \lambda_{p+1}$, where λ_p is the eigenvalue of dimension p. This corresponds to finding the dimension in figure 4.6 to the left of the steepest slope. First consider how the eigenvalues for the sensor field of one row change over the dimensions. The steepest slope is between dimension one and two, correctly indicating that this is a one-dimensional sensor field. For all of the other six shapes the situation is different, with the steepest slope between dimension two and three, indicating that the most appropriate dimension is two. This is correct since their original sensor layouts all are two-dimensional. Fig-

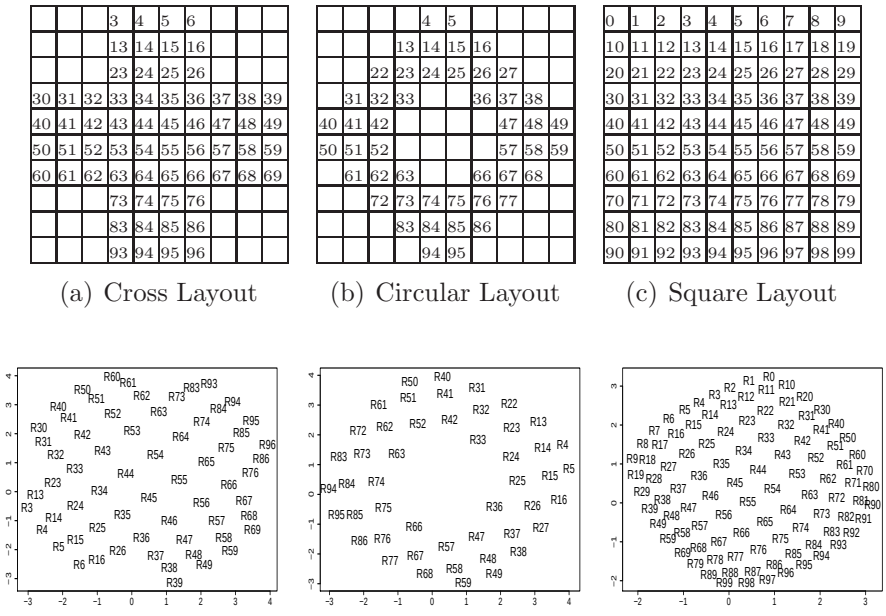

(a) Cross Layout (b) Circular Layout (c) Square Layout

(d) Cross Visual Field (e) Circular Visual Field (f) Square Visual Field

Figure 4.7: Layout of the sensors, figure 4.7(a) to 4.7(c), and the reconstructured visual fields represented as sensoritopic maps, figure 4.7(d) to 4.7(f).

ure 4.6 shows the average eigenvalues for a particular sequence, but all results for the 30 sequences always yielded the same dimensionality for all the seven different sensor fields.

Now consider the examples of the reconstructed visual fields in figure 4.7(d) to 4.7(f) and figure 4.8(d) to 4.8(f). Clearly, in each case they bear a close resemblance to the layouts of the real sensors from which the sensory data was collected, albeit more so for some layouts than others. For each of the six layouts in figures 4.7 and 4.8, the average reconstruction distance (equation 3.8) was computed between the real layout and 100 reconstructed sensoritopic maps for all 30 sequences and red, green and

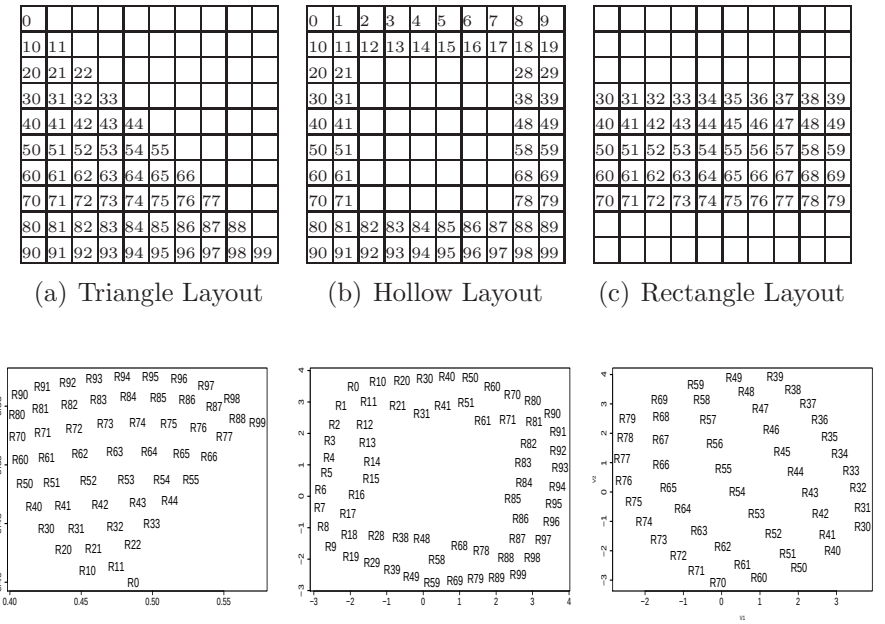

(a) Triangle Layout (b) Hollow Layout (c) Rectangle Layout

(d) Triangle Visual Field (e) Hollow Visual Field (f) Rectangle Visual Field

Figure 4.8: Layout of the sensors, figure 4.8(a) to 4.8(c), and the reconstructured visual fields represented as sensoritopic maps, figure 4.8(d) to 4.8(f).

Cross	Circular	Square	Triangle	Hollow	Rectangle
0.075	0.057	0.051	0.091	0.11	0.18
(0.016)	(0.013)	(0.012)	(0.014)	(0.011)	(0.021)

Table 4.4: Average reconstruction distances for the different visual sensor layouts of figure 4.7 and 4.8 with standard deviation in parentheses.

blue sensors, resulting in a total of $100 \times 30 \times 3 = 9000$ sensoritopic maps for each sensor layout. Table 4.4 shows the resulting averaged reconstruction distances with the standard deviation in parentheses. The results of table 4.4 quantitively confirm the intuitive resemblance of the recon-

structed visual fields of figure 4.7(d) to 4.7(f) and figure 4.8(d) to 4.8(f) to their respective real layouts in figure 4.7(a) to 4.7(c), and figure 4.8(a) to 4.8(c). The square, circle, triangle, and cross reconstructed layouts are all below an average reconstruction distance of 0.10, indicating a close similarity to the real sensor layouts. For the other three layouts, most notably the rectangle layout, the reconstruction distances were slightly higher, although still much lower than the a random map, which would have an average reconstruction distance of 0.52.

One question to ponder is why some arrangements of sensors are easier to reconstruct than others. This is an interesting question but has not been considered in detail by the author.

4.3.3 Visual Fields of Different Modalities

Now imagine a visual field consisting of sensors of different modalities such as the two layouts in figure 4.9, where some sensors measure the red channel, others green, and some the blue channel of a pixel. In the ordered layout of 4.9(a), the sensor layout has 33 red sensors, 33 green sensors, and 34 blue sensors, ordered from left to right, top to bottom. The random layout of figure 4.9(b) was created by selecting for each position in the layout a sensor in the set $\{R, G, B\}$, with an equal probability of 1/3. Again all 30 sequences of data were used and figure 4.10 shows two typical sensoritopic maps.

The first thing to notice about the top two reconstructed maps of figure 4.10 is that the spatial layout of the maps closely resemble that of the real layouts, even though the sensors are of different modalities. Con-

R	R	R	R	R	R	R	R	R	R
R	R	R	R	R	R	R	R	R	R
R	R	R	R	R	R	R	R	R	R
R	R	R	G	G	G	G	G	G	G
G	G	G	G	G	G	G	G	G	G
G	G	G	G	G	G	G	G	G	G
G	G	G	G	G	G	B	B	B	B
B	B	B	B	B	B	B	B	B	B
B	B	B	B	B	B	B	B	B	B
B	B	B	B	B	B	B	B	B	B

(a) Ordered layout

R	B	R	B	G	G	B	G	B	R
G	R	G	B	R	G	B	G	R	G
G	G	G	B	B	R	R	R	R	G
B	R	G	R	R	G	G	R	B	G
G	R	B	R	B	G	G	G	B	R
B	G	B	R	G	R	G	B	R	R
G	R	R	G	G	G	G	B	R	R
G	G	R	B	R	G	B	B	B	R
B	G	G	G	B	G	B	R	G	B
B	B	R	R	B	R	B	B	G	G

(b) Random layout

Figure 4.9: Layout of visual field with different modalities.

sidering the different distributions of the sensors shown in figure 4.4, one realizes that this would not be the case if the 1-norm distance of Pierce and Kuipers (1997) were used – see the lower two sensoritopic maps of figure 4.10 and chapter 7 for a comparison between different distance metrics and measures applied to the sensory reconstruction method.

The reason that using the 1-norm distance in this case would not result in reconstructed maps is that it only captures linear relationships between sensors.

As in previous experiments the average reconstruction distance was computed for the two layouts of figure 4.9 averaged over 100 created maps for each of the 30 sequences of data. The average reconstruction distance for the ordered map of figure 4.9(a) was 0.059 with a standard deviation of 0.011. For the random layout map of figure 4.9(b) the average reconstruction distance was 0.060 and the standard deviation 0.010.

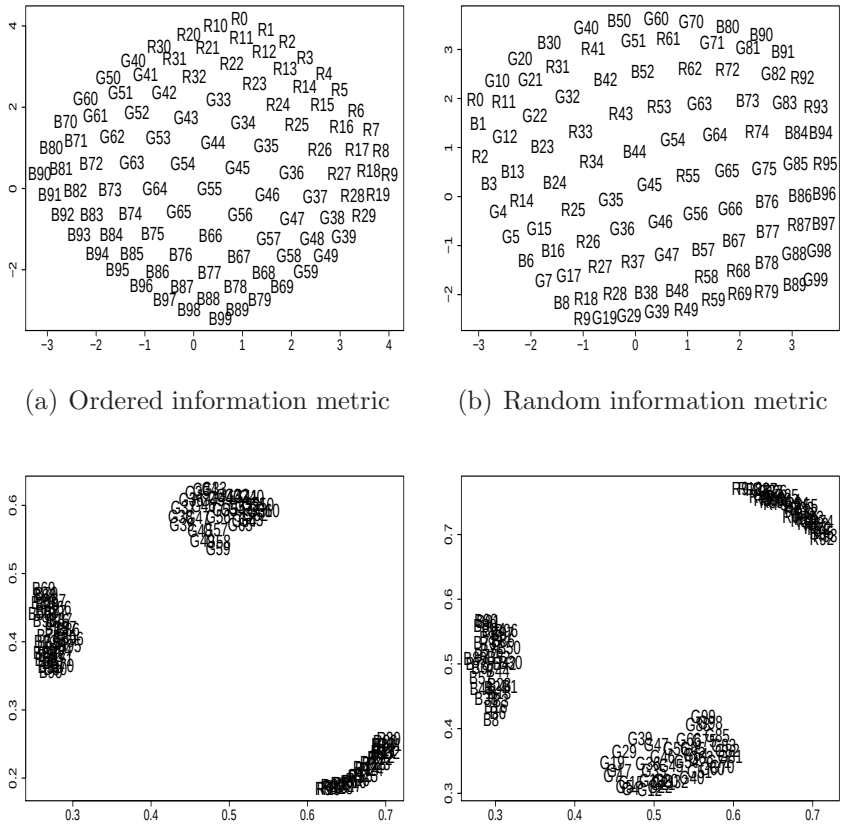

(a) Ordered information metric

(b) Random information metric

(c) Ordered 1-norm

(d) Random 1-norm

Figure 4.10: Reconstruction of sensor fields of different visual modalities using the information metric and 1-norm distance. In the lower two maps are all the sensors of each modality, red, green, and blue, clustered.

4.3.4 Reconstruction of Scrambled Visual Fields

This section describes an application of the sensory reconstruction method where "scrambled" sensor fields can be "de-scrambled" by exploiting the statistical structure of the input. The application and method is easiest

explained using an example.

Imagine that a camera is connected to a screen, where one pixel in the camera is connected to the corresponding pixel on the screen. Thus, the screen will display the exact image recorded by the camera, with each pixel of the camera displayed in the corresponding position on the screen. Now, imagine what would happen if an evil individual were to randomly reconnect the wires to the screen. It would, if the camera was in a non-uniform visual environment, seem like the screen would display random pixels without any structure, similar to the "snow" seen on a TV tuned to a dead channel[3]. Figure 4.11 shows an example where 4.11(a) is the original image from a time-series of images, figure 4.11(b) a random map equivalent of re-wiring the camera to the screen at random, and figure 4.11(c) the resulting (perceived) random image. This information-preserving random mapping can in fact be discovered and "undone" using the sensory reconstruction method and time-series of visual data similar to the previous sections.

The first step is to compute the informational relationships between the sensors using the sensory reconstruction method which results in a sensoritopic map of the sensors – see figure 4.11(d). As seen in previous sections, spatial sensoritopic maps of visual sensors do reflect the sensors' relative positions although the coordinates of the sensor placements are continuous. To map these coordinates to a two-dimensional discrete grid the angle of the rectangle formed by the sensors can be found by rotating

[3] "TV tuned to a dead channel" inspired by the first sentence in William Gibson's *Neuromancer* (Gibson, 1986).

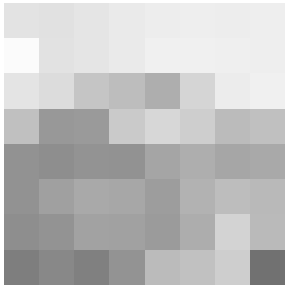

(a) Original image

53	7	63	38	18	56	2	44
21	32	5	43	8	4	59	49
33	35	3	15	23	47	26	64
27	1	54	48	42	17	34	11
45	16	20	30	40	25	10	39
46	13	55	62	58	24	51	61
29	41	50	9	31	6	36	52
60	22	19	37	57	14	28	12

(b) Random scrambling map

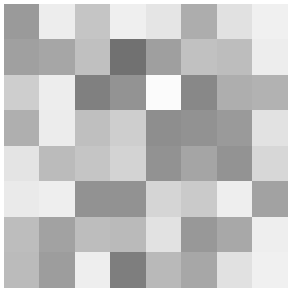

(c) Randomized image

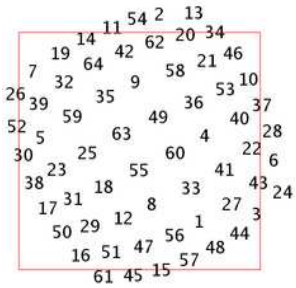

(d) Sensoritopic map

13	34	46	10	37	28	6	24
2	20	21	53	40	22	48	3
54	62	58	36	4	41	27	44
11	42	9	49	60	33	1	48
14	64	35	63	55	8	56	57
19	32	59	25	18	12	47	15
7	39	5	23	31	29	51	45
26	52	30	38	17	50	16	61

(e) Reconstructed map

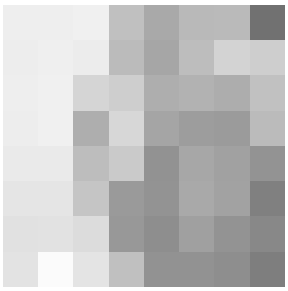

(f) Reconstructed image

Figure 4.11: Position 1 is in upper left corner and 64 in lower right. The random map scrambles the input by moving the sensor in position p to the position specified by the value in position p. For example, sensor 1 is moved to position 53. The reconstructed map is applied by moving the sensor specified by the value in position p to position p. For example, sensor 26 from the scrambled image is moved to the lower left corner of the reconstructed image.

a rectangle and noting the angle at which most sensors are inside the rectangle. Then each sensor is assigned a discrete position by dividing the rectangle into 64 squares and then assigning a sensor to each square. This map shown in figure 4.11(e) can now be used to recover the original image as shown in figure 4.11(f).

It is also possible to recreate the visual field without discretizing it. Then the value of each sensor is simply placed in its position in the

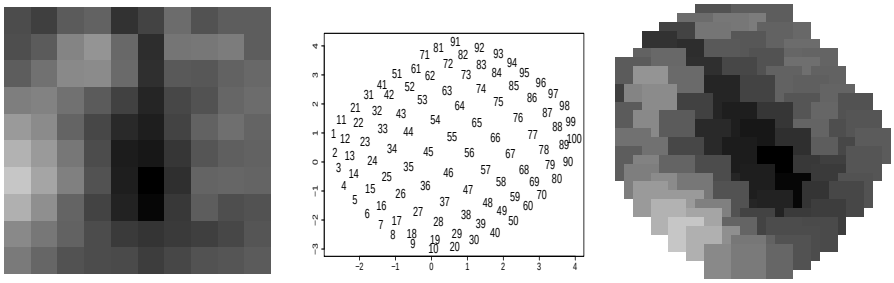

(a) Original image (b) Sensoritopic map (c) Reconstructed image

Figure 4.12: Reconstructed visual field.

sensoritopic map. This means that the resulting image in most cases will have a non-rectangular shape. Figure 4.12 shows an example of this method. Here figure 4.12(a) is an example of the original image, figure 4.12(b) the reconstructed sensoritopic map after 1000 time steps of data, and figure 4.12(c) the reconstructed image from the same time step as the example image of figure 4.12(a). The descrambled image was reconstructed by first creating a 28 by 28 pixel image, where the value 28 was selected after some trial and error using different images sizes. The value of each pixel is placed in the position indicated by the position in the sensoritopic map as a four by four square with the intensity value of that particular sensor. Again the size four by four was found after some experimentation.

It should be noted that the recreated visual fields are based on the informational relations found in the reconstructed sensoritopic maps. This means that the recreated images, just like the sensoritopic maps, reflect the spatial relations rather than the real physical organization of the visual field, and that the recreated images might be rotated and/or mir-

rored compared to the real physical organization of the sensors. This also means that how well the images are de-scrambled is determined by how well the informational relations reflect the real physical layout of the sensors. This can, as shown in section 4.3.2, be computed by the average reconstruction distance, and the results there showed how close the reconstructed sensor fields were to the real spatial organization of the sensors.

4.4 Statistical Structure of Visual Data

In the previous sections we have seen how the sensory reconstruction method manages to reconstruct visual fields consisting both of sensors of the same modality as well as sensors of different visual modalities. How does this actually work? The basic answer is that it exploits the statistics of the environment – in particular, power law correlations in time and space as will be illustrated here. Consider the graph showing the normalized information distance between all pairs of sensors of a 10 by 10 visual field in figure 4.13, taken from the square visual field of section 4.3.2 from a typical run after 1000 time steps. The distance between a sensor and itself is zero and the 10 by 10 squares visible in the matrix suggest that the visual field is 10 by 10 sensory field. The key here is that the closer two sensors are in the physical visual field, the smaller the informational distance is between the two sensors.

Another way to look at how sensors are informationally related to each other is to plot the informational distance as a function of the phys-

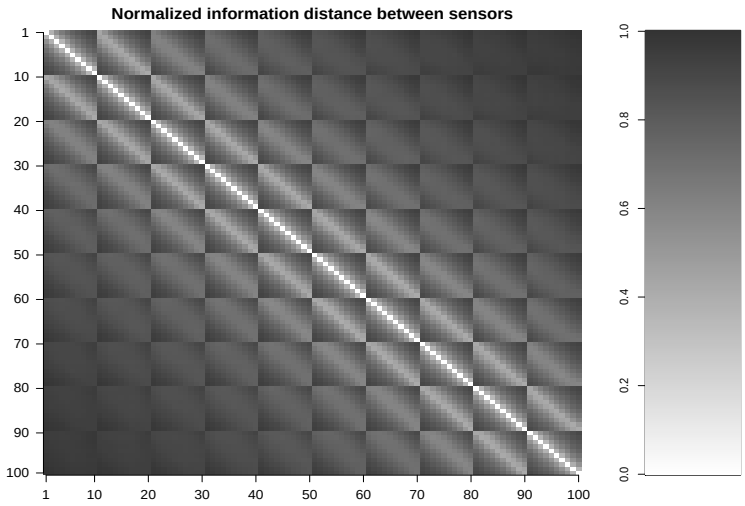

Figure 4.13: Normalized information distances between all pairs of sensors for the square visual field of 4.7(c) with 0 and 1 visualized as white and black, respectively. The distance between a sensor and itself is always zero, hence the white diagonal line. The further away two sensors are the less they are correlated and the greater is the information distance.

ical distance between the sensors. Let $d_i(S_x, S_{x+d})$ be the informational measure, e.g., information metric or mutual information, between the sensor S_x and a sensor S_{x+d}, which is at physical distance d in pixels between the sensors.

Figure 4.14 shows the informational distance in bits as a function of the pixel distance from the sensor data used in this chapter, for the red channel and intensity in each pixel. The presented results come from the raw 88 by 72 images but similar results were obtained for the averaged 10 by 10 images – see the discussion below about scale invariance. The graph was created averaging over all sensors at vertical distance d, but

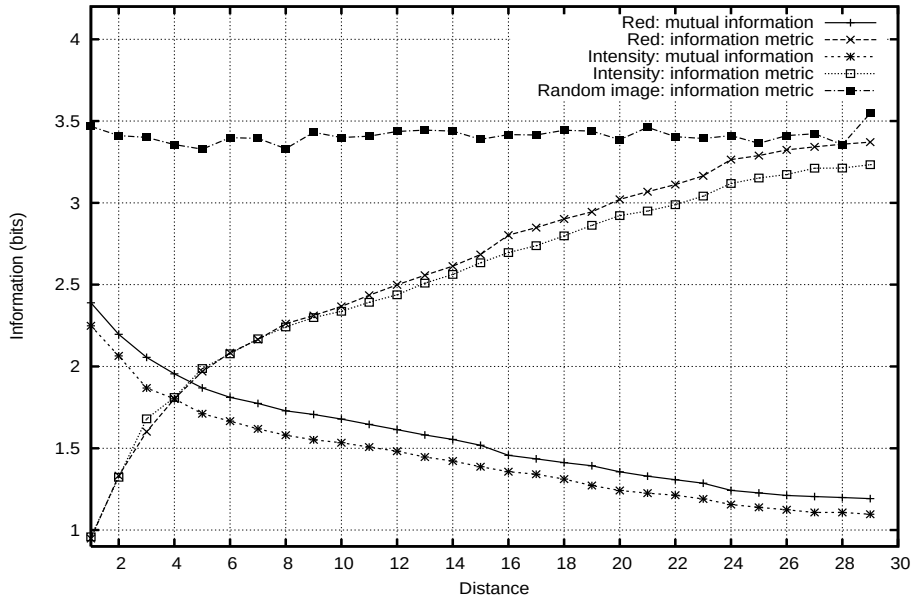

Figure 4.14: Information metric and mutual information versus distance between pixels. The mutual information for the random images has been omitted for clarity as it is very close to zero. The values for information metric of the random images were divided by two (roughly 3.5 instead of 7), to make the graph clearer.

similar results, which are not shown, were obtained by looking at horizontal distances and also distances from several directions combined. For comparison, images were generated at random, with each channel of each pixel selected at random from the set $\{0, 1, \ldots, 255\}$. For each distance the mutual information and information metric were computed.

As expected the information metric for the random images is more or less constant for the different distances, while it increases for the red and intensity sensors at a similar rate. The mutual information between sensors decreases when the distance increases since the correlation be-

tween two sensors further away is smaller. Looking more closely at the graph of figure 4.14, it seems that for the both the mutual information and information metric the relationship between the physical distance and informational distance is a power law. This would mean that

$$d_i(S_x, S_{x+d}) \approx ad^k \tag{4.1}$$

where a (the constant of proportionality) and k (the exponent of the power law) are constants. If the relationships for the information metric and mutual information in figure 4.14 are power laws, they would appear as a straight line if plotted in a log-log graph, since

$$\log d_i(S_x, S_{x+d}) = k \log d + \log a \tag{4.2}$$

has the same form as the equation for a straight line.

Figure 4.15 shows the same data as figure 4.14 plotted on a log-log scale with fitted straight lines[4]. The fitted straight lines and the asymptotic standard errors shows that the points are not exactly straight lines on a log-log scale, but they are still quite close.

This result is similar to what has been found by neuroscientists that have studied the statistics of natural environments – see section 2.2. For instance, Ruderman (1994) and Simoncelli and Olshausen (2001) found that the mutual information between pixels of different distances follows a power law for natural images. There has been considerable debate and speculation about the environmental causes of this power law behaviour

[4]The fitting was done using the least-square fitting method of the program *gnuplot*.

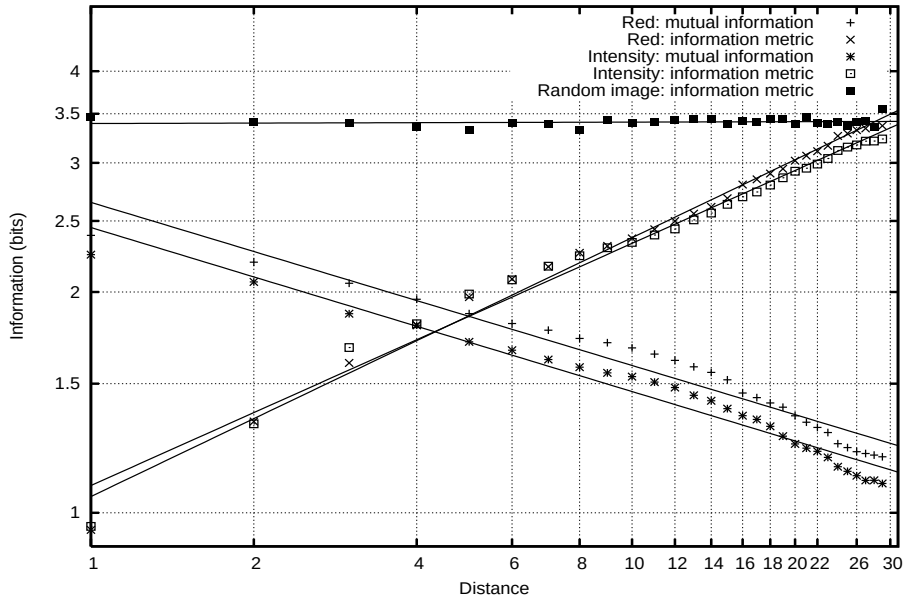

Figure 4.15: Log-log plot of information distances versus spatial distances. $k = -0.222$ ($ase = 4.47\%$) for the red mutual information, $k = -0.223$ ($ase = 3.91\%$) for the intensity mutual information, $k = 0.351$($ase = 1.93\%$) for red information metric, and $k = 0.330$ ($ase = 1.97\%$) for the intensity information metric, where ase is the asymptotic standard error of the fitting.

of natural images – see for example (Simoncelli and Olshausen, 2001; Simoncelli, 2003). Perhaps the most commonly held belief is that the power law is due to the scale invariance of the natural visual world, but it might also be the case that the presence of edges in natural images is important (Simoncelli and Olshausen, 2001). Scale invariance of the images used in our experiment is also suggested by our results – we first tried plotting the same graphs as above using the averaged 10 by 10 as well as 30 by 30 images with very similar results to the results presented

here.

As mentioned in section 2.2.1 time-series flows for natural images also often have *temporal coherence*. This means that the value of a particular part of the image in one time step is correlated with the value of the same part of the image at a later time step. To find how this correlation is related to time, we computed the information metric distance and mutual information between a pixel and the same pixel time-shifted using the same data from the AIBO as used above. Let S_x be a visual sensor (pixel) and S_{x+t} be the same sensor with the sensor values shifted t time steps, where in the experiments performed there were 20 time steps per second, and a total of 1.5 seconds. Then the mutual information over this time-shift is $I(S_x; S_{x+t})$, and the information metric $d_{im}(S_x, S_{x+t})$, where $1 \leq t < 30$.

Figure 4.16 shows the mutual information and information metric for the red and intensity channel. Here the mutual information is smaller and the information metric higher than the graph of figure 4.14, which showed the informational relations as a function of spatial distance, but with similar shapes of the curves. This indicates that also the temporal coherence in visual sensors is a power law.

To see whether the temporal coherence scales as a power law we plotted the data using a log-log scale, which is shown in figure 4.17. Similarly to the spatial coherence above, the temporal coherence of figure 4.17 does scale more or less as a power law, with asymptotic standard errors of the line fitting similar to the ones for the spatial coherence. One difference, though, between the temporal and spatial coherence, is

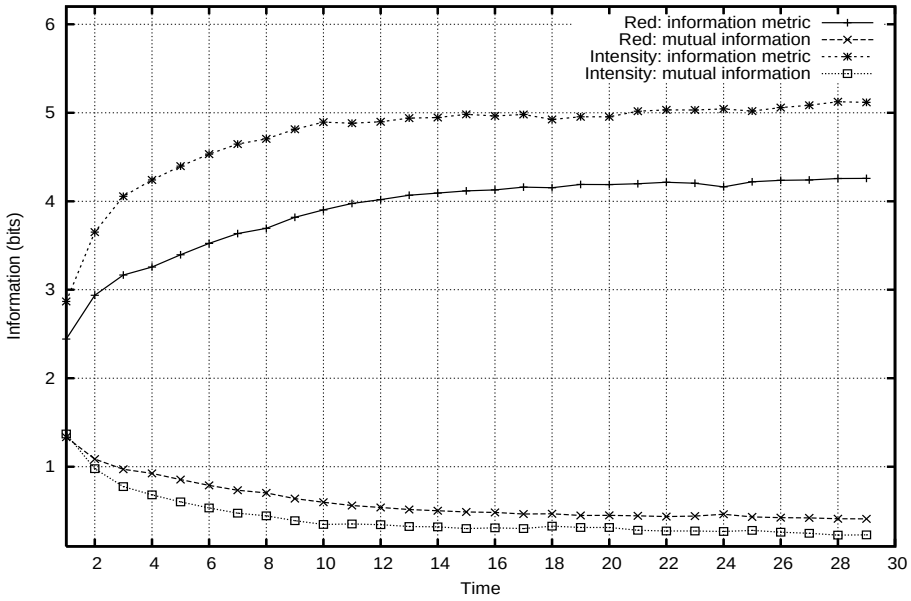

Figure 4.16: Information metric and mutual information versus time for one pixel.

the slope, k, of the fitted curves. For the temporal coherence the slopes are steeper, both for the information metric and the mutual information, compared to the spatial coherence.

The same data was also used to examine the scaling of the 1-norm distance. Figure 4.18 shows the 1-norm distance versus both the temporal as well as spatial distance. Just as for the information metric the 1-norm distance grows with the spatial and temporal distance.

Figure 4.19 shows the same data plotted on a log-log graph. Similarly to the information metric graphs above, the 1-norm distance scales more or less as a straight line in the temporal as well as spatial domain.

What kind of statistical structure of the sensor data is necessary for

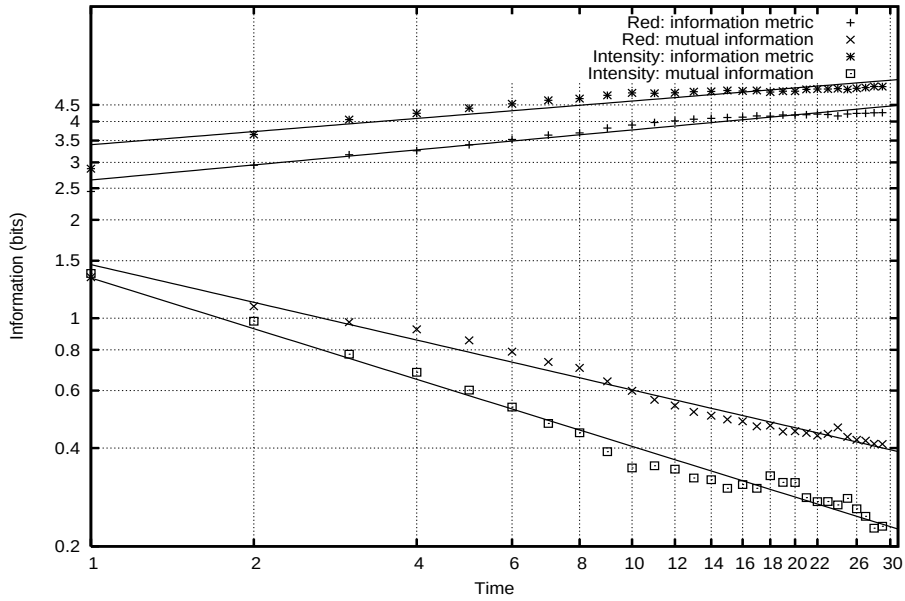

Figure 4.17: Log-log plot of information distances versus time for one pixel. $k = -0.389$ ($ase = 2.80\%$) for the red mutual information, $k = -0.510$ ($ase = 2.87\%$) for the intensity mutual information, $k = 0.151$($ase = 1.97\%$) for red information metric, and $k = 0.133$ ($ase = 2.24\%$) for the intensity information metric, where ase is the asymptotic standard error of the fitting.

reconstruction to be possible? Starting with the obvious, neither random data nor completely static data is possible, since the distances between all sensors will be the same. In general, the statistical structure of the environment and the actions of the robot should have an informationally piecewise smooth effect on the sensory data, where the smoothness can be either linear, or exponential as the results above indicated, where relative information distances between sensors should correspond to their physical organization.

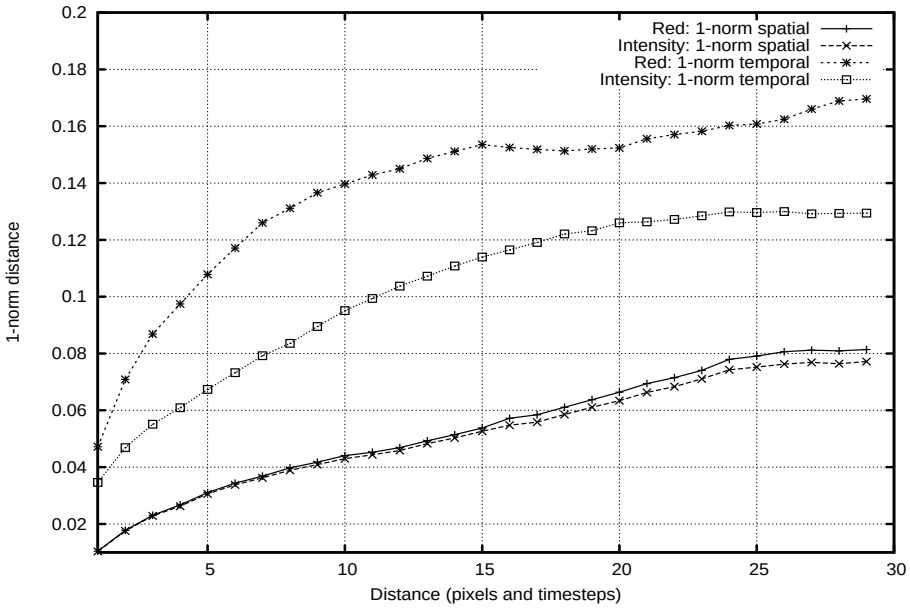

Figure 4.18: 1-norm versus spatial and temporal distance.

4.5 Conclusion

In this chapter we studied the reconstruction of sensors using the sensory reconstruction method, where the sensor data came from different experiments using the SONY AIBO robot. First we looked at all the sensor data from the robot walking around in an office environment. The resulting sensoritopic maps showed that some of the symmetry and organization of the body of the robot was found in the maps. The distance between sensors in the maps reflects their informational distance where sensors that have a smaller informational distance are close in the map. This generally means that the closer two sensors are in the map, the less extra information is needed to predict one sensor knowing the current

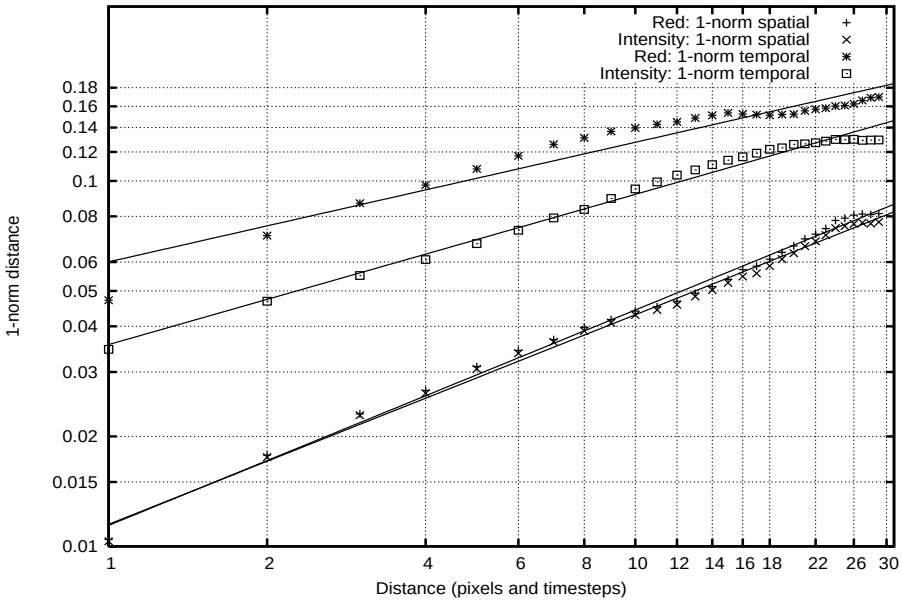

Figure 4.19: Log-log plot of 1-norm versus spatial and temporal distance. $k = 0.581$ ($ase = 1.45\%$) for the red spatial, $k = 0.573$ ($ase = 1.48\%$) for the intensity spatial, $k = 0.0.376$($ase = 5.44\%$) for red temporal, and $k = 0.411$ ($ase = 2.25\%$) for the intensity normal, where ase is the asymptotic standard error of the fitting.

state of the other. This was exemplified by the paw sensors where one paw sensor can be used to predict the others.

The reconstruction of only visual sensors was studied in more detail where it was shown how sensors arranged in different spatial layouts, as well as sensors of different visual modalities, can be reconstructed and their physical relations recovered. The reconstruction of visual sensors of different modalities is possible because the information metric is based on informationally smooth effects on movements, while the 1-norm distance used by Pierce and Kuipers (1997) only works when the absolute values

of the sensors are piecewise smooth and linearly correlated – see also chapter 7. We then analyzed the statistics of the visual data collected from the AIBO and found that the relations between the informational distances and distances in time and space were a power law – something that has also been found by neuroscientists analyzing the statistics of natural images in nature.

In the experiments presented in this chapter the robot was always moving. In general, the sensory reconstruction needs sensor data that change somehow over time – in sensor data with no changes the information distance between two sensors will always be zero, and with random changes the distances between all pairs of sensors will be more or less the same. For reconstruction of sensory organization to take place, there need to be changes of certain characteristics in the sensors' values, either from self-induced movement or movements of objects in the world.

In the presented results of the visual sensors in this chapter we measured reconstruction in terms of relative distances, with no reference to a particular orientation of the sensory field. An example of this is the reconstructed square visual field of figure 4.7(f). Here the relative organization of the sensors is very similar to the real layout of figure 4.7(c), but the reconstructed visual field is a mirrored version of the real layout with sensor 0 to the right and also angled at 45% compared to the real layout. This is a natural consequence of using raw and uninterpreted sensor data as experienced by the robot itself – without any analysis invoking external knowledge such as scene analysis or knowledge about the movements of the robot, it is impossible to find the "real" physical

organization of the sensors, and only the relative spatial organization from the perspective of the agent's own "experience" of its Umwelt can be found.

Finally it should be emphasized that the reconstruction of sensor fields is not restricted to just sensors of visual modalities, like the sensors used in this chapter. It can rather be applied to sensors of any modalities such as tactile sensors in skin or infrared sensors where the statistical structure of the measured environment has an informationally piecewise smooth effect on the sensory data.

Chapter 5

Development of Sensoritopic Maps

In the previous chapter we showed how the sensory reconstruction method finds the informational relationships between sensors and can reconstruct, for example, visual sensor fields. In this chapter we look at how sensoritopic maps develop over time as the agent acts in the world. The previous chapter also discussed the statistics of natural visual environments and how these statistics are reflected in the informational distances between pairs of sensors. Here we look at how sensoritopic maps develop in less normal environments, in our case an environment with only vertical contours, which means that the statistics of the environment are different. This is something that has also been studied in neuroscience – see for example section 2.2.2 and Wiesel (1982) – where it has been found how the visual environment of kittens affects the development of their visual system. In this chapter we see what effect an environment

with oriented contours has on the informational relationships between the visual sensors.

We start by looking the development of sensoritopic maps for all AIBO sensors, before looking in more detail at the development of the maps of only the visual sensors. Finally, we show results of the visual field of the SONY AIBO robot developing in a world with only vertical contours.

5.1 Development of AIBO Sensoritopic Maps

We first consider how the sensoritopic maps of all the SONY AIBO sensors and actuators, as described in section 4.2, develop as the robot interacts in the world. Here we use the same data as in section 4.2, and the presented maps show examples of development, but all the collected time-series of data showed very similar results.

Figure 5.1 shows the development of a typical run of the robot acting in the world. Starting with only five time steps of sensor and actuator data, there is no real discernible structure, apart from most of the visual sensors still being clustered together in a small number of groups. As the robot interacts for longer in the world, more and more structure emerges. After 50 time steps all the visual sensors, sensors 1 to 100, have separated from the other sensors. There is also more order among the visual sensors, with, for instance, sensors $10, 20, \ldots, 100$ (apart from 30) clustered to the right of the visual sensors, and sensors $1, 11, \ldots, 91$ to the left.

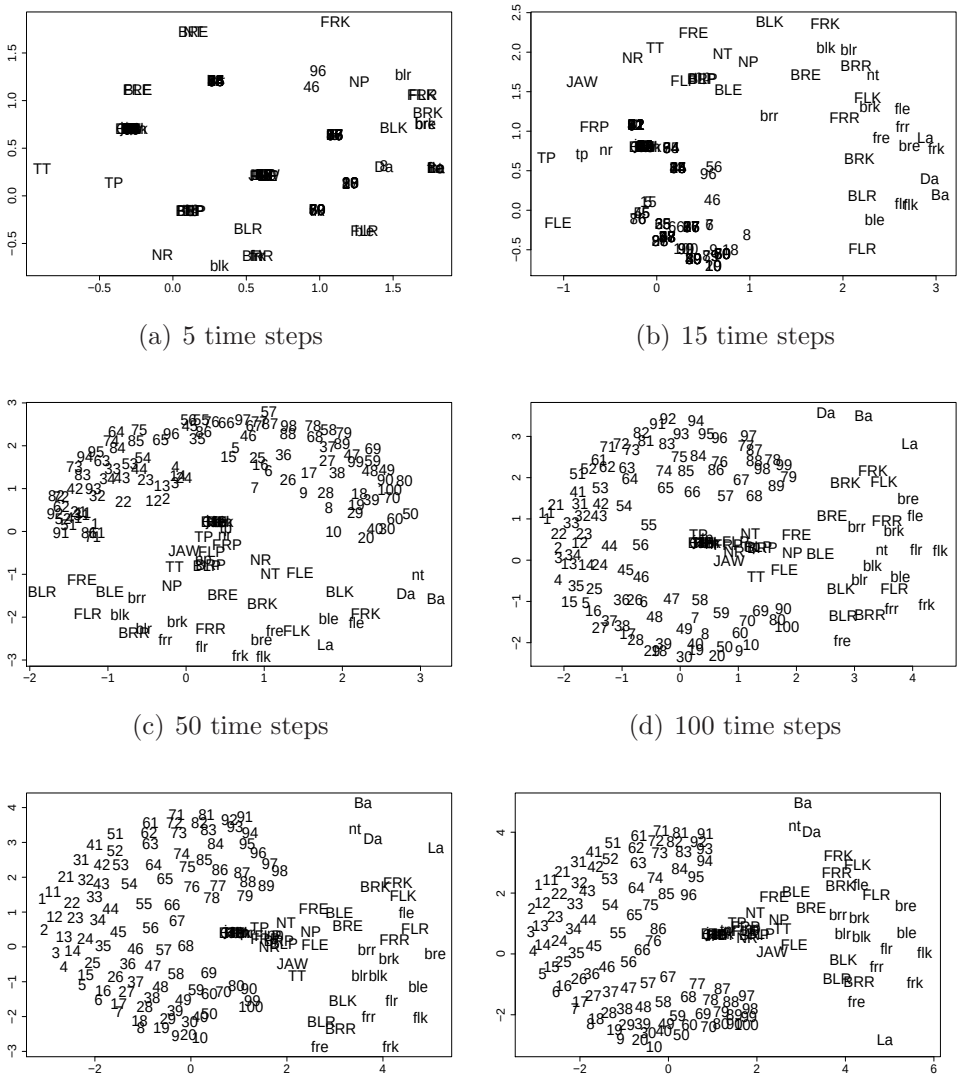

(a) 5 time steps

(b) 15 time steps

(c) 50 time steps

(d) 100 time steps

(e) 500 time steps

(f) 1000 time steps

Figure 5.1: Development of AIBO sensoritopic maps of over time for a typical run.

In the centre of the sensoritopic map we find the sensors that always, or nearly always, had the same values in this particular run. These

include the temperature, battery level, tail and jaw duties. Since the entropy of all these sensors is zero or very close to zero, the information distances between these pairs of sensors are zero or close to zero.

5.2 Development of Visual Fields

Here we study how only the visual fields of chapter 4 developed over time as the robot interacted in the environment over time, starting from no structure in its sensors. The 30 sequences of 1000 time steps of data collected as described in the previous section were used. For each of the 30 sequences, 100 sensoritopic maps were created with random starting positions for every 10 time steps to calculate the average reconstruction distance presented in figure 5.3.

Figure 5.2 shows the sensoritopic maps developed over time, with maps created after 10 time steps up to 1000 time steps for a typical run.

After only 10 time steps the map seems more or less random, with no discernible structure. With more time, the statistics of the movement and environment was captured by the information metric and the sensoritopic maps more closely reconstruct the real layout of the sensors.

The graph in figure 5.3, which shows how the reconstruction distance of section 3.6 develops over time, confirms this, where the sensoritopic map after ten time steps has an average relative reconstruction distance of 0.45. This is close to a random map, which would have a reconstruction distance of 0.52. While the sensoritopic maps in figure 5.2 are from a particular run, the data collected from all the 30 collected sequences

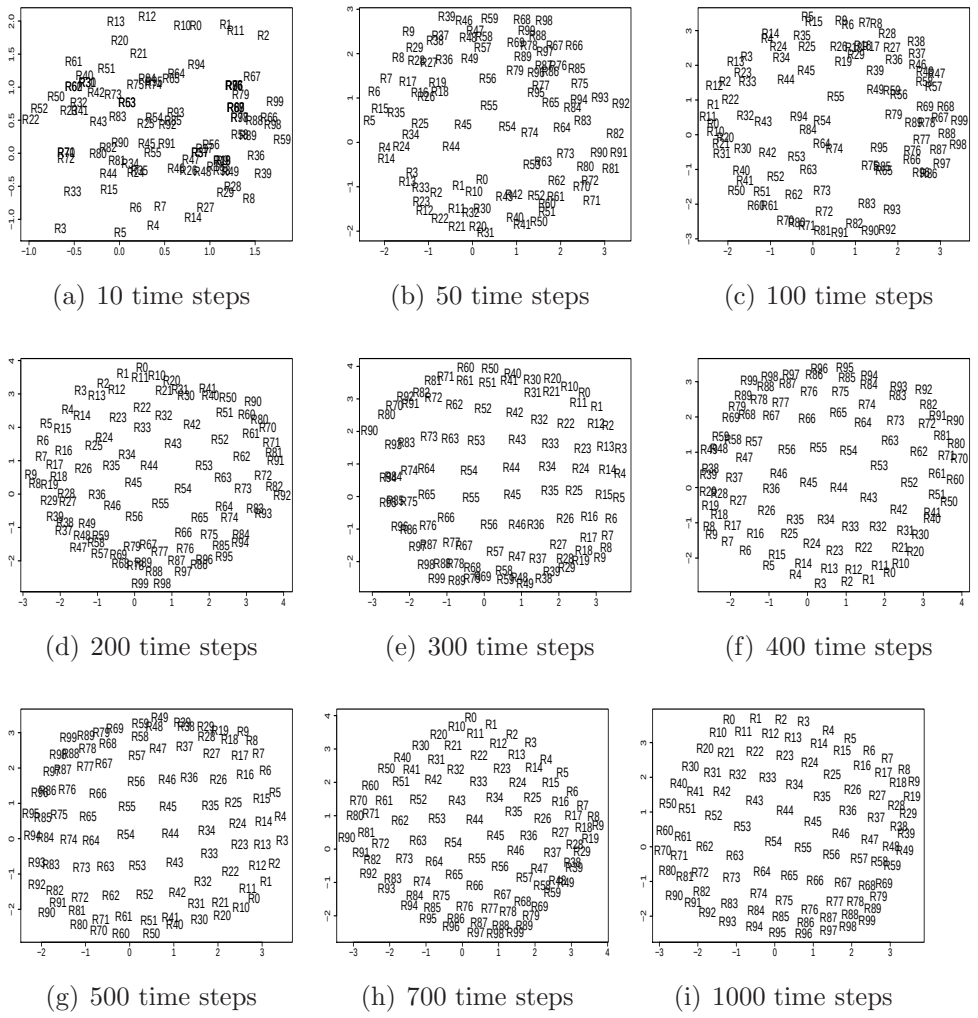

(a) 10 time steps (b) 50 time steps (c) 100 time steps

(d) 200 time steps (e) 300 time steps (f) 400 time steps

(g) 500 time steps (h) 700 time steps (i) 1000 time steps

Figure 5.2: Development of sensoritopic map of visual field over time from 10 to 1000 time steps of data for a typical run.

produced very similar results, with a standard deviation of the values in figure 5.3 close to 0.01. The reason for this deviation was partly due to the statistics of the sensor data, but the initial random placements of the sensors in the sensory reconstruction method accounts for most of the

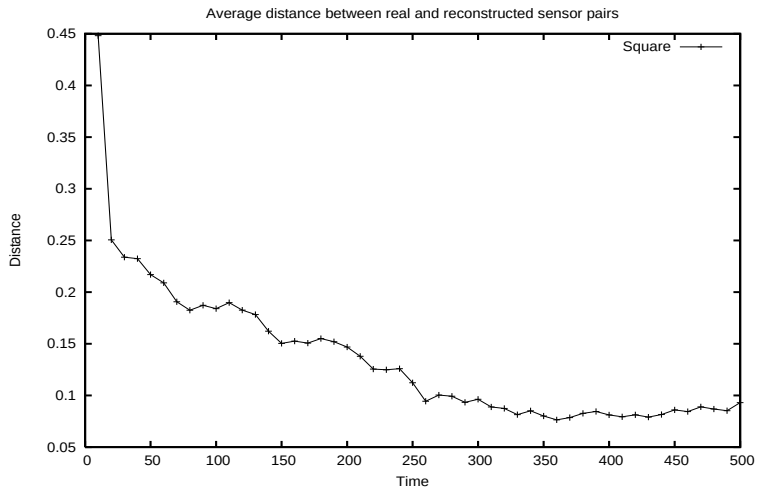

Figure 5.3: Average distance between real and reconstructed sensor pairs.

variance.

5.3 Development in Environments with Oriented Contours

As we discussed in section 2.2.2 the development of the visual field, at least for some animals such as cats, is partly dependent on the stimuli it receives while developing after birth. It has, for instance, been found that kittens reared in environments with only vertical contours have more neurons selective for vertical contours than contours of other angles (Blakemore and Cooper, 1970; Wiesel, 1982; Callaway, 1998). Here we describe a similar experiment performed with a robot acting in an environment with only vertical contours. The experiment shows how the sensoritopic

Figure 5.4: The SONY AIBO robot in its environment with vertical contours.

maps develop a different organization compared to those developed in normal visual environments.

The environment with only vertical contours was created with big white sheets of paper with 2cm wide stripes of black paper glued to the white paper, see figure 5.4. The AIBO was standing in front of the sheets of paper moving its head in such a way to avoid looking outside the white sheets with the black stripes.

Figure 5.5 shows the development of the sensoritopic maps from the first time steps up to 600 time steps. Naturally, the maps from the early time steps show little structure, albeit some structure can be found after 50 time steps. For instance, there is a grouping of 9,19,29,39 in the upper left corner. After more time steps these clusters become more and more noticeable, and after 500 time steps the sensors are grouped in a horse-shoe shape of 10 clusters with 10 sensors in each. This is very different

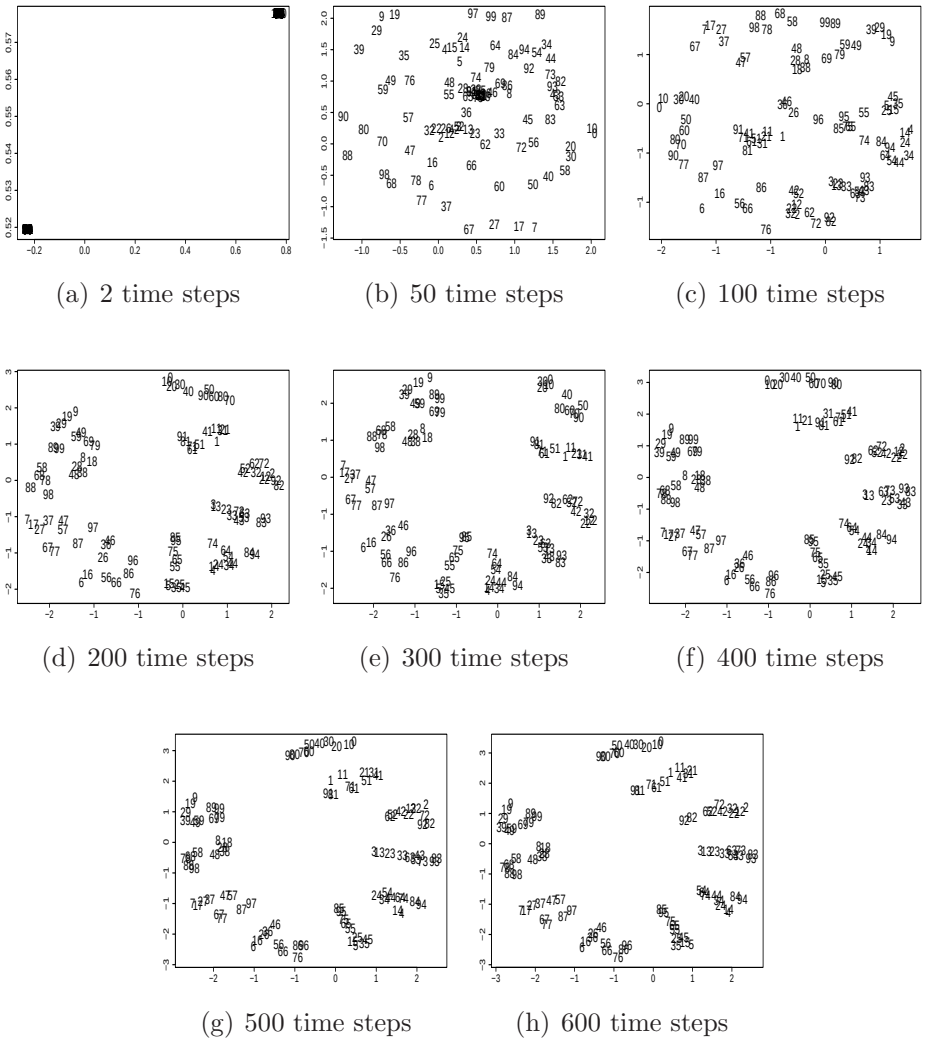

(a) 2 time steps (b) 50 time steps (c) 100 time steps

(d) 200 time steps (e) 300 time steps (f) 400 time steps

(g) 500 time steps (h) 600 time steps

Figure 5.5: Sensoritopic maps of the sensors after 50, 100, 200, 300, 400, 500, and 600 time steps of visual data in the vertical environment.

from the sensoritopic maps formed after the same number of time steps from normal environments. Looking more closely at these clusters we find that each cluster corresponds to one column in the sensor layout

in figure 4.1(b). The upper right end of the horse-shoe contains the sensors $0, 10, 20, \ldots, 90$, which are the sensors of the leftmost column of the layout of visual sensors in figure 4.1(b). If we follow the horse-shoe shape starting from sensors $0, 10, 20, \ldots, 90$, we find that the next cluster consists of all sensors in the second column (ending with 1), and so forth. Finally, the leftmost cluster of the horse-shoe shape contains all sensors of the rightmost column of sensors $(9, 19, \ldots, 99)$ in figure 4.1(b).

What is the reason for this clustering of columns of sensors in the vertical environment? In an environment with only vertical contours and a uniform background all sensors with the same vertical position will at each time step return more or less the same value. Thus, the informational distance between the sensors in the same vertical position will be close to zero.

In the results presented in figure 5.5 we note that the distance between the sensors in the same column is larger than 0.0. This is due to the fact this is data from the real world, and hence the light is different in different parts of the visual field, and not all lines are aligned at exactly the same angle. The shape of the group of clusters is dependent on the distribution of vertical lines within the environment, the width of the lines, and the robot's distance to the lines. In this particular experiment the vertical lines were often thinner than the width of the visual field (10 pixels). Thus we find that the informational distance between the two outermost columns is shorter than the distance between, for example, the leftmost column and the middle columns. This, along with the horse-shoe effect (Krzanowski, 1988), is the reason for the horse-shoe shape of the clusters.

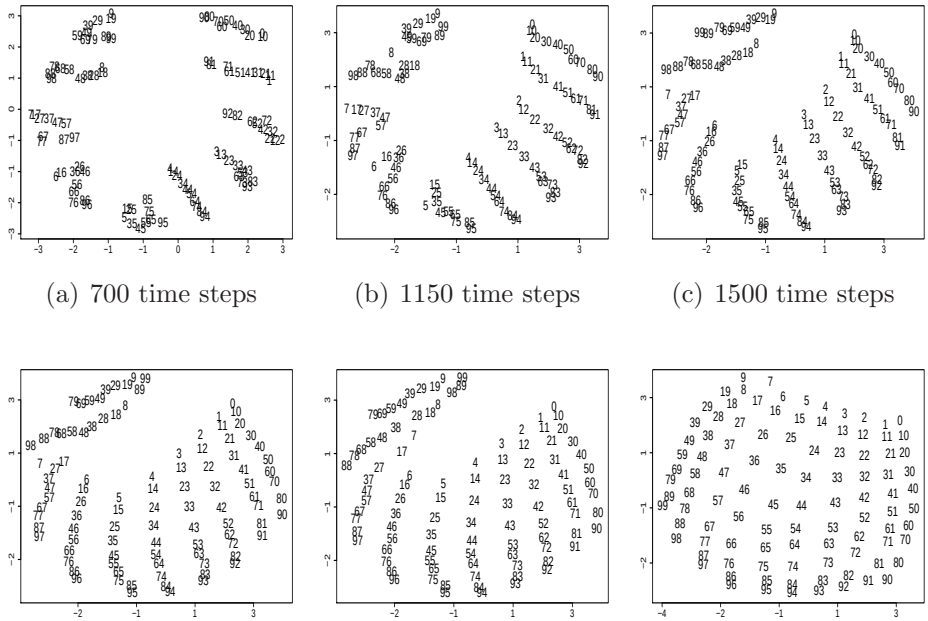

(a) 700 time steps (b) 1150 time steps (c) 1500 time steps

(d) 1900 time steps (e) 2100 time steps (f) 2300 time steps

Figure 5.6: Sensoritopic maps of the sensors after 700, 1150, 1500, 1900, 2100, and 2300 time steps of visual data in the normal environment where the robot moved after 600 time steps from the vertical environment.

Now consider a situation where the AIBO after 600 time steps moves from the environment with only vertical contours to a normal office environment with contours of all angles. In figure 5.6 sensoritopic maps are shown of the visual sensors after the robot has moved from the vertical environment to the office environment. After 700 time steps the sensors of each vertical column are still clustered together even though they have started to move apart. The longer the time that the AIBO has spent in the normal environment, the more the sensoritopic map looks like the map in figure 5.2(i), which is the layout of sensors in the normal environment. This is an example of *unfolding* of sensors, where the sensors in the

columns are separated in the sensoritopic map when they are exposed to different information and hence become less correlated.

5.4 Conclusion

In this chapter we have considered how sensoritopic maps develop as the robot interacts with its environment and receives more sensory data, and the effect of the structure of the environment on the development. First the development of all the sensors and actuators was presented. After only a few time steps of interaction, no real structure was found. As time progressed, more structure was found, and the symmetry of the body discussed in section 5.2 as well as the visual field appeared. When looking at only the visual sensors, the average reconstruction distance decreased over time as more structure was found with more sensor data. We then looked at how the sensoritopic maps developed in a visual environment with only vertical contours. The resulting sensoritopic maps showed that all sensors from each column in the visual field were clustered together, indicating small informational distances.

The sensory reconstruction method can be applied to robots that adapt and evolve over time, where the robot is constrained by the available number of sensors and the processing power available to process the information from the sensors. First of all is it important to note that all robots interact with some environment and that knowledge about this environment usually can be utilized to optimize the robots' sensors. Consider for example the fact that most mammals have more neurons

selective for vertical and horizontal contours than contours of other orientations (Callaway, 1998). This can be explained by the fact that most environments contain more contours of those orientations (Coppola et al., 1998). Thus, the mammal visual system has been adapted by finding generic properties of many different environments. Similarly, it is possible to adapt the visual system of robots by varying the properties of the environment that the robot will interact in. This was illustrated here in the experiment in the vertical environment where the sensors were clustered in 10 groups and most of the sensors could have been discarded or moved to other positions on the robot.

One important question is how this specialization might affect future adaptations to other environments. For instance, consider a robot with a sensoric system optimized for the environment with only vertical contours. How can the robot detect that it has moved to a more complex forest environment using sensors adapted to the restricted vertical environment?

Chapter 6

Adaptation in Individual Sensors by Entropy Maximization

In section 2.2 we discussed the statistics of natural environments and how biological organisms can exploit these low level statistical structures. Among other things, it has been found that the contrast-sensitive neurons of the fly optimize the encoding of the contrast (Laughlin, 1981). This is achieved by the individual neuron by maximizing the entropy of the voltage response to the contrast distribution of the incoming signals. While the contrast-related entropy maximization found by Laughlin (1981) has evolved over evolutionary time and is constant, there are also indications that some neural systems adapt to changing statistics in a matter of seconds or minutes. This is the case in, for instance, some motion-sensitive neurons of the fly (Brenner et al., 2000), and maybe also in the vertebrate

retina (Bialek and de Ruyter van Steveninck, 2004).

The problem of encoding a wide range of contrasts in the fly neuron to a smaller range of voltages is similar to the problem of binning discussed in section 3.2, and in this chapter we show how entropy maximization can be used to add more resolution in sensor data where it is needed. In binning, a larger input range, or discretized alphabet, is mapped to a smaller output range, or alphabet, of symbols. In all the results we have presented in the previous chapters, uniform binning has been used, where each symbol of the smaller output alphabet is assigned to the same number of consecutive symbols of the larger input alphabet. As discussed in section 3.2, there are several problems with uniform binning. One is the placement and size of the bins; what if all the values of the input data vary between values in the range of one of the output symbols? This is the problem that entropy maximization solves by arranging the bins, which can be of different size, in such a way as to add more resolution in the sensor where most of the input data is located.

In this chapter we first look in more detail at how entropy maximization works, and how it can be implemented on a robot. We then present results from an exploratory simulation as well as more detailed experiments with a robot. The results show that entropy maximization enables the sensory reconstruction method to find correlations between sensors of different modalities by adding more resolution in the data where it is needed.

6.1 Entropy Maximization

Consider the grey-scale image depicting Claude Shannon in figure 6.1(a). Here each pixel can have a value between 0 and 255, meaning that $\mathcal{X}_{raw} = \{0, 1, \ldots, 255\}$. How can this image be encoded, or compressed, to only five different pixel values, $\mathcal{X} = \{25, 75, 125, 175, 225\}$? Figure 6.1(b) shows the image compressed using uniform binning, and, as seen in figure 6.1(e), the distribution of grey-scales in figure 6.1(a) is not uniform, with most pixels in the range $\{100, 101, \ldots, 200\}$. The entropy of the encoded image is approximately 1.97 bits per pixel, which is less than the maximal theoretical entropy of $\log_2 5 \approx 2.32$ bits. From an information theoretical point of view, this means that this encoding is non-optimal since the entropy of the encoded image is less than the maximal possible entropy of the image. Now, consider figure 6.1(c) which also uses five bins, where (at least if studied from a distance) the image subjectively seems to convey more detail about the original image. Here the original values have been binned in such a way that each bin contains approximately the same number of pixels, which means that the entropy of the image is close to the maximum of $\log_2 5 \approx 2.32$ bits per pixel. This can also be considered as adding more resolution where most of the data is located.

More formally, given a raw sensor X_{raw}, the aim is to find a partitioning of the data into the N bins of the alphabet $\mathcal{X}$, $\mathcal{X}_{raw} = B_1 \cup \cdots \cup B_N$ such that each bin B_i is equally likely given a certain set of data. That is,

$$P(X_{raw} \in B_i) \approx \frac{1}{N}, \tag{6.1}$$

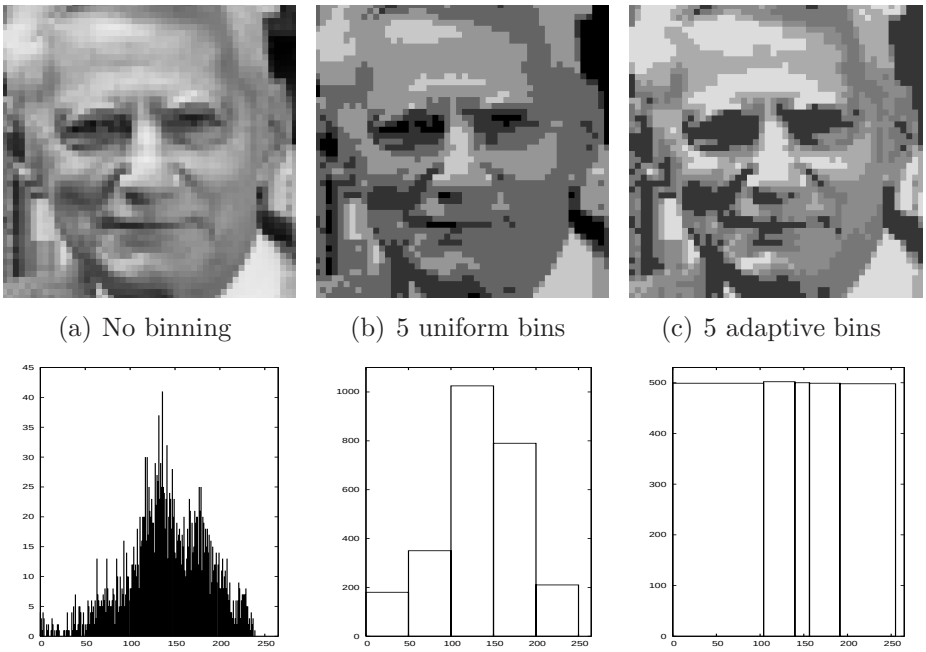

(a) No binning (b) 5 uniform bins (c) 5 adaptive bins

(d) No binning - histogram (e) 5 uniform bins - histogram (f) 5 adaptive bins - histogram

Figure 6.1: Figure 6.1(a) shows a 50 by 50 pixels grey-scale image of the founder of information theory, Claude Shannon, and figure 6.1(d) the corresponding histogram of pixels between 0 and 255. Figure 6.1(b) shows the same picture where the pixel data (0-255) is binned into only five different pixel values using uniform binning and figure 6.1(e) the frequency of pixel values. Finally, figure 6.1(c) shows the same picture with the pixel data binned into five bins using adaptive binning and figure 6.1(f) the corresponding histogram [after (Olsson et al., 2005b)].

which is equivalent to the entropy of the distribution being maximized. Another way to view this is to make the distribution as close as possible to equidistribution, given a particular set of data. It is important to note that while entropy maximization changes the entropy of individual sensors to their maximal values, it still maintains correlation between sensors.

The experiments performed by Brenner et al. (2000) also indicate that this kind of entropy maximization is constantly happening in the motion-sensitive neurons of the fly. This can be implemented using a sliding window where the last T time steps of sensor data are considered to estimate the frequency distribution of the sensor. To calculate the value of sensor $S_x \in \mathcal{X}$ at time t using entropy maximization, the following algorithm can be used:

Algorithm 1 EntropyMaximization(raw, histogram, t)

```
1: valuesPerBin = T/numBins
2: if t < T then
3:    return (int)(raw/valuesPerBin) /* uniform binning */
4: else
5:    sum = curBin = 0
6:    for i = 0 to histogram.length do
7:       sum = sum + histogram[i]
8:       if sum > valuesPerBin then
9:          curBin = curBin + 1
10:         sum = 0
11:      end if
12:      if i > raw then
13:         return curBin
14:      end if
15:   end for
16:   return curBin
17: end if
```

Here $raw \in \mathcal{X}_{raw}$ is the raw sensor input and *histogram* a histogram (represented as an array of size $|\mathcal{X}_{raw}|$) of the last T time steps of data where each element specifies how many times that raw value has been seen during the last T time steps. When $t < T$, it means that there is

not enough data to fill the window and standard uniform binning is used. In our experiments we have used a window size of $T = 100$, which means that uniform binning was used the first 100 time steps. It should also be noted that in this implementation, all instances of the same value of X_{raw} are added to the same bin. This means that the distribution need not be completely uniform, as in figure 6.1(f).

6.2 Experiments

To test the entropy maximization technique we performed two types of experiments: one using a basic simulation and one using the SONY AIBO robot. In both experiments the problem is to see whether sensors of different modalities in the same physical position are in the same position in the reconstructed sensoritopic maps. This is an example of sensor integration that can be verified by the average reconstruction distance of the sensoritopic maps.

6.2.1 Simulation Experiments

On a 500 by 350 pixel environment – see figure 6.2 – an eight by eight pixel agent represented as a square moves a maximum of one pixel per time step in the x-direction and a maximum of one pixel in the y-direction. Hence $dx, dy \in \{-1, 0, 1\}$, but both cannot be 0 at the same time, which means that the agent is always moving. At each time step there is a 15% probability that either dx or dy, or both, change value by -1 or 1. Every pixel n ($1 \leq n \leq 64$) of the agent has four sensors, one for the red

Figure 6.2: The environment where the agent is moving. The image depicts autumn leaves and has higher variation in the red and green channels than the blue channel.

intensity (R_n), one for the green (G_n), one for the blue (B_n), and one for the average intensity of that pixel (I_n). Thus, the agent has a total of 256 sensors. For each time step the values of all 256 sensors are used as the input to the sensory reconstruction method.

Figure 6.3 shows the histograms of all sensors of each type accumulated over the whole simulation of 6000 time steps, and also examples of histograms for each sensor type over 10 consecutive time steps. The red and green sensors are quite uniformly distributed over almost the whole range while the blue has a high peak at 0. In figure 6.3(d) to 6.3(f) we can see that the ranges of values in the red and green sensors are greater than in the blue sensors during these 10 time steps, something that was true for most frames of data.

Given the structure of the input data it was expected that adaptive binning with a sliding window would be advantageous for the sensory reconstruction method. Different numbers of bins between four and 20 bins

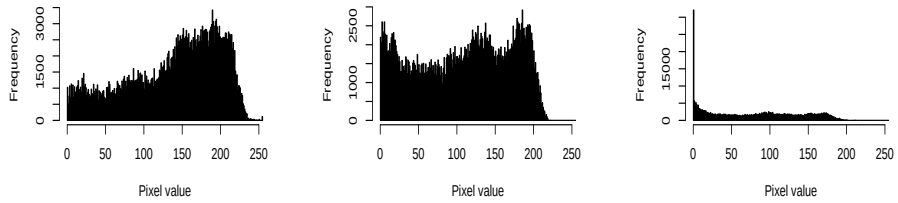

(a) Red histogram 6000 time steps

(b) Green histogram 6000 time steps

(c) Blue histogram 6000 time steps

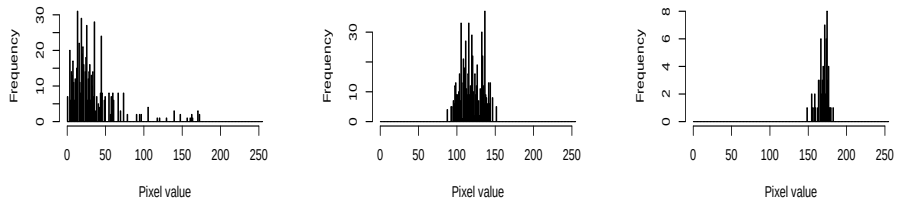

(d) Red histogram 10 time steps

(e) Green Histogram 10 time steps

(f) Blue Histogram 10 time steps

Figure 6.3: Figures 6.3(a), 6.3(b), and 6.3(c) shows histograms of red, green, and blue sensors from the image in figure 6.2 collected from 6000 timesteps of movement from all sensors. Figures 6.3(d), 6.3(e), and 6.3(f) show examples of histograms from 10 consecutive time steps.

were used with similar results and the presented sensoritopic maps show typical maps – section 6.2.2 shows more detailed results using different numbers of bins for the collected AIBO data.

Figure 6.4(a) shows a sensoritopic map of the 256 sensors where the sensor data was partitioned into 16 uniform bins (four bits per sensor). The graph shows that some structure is found and some sensors that are closely positioned in the agent are close in the sensoritopic map. One exception is that the blue sensors, B_1 to B_{64}, all located to the left.

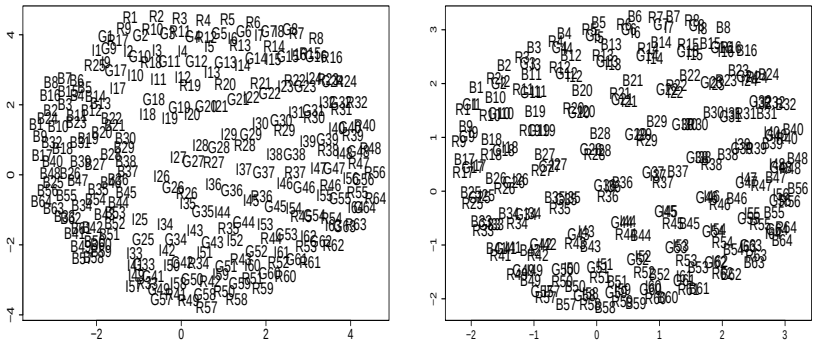

(a) Uniform binning - 16 bins (b) Adaptive binning - four bins

Figure 6.4: Sensoritopic maps of the sensory data where R1-64 is the red channel sensors, G1-64 the green, B1-64 the blue, and I1-64 the intensity sensors using uniform and adaptive binning .

Clearly, if all the informational structure could be found the map should correspond to the physical organization and, for instance, R_1 should be close to B_1. Now consider figure 6.4(b). Here the input data was binned into only four bins (two bits per sensor) using entropy maximization with a sliding window of size 100. Here the sensoritopic map clearly shows the informational and physical relationships between the sensors, where sensors that are closely located in the layout of the agent are clustered in the map. This means that the real physical layout of the sensors has been recovered from the raw input data, something that the same method failed to do using uniform binning and twice the amount of resolution per sensor (two instead of four bits).

6.2.2 AIBO Experiments

The robotic experiments were performed with a SONY AIBO robot wandering in an office environment with both artificial lights and two windows. As described in section 4.1.1, images of size 88 by 72 pixels from the robot's camera were saved over a dedicated wireless network with an average frame rate of 20 frames per second. The images were transformed to eight by eight pixels images by either pixelation with averaging or by using only eight by eight pixels from the centre of each image. Either transformation produced similar results in subsequent experiments. The robot performed a simple exploring behaviour with obstacle avoidance walking around in the office.

Figure 6.5 shows histograms of all sensors of each type (red, green, blue, intensity) combined over 1000 time steps where each sensor can have a value in the range $\{0, 1, \ldots, 255\}$. The red and green sensors have most values between 0 and 170 with two clear peaks at roughly 70 and 150. The blue sensors had a narrower range, with most sensor values between 0 and 80, and two narrow peaks at roughly 25 and 75. The peaks are due to the windows; when walking towards the windows the ambient light is brighter. Similarly to the simulation previously discussed, the histograms in any given frame show a narrower range of the data for the blue sensors. Thus, it is expected that the blue sensors are more difficult to reconstruct using uniform binning.

As seen in figure 6.6 this is the case. Figure 6.6(a) shows a sensoritopic map of the blue sensors constructed from 16 uniform bins. Contrast this with figure 6.6(b) using only six adaptive bins where the organization of

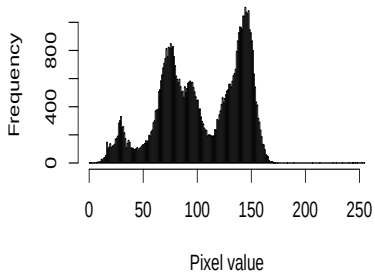

(a) Red histogram

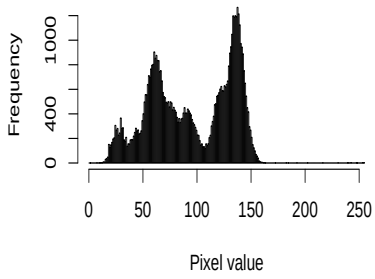

(b) Green histogram

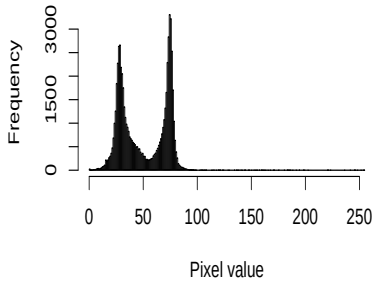

(c) Blue histogram

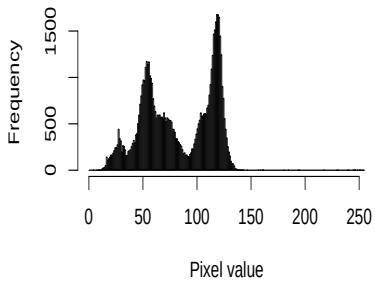

(d) Intensity histogram

Figure 6.5: Histograms of red, green, blue, and intensity sensors.

the visual field has been reconstructed.

In figure 6.7 sensoritopic maps of all the red, green and blue sensors combined are shown. Here we can again see how the adaptive binning enables the sensory reconstruction method to find the positional relations of the sensors of the different types of sensors, where sensors from the same physical position, e.g. $R8$, $G8$, and $B8$, are clustered together. We can also see that the order with $R1$ at the opposite corner of $R64$ has

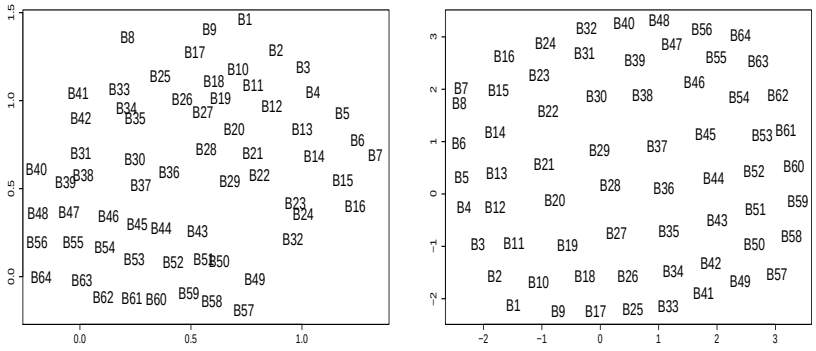

(a) Uniform binning - 16 bins (b) Adaptive binning - six bins

Figure 6.6: Sensoritopic maps of blue sensors. Figure 6.6(a) shows the sensoritopic map created with 16 uniform bins and figure 6.6(b) with six adaptive bins using a sliding window.

been found. In the sensoritopic maps in figure 6.7(c) and 6.7(a) using six and 16 uniform bins we see that the blue sensors are separated from the red and green. The structure of the red and green sensors is also less clear compared to the adaptive binning of figure 6.7(b) and 6.7(d).

To study the effect of different bin sizes on the two different binning methods, sensoritopic maps were created using different bin sizes for both uniform and adaptive binning. For each number of bins in the range $\{4, 6, \ldots, 20\}$, 100 sensoritopic maps were created with each of the two methods. These reconstructed maps were compared to the real layout of the sensors by computing the average reconstruction distance described in section 3.6. This distance is the average of all distances between all pairs of sensors in the reconstructed map and the known real layout of the sensors, where 0 means that the sensors of the reconstructed map has the same distances as the real layout. If the sensors are placed at

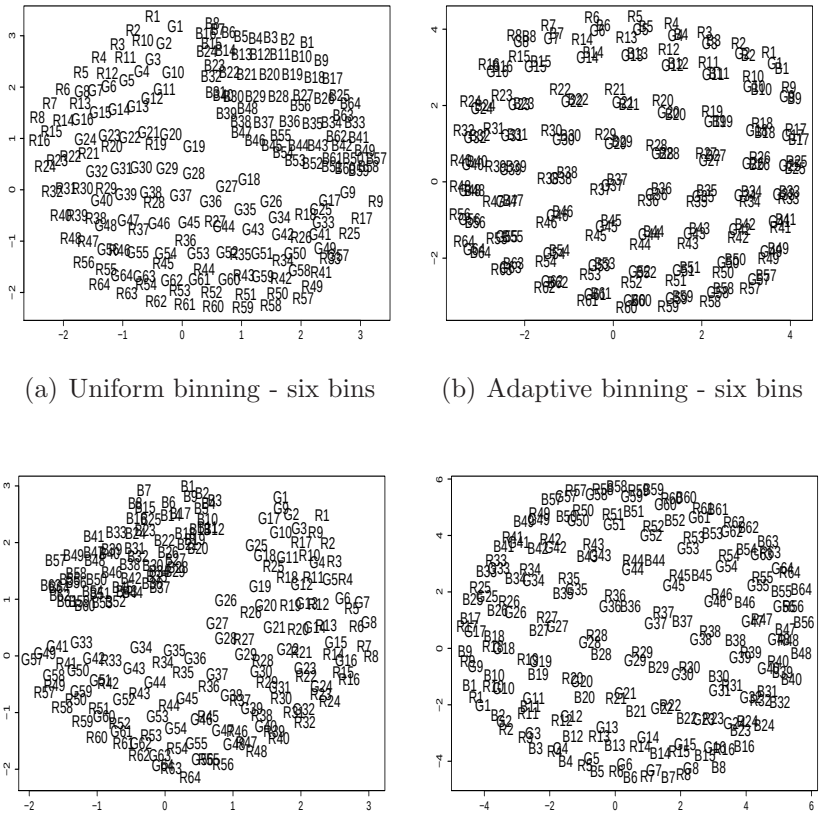

(a) Uniform binning - six bins

(b) Adaptive binning - six bins

(c) Uniform binning - 16 bins

(d) Adaptive binning - 16 bins

Figure 6.7: Combined sensoritopic maps of red (R), green (G), and blue (B) sensors using six and 16 bins with uniform and adaptive binning

random positions, the average reconstruction distance for a rectangular visual field is 0.52.

The results of table 6.1 show the average reconstruction distance for the 100 created maps and the standard deviation for each bin size for uniform and adaptive binning. The average reconstruction distances in the table confirm the anecdotal evidence of the previously shown sensoritopic maps – the average reconstruction distances are, for all the different

#Bins/Exp.	RGB Uniform	RGB Adaptive.
4	0.259 (0.007)	0.082 (0.009)
6	0.226 (0.006)	0.075 (0.012)
8	0.215 (0.009)	0.072 (0.011)
10	0.219 (0.003)	0.069 (0.013)
12	0.179 (0.011)	0.068 (0.011)
14	0.202 (0.008)	0.069 (0.009)
16	0.206 (0.006)	0.067 (0.011)
18	0.207 (0.003)	0.069 (0.011)
20	0.207 (0.004)	0.072 (0.009)

Table 6.1: Average reconstruction distances for AIBO experiments for uniform and adaptive binning with different bin sizes. Standard deviation in parentheses.

bin sizes, significantly smaller for the adaptive binning than the uniform binning, with the adaptive distances roughly a third of the uniform reconstruction distances. With only four bins, the uniform binning method had an average reconstruction distance of 0.259, which is more than three times as much as the adaptive binning with four bins. With more bins, the uniform method performs better, with a lowest average reconstruction distance of 0.179 with 12 bins. Still, this is much higher than the adaptive binning method, which had an average reconstruction distance of 0.068 using 12 bins.

6.3 Conclusion

This chapter has discussed entropy maximization of sensory data in the fly visual system and how a similar system can be implemented in a robot. The system constantly adapts the input/output mapping of sensory data by estimating the distribution of input data and adapts the output distribution by entropy maximization of the data. This mapping of input/output data compresses the data while maintaining correlations between sensors.

Results from simulation show how an agent using this adaptive technique can reconstruct its visual field with a resolution of only two bits per sensor using the sensory reconstruction method. Using four bits per sensor and uniform binning, the sensory reconstruction method failed to reconstruct the visual field. This result indicates that adaptive binning is useful for compressing sensory data and to find correlations between sensors. Results from experiments with a SONY AIBO robot show some statistical properties of different indoor environments and how adapting to this structure helps the robot find structure in the sensory data.

One interesting question is whether entropy maximization is more effective for the agent on a higher level on sets of sensors or at the single sensor level. In this case, how are these sets or objects selected? There are also many problems associated with entropy estimation. For example, what is the best method to estimate entropy given distributions with empty bins? Here other methods like Miller-Madow bias correction (Paninski, 2003) could be investigated.

Chapter 7

Informational Distance Measures

After the information metric (Crutchfield, 1990) was introduced by Olsson et al. (2004a) as a method to compute the informational relationships between sensors in robotics, a number of papers have been published where it has been used for robotic applications – see for example (Olsson et al., 2004c, 2005a,b,c; Mirza et al., 2005a,b; Kaplan and Hafner, 2005; Hafner and Kaplan, 2005). Even though the information metric has produced good and interesting results in a number of applications, including the results presented in the other chapters of this thesis, a natural question to ask is still "why the information metric?". Some possible arguments against using the information metric are: 1) it is costly to compute, 2) too much data is needed to estimate the probabilities needed, and 3) other, less complicated, distance measures might produce the same results.

In this chapter we focus on the third argument and come back to the other two in the conclusions in section 7.3. Here we present five alternative distance measures, some of which have been suggested by reviewers of our papers and by colleagues, and compare them to the information metric, which was introduced in section 3.3. The five distance measures are 1-norm (one dimensional Euclidean distance), correlation coefficient, Kullback-Leibler divergence, Hellinger distance, and Jensen-Shannon divergence. To compare the potential utility of the methods we applied them as the distance measure used in the sensory reconstruction method. In the presented experiment the sensors of the visual field of a robot were split into three different modalities: red, blue, and green. Performance of the different distance measures is measured by comparing how well the resulting sensoritopic maps reconstruct the real visual field.

One key concept when discussing distance measures is whether the distance measure is a metric in the mathematical sense. Why this is important and the definition of a metric was discussed in section 3.3.

The next section presents the different distance measures and whether they are metric in the mathematical sense or not. Then the results of using the different presented distances measures are presented, and finally we conclude the chapter.

7.1 Different Distance Measures

As described in section 3.1 a sensor is denoted by S_x, where the sensor can be viewed as a time-series where S_x^t is the value of the sensor at time

step t.

The computational costs for the presented methods are roughly the same, apart from the Jensen-Shannon divergence which is more costly due to the need – just like for the information metric – to compute the joint entropies of all pairs of sensors – see section 3.3.

7.1.1 1-Norm distance

The *1-norm distance* used by Pierce and Kuipers (1997) is different from the distance measures that follow in that it does not take into account the probabilities of the different values that a sensor can take. It is normalized between 0.0 and 1.0 and is defined as

$$d_{1n}(S_x, S_y) = \frac{1}{T}\sum_{t=1}^{T} |S_x^t - S_y^t|. \tag{7.1}$$

This measure is a metric in the mathematical sense and computes for each time step the absolute distance between the two sensors.

7.1.2 Correlation Coefficient

The *correlation coefficient* is defined as

$$r = \frac{\sum_{t=1}^{T}(S_x^t - \bar{S}_x)(S_y^t - \bar{S}_y)}{\sqrt{\sum_{t=1}^{T}(S_x^t - \bar{S}_x)^2}\sqrt{\sum_{t=1}^{T}(S_y^t - \bar{S}_y)^2}} \tag{7.2}$$

where $\bar{S}_x$ and $\bar{S}_y$ are the mean of S_x and S_y respectively. The range of r is $-1.0 \leq r \leq 1.0$, where 1.0 means that they are perfectly linearly

correlated, 0 that the two sensors are not linearly correlated, and -1.0 perfectly negatively correlated. This can be made symmetric by computing the squared correlation coefficient, which is in the range $0 \leq r^2 \leq 1.0$, and then

$$d_{CC}(S_x, S_y) = 1 - r^2_{S_x,S_y}. \tag{7.3}$$

This is still not a metric since it does not satisfy the triangle inequality (Ernst et al., 2005).

7.1.3 Kullback-Leibler

The *Kullback-Leibler divergence* (Cover and Thomas, 1991) is defined as

$$D(p_x||p_y) = \sum_{x \in \mathcal{X}} p_x(x) log_2 \frac{p_x(x)}{p_y(x)}, \tag{7.4}$$

where $0\ log_2 \frac{0}{p_y} = 0$ and $p_x\ log_2 \frac{p_x}{0} = \infty$. These two special cases never happened in the experiments described below. The Kullback-Leibler measure is not a metric because it is not symmetric and because that the triangle inequality does not hold (Cover and Thomas, 1991). It can be made symmetric by adding the two possible Kullback-Leibler divergences of S_x and S_y,

$$d_{KL}(S_x, S_y) = D(p_x||p_y) + D(p_y||p_x), \tag{7.5}$$

where p_x is the probability distribution associated with sensor S_x and p_y with S_y. It should be noted that this is still not a metric.

7.1.4 Hellinger Distance

The square root of the *Hellinger distance*, also known as *Bhattacharya distance* (Basu et al., 1997) , is a metric and is defined as

$$d_H(S_x, S_y) = \sqrt{\frac{1}{2}\sum_{x\in\mathcal{X}}\left(\sqrt{p_x(x)} - \sqrt{p_y(x)}\right)^2}. \tag{7.6}$$

7.1.5 Jensen-Shannon Divergence

Finally, the *Jensen-Shannon divergence*, presented in Lin (1991), is defined as

$$d_{JS}(S_x, S_y) = H(\pi_X X + \pi_Y Y) - \pi_X H(X) - \pi_Y H(Y), \tag{7.7}$$

where $\pi_X, \pi_Y \leq 0, \pi_X + \pi_Y = 1$, are the weights associated with the sensors S_x and S_y. In this paper the weights were always $\pi_X = \pi_Y = 0.5$. In (Endres and Schindelin, 2003) it was proved that the Jensen-Shannon is the square of a metric, i.e., $\sqrt{d_{JS}}$ is a metric, which was used in the experiments presented in this paper.

7.2 Reconstruction Using Different Measures

In the experiments a SONY AIBO robotic dog was placed in a sitting position on a desk in the lab as previously described in section 4.2.1. The robot only moved its head with uniform speed using the pan and

tilt motors in eight directions; up, down, left, right, and four diagonal directions. Five sequences of 6000 frames each of visual data were collected from the camera at a resolution of 88 by 72 pixels, with eight bits for each channel (red, green, blue) at an average rate of 20 frames per second. The collected images were downsampled to eight by eight pixels using averaging. In the collected data the range of the blue sensors was slightly lower than the red and green sensors with a slightly smaller variation.

Sensoritopic maps were created from each of the five sequences of data by the sensory reconstruction method using the different distance measures previously described. The presented maps are examples but all maps created using one particular distance measure had roughly the same characteristics as the ones presented here, verified by ocular inspection and the average reconstruction distance. Table 7.1 shows the results for the different measures which will be referred to below, where 100 sensoritopic maps were created for each of the five sequences of data. Thus, the averages are from 500 sensoritopic maps.

7.2.1 Only Red Sensors

Figure 7.1 shows sensoritopic maps computed with the different distance measures of only the red sensors $R1 - R64$. First, if we look at the maps for the Kullback-Leibler, Hellinger, and Jensen-Shannon distance, we find no real structure. For the correlation coefficient distance, figure 7.1(b), we find that sensors that are close in the visual field tend to be closer in the sensoritopic map, but it is not very clear. Now, compare this

Measure \ Exp.	R64	RGB192	ARGB192
1-norm	0.06 (0.01)	0.32 (0.01)	–
Correlation coefficient	0.19 (0.02)	0.23 (0.03)	0.21 (0.05)
Information metric	0.07 (0.02)	0.12 (0.03)	0.09 (0.03)
Kullback-Leibler	0.37 (0.03)	0.35 (0.01)	0.41 (0.05)
Hellinger	0.45 (0.05)	0.40 (0.02)	0.46 (0.04)
Jensen-Shannon	0.45 (0.04)	0.39 (0.01)	0.45 (0.04)

Table 7.1: Average distances between all pairs of correct and reconstructed sensors using equation 3.8 with standard deviation in parentheses. The column R64 shows the average distances for the 64 red sensors of figure 7.1 and RGB192 the red, green, and blue sensors of figure 7.2, both using normal binning. AB-RGB192 shows the results for the adaptive binning of figure 7.3.

to the sensoritopic maps for both the 1-norm distance, figure 7.1(a), and the information metric, 7.1(c). Here the spatial relationships of the red sensors have been found, with sensor $R1$ in the upper left corner and $R64$ in the lower left corner for the 1-norm distance and the $R1$ sensor in lower left corner for the information metric. Since the sensory reconstruction method cannot find the real physical location of the sensors, but only the relative spatial relationships, both of these maps are valid representations of the visual field.

The results in table 7.1 confirm the initial conclusions from the sensoritopic maps above. The average reconstruction distance for the Hellinger

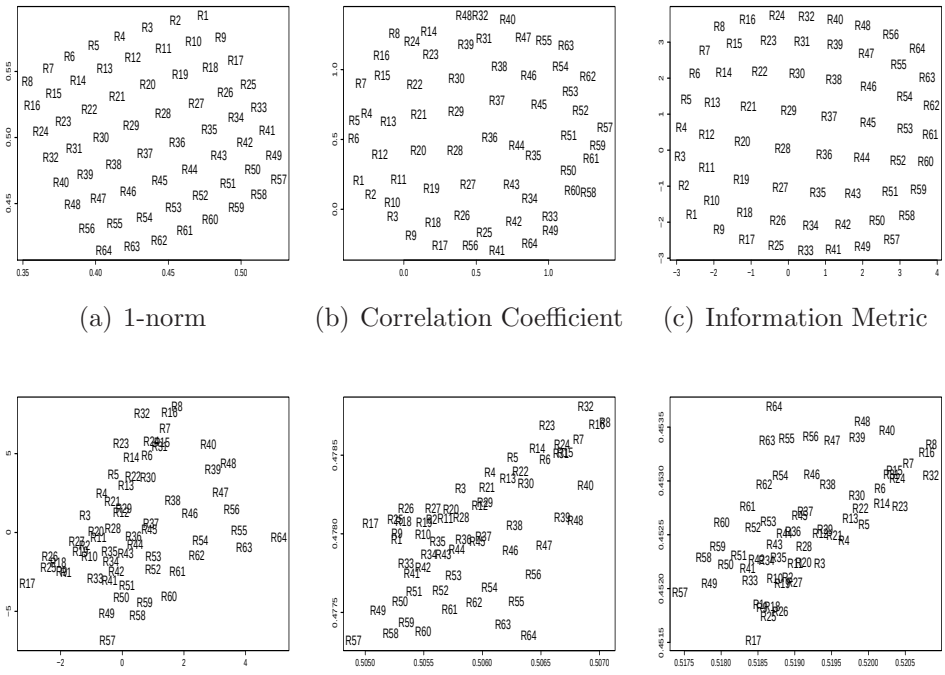

(a) 1-norm (b) Correlation Coefficient (c) Information Metric

(d) Kullback-Leibler (e) Hellinger (f) Jensen-Shannon

Figure 7.1: Sensoritopic maps of the red sensors created using the different distances measures.

and Jensen-Shannon distance were close to the average random distance of 0.52 and the Kullback-Leibler distance is slightly less random with a an average distance of 0.37. As expected, the correlation coefficient had an average reconstruction distance smaller than the three previously mentioned distance measures, but higher than the 1-norm distance and the information metric.

7.2.2 Red, Green, Blue Sensors with Uniform Binning

Figure 7.2 shows sensoritopic maps with both red, green, and blue sensors, and column RGB192 of table 7.1 the corresponding average distances. This is an example of sensor integration where the problem is to find which sensors are from the same location in the visual field, when the only input data to the system is the raw and unstructured data from the 192 sensors without any classification. Here the Hellinger map and Jensen-Shannon map both contain three clusters, one for each modality. The Kullback-Leibler map is divided into four clusters, where the uppermost left cluster contains nine of the blue sensors. The 1-norm distance shows how structure within the modalities is present but there is no fusion of the sensors from different modalities. The correlation coefficient measure show a similar structure but there is some overlap between the red and the green sensors. For the information metric, figure 7.2(c), the situation is different. Here the sensors of different modalities from the same location in the visual field are clustered together. This is an example of autonomous sensory fusion where sensors of different modalities are combined.

Again, the results in table 7.1 confirm the anecdotal evidence from the typical sensoritopic maps of figure 7.2. The Kullback-Leibler, Jensen-Shannon, and Hellinger distance measures have similar average reconstruction distances, while the 1-norm distance has a much higher reconstruction distance than the experiment with only one sensor modality

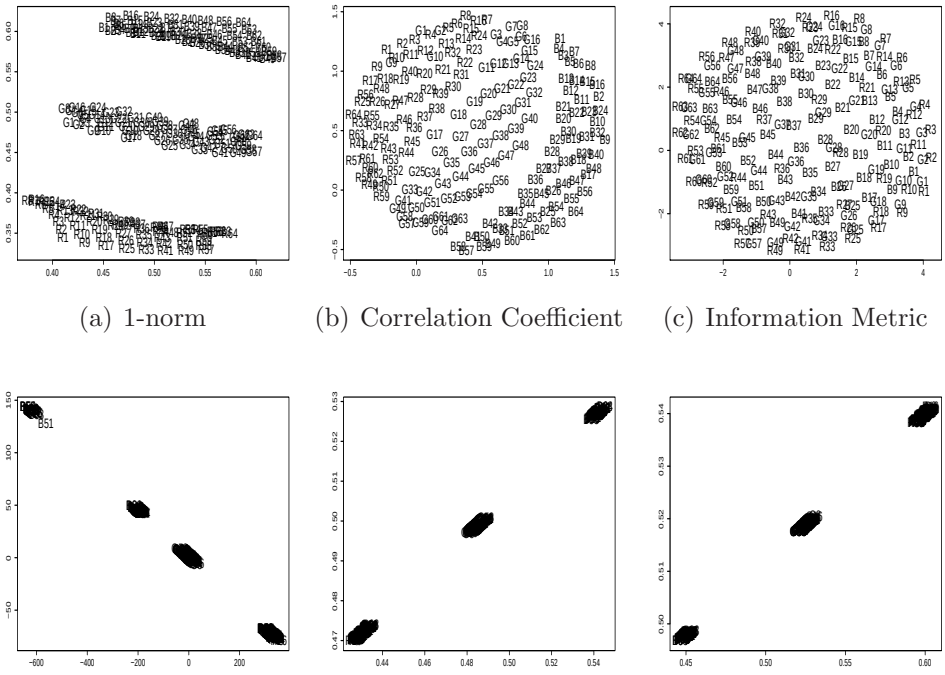

(a) 1-norm (b) Correlation Coefficient (c) Information Metric

(d) Kullback-Leibler (e) Hellinger (f) Jensen-Shannon

Figure 7.2: Sensoriopic maps of 192 sensors using uniform binning.

of section 7.2.1. This is due to the 1-norm distance comparing absolute values of the sensors and not the probabilities. This, of course, might lead to problems when the sensors are of different modalities, since they might have informational relationships which are more complicated than linear relationships, which is the case in this experiment. The average reconstruction distance of the information metric, although double the one for only red sensors, was significantly lower than the others.

7.2.3 Red, Green, Blue Sensors with Adaptive Binning

In chapter 6 it was shown that entropy maximization of the data in individual sensors might be useful to find correlations between sensors of different modalities. Figure 7.3 shows sensoritopic maps and column AB-RGB192 of table 7.1 the average distance computed using the same data as before, where it has been preprocessed by maximizing the entropy in each sensor using a window of 100 time steps – see chapter 6 for details of this method. The 1-norm distance is not included since it is operating on raw sensor values and not on probabilities.

In the Kullback-Leibler, Hellinger, and Jensen-Shannon maps, the red and green sensors are clustered together, and the blue in another cluster, less concentrated than in the previous section where uniform binning was used. The map of the correlation coefficient is similar, albeit with with more structure showing the layout of the individual sensors of the different modalities, as also can be seen in the average distance in table 7.1. The information metric in figure 7.3(b) again shows clustering of the different modalities according to their spatial location in the visual field. For example sensor $R28$ is clustered together with $B28$ and $G28$. Again, these anecdotal results are confirmed by the average reconstruction distances in table 7.1, where the information has by far the lowest average reconstruction distance.

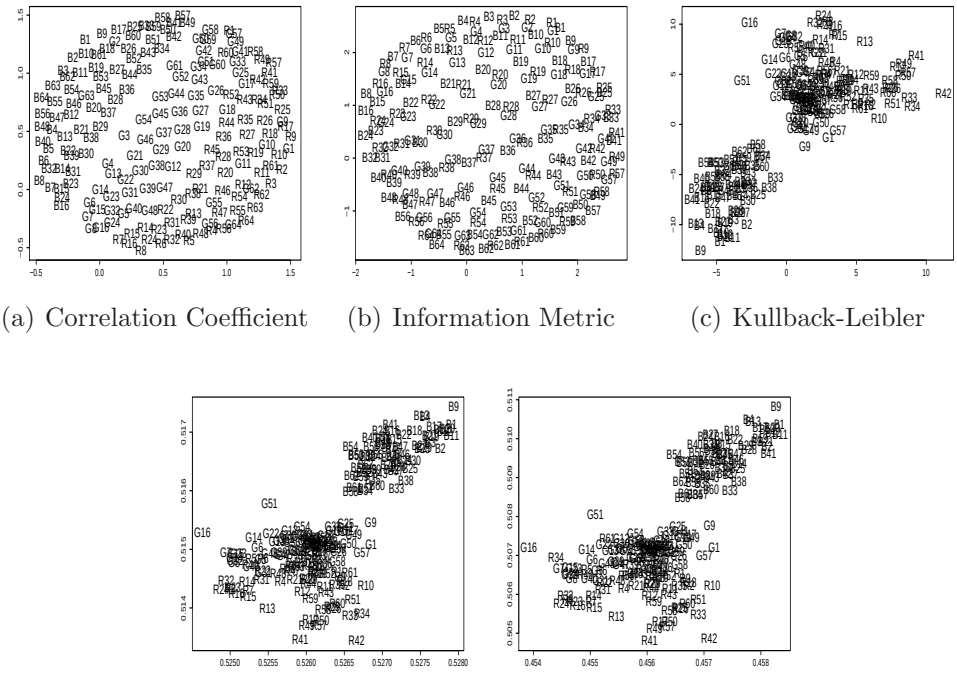

(a) Correlation Coefficient (b) Information Metric (c) Kullback-Leibler

(d) Hellinger (e) Jensen-Shannon

Figure 7.3: Sensoritopic maps of 192 sensors using entropy maximization of the sensor data.

7.3 Conclusion

In this chapter we compared the information metric to five other distance measures: the 1-norm distance, the correlation coefficient, Kullback-Leibler divergence, Hellinger distance, and the Jensen-Shannon divergence. These distance measures were suggested to us by reviewers of our papers and colleagues, as less complicated alternatives to the information metric. Among the compared distances the information metric, 1-norm distance, Hellinger distance, and the squared Jensen-Shannon divergence are metrics in the mathematical sense. The comparison was performed

by applying these distance measures as the distance measure used in the sensory reconstruction method. The created sensoritopic maps were compared by how close the reconstructed maps were to the real layout of the sensors using the average reconstruction distance described in section 3.6.

The results showed how the maps created using the information metric had significantly shorter average reconstruction distances than all the other maps, when the sensors were of different modalities. When using sensors from one modality the average distance was similar to the 1-norm distance. Among the other proposed measures the correlation coefficient had a shorter average distance than the others, but still significantly longer than the information metric.

Why is it the case that the information metric enables the sensory reconstruction method to find these relations between sensors of different modalities when the other measures do not? By considering the individual as well as joint entropies of the sensors, the information metric provides a general method for quantifying all functional relationships between sensors, while many other methods only find some relationships. For example, a correlation coefficient approaching zero does not imply that two variables actually are independent (Steuer et al., 2002).

One argument against the information metric is that it is quite costly to compute. That is to a certain extent true, but also true for other measures using joint probabilities such as Jensen-Shannon divergence. But, in our experience, it is possible to compute in real-time if implemented correctly. As an example, we have had an AIBO robot connected to a 1.7

GHz PC using the de-scrambling method of section 4.3.4, reconstructing its 25 by 25 pixel visual field in real time using roughly 19 frames per second.

Another argument against using the information metric is that it requires a significant amount of sensor data to estimate the individual and joint probability distributions and entropies of section 3.2. This is also true to some extent, but in many applications this is not a problem, and it is also a problem for other statistical methods. It is also the case that it works quite well even without perfect estimation, or using very few bins as showed in earlier chapters.

To say what distance measure is "best" is of course always dependent on the particular problem one is trying to solve. What the results above showed was that for this particular problem, and many of the other problems discussed in this thesis, the power of the information metric to capture all informational relationships between sensors is an advantage.

It should be noted that the sensoritopic maps reflect the informational geometry of the sensors, where sensors that are highly correlated are close in the map. Such proximity need not respect sensory modality, as seen in the experiments above, where it was found that sensors of different modalities from the same physical location were placed close in the information metric based sensoritopic maps. Similar cross-modal sensor fusion has also been found in nature, e.g., in the optic tectum of rattlesnakes, where bimodal neurons receive input from the retina as well as infrared-sensing pit organs, and the neurons cross-modally integrate sensory information (Newman and Hartline, 1981).

Chapter 8

Discovering Motion Flow

It is often the case that a robot is in an environment where movement has a piecewise smooth effect on the sensory data produced by some of the sensors. For example, most real world scenarios have this effect on visual sensors unless there is complete darkness or the visual input is random. The same is also true for, for example, infra-red sensors that measure the distance to the closest obstacle, and in some cases, tactile sensors. This effect can be exploited by a robot to perform sensory guided movement by computing motion flow in the sensors which can tell the robot about the velocity and direction of movement, caused by the robot itself or by movement of objects in the environment.

In traditional optical flow techniques it is assumed that the sensors that make up the visual field are of the same modality, and that the brightness values of the sensors vary smoothly over time and also spatially over the other sensors that make up the image. In this chapter we generalize the concept of optical, or more generally, motion flow, to

assume only that the informational relations vary smoothly over the sensors, as seen, for instance, in section 4.4. This enables us to describe a novel method for adapting some sensors in a multimodal sensory field requiring only smooth informational relations rather than the sensor value smoothness assumed in traditional optical flow analysis.

The rest of this chapter is structured as follows. We first give an overview of the ideas behind the classical optical flow algorithm in section 8.1. Then an alternative flow algorithm, based on temporal-informational correlations between sensors in the field, rather than the smoothness of sensor values as in traditional optical flow, is presented in section 8.2. Then in section 8.3 we describe how traditional optical flow techniques can be applied to reconstructed visual fields of the same modality, before describing in 8.4 how sensors can be adapted to compute traditional optical flow, or more generally motion flow, in sensors that are only informationally correlated.

8.1 Traditional Optical Flow

Optical flow is an approximation for detecting and measuring local motion in images, where the motion is found by computing how much each pixel or small part of the image has moved between consecutive images. As an example, consider the two images schematized in figure 8.1. Here the part of the image at position (x, y) at time t, $I(x, y, t)$, has moved to the position $(x + \delta x, y + \delta y)$ at time $t + \delta t$. This means that $I(x, y, t) = I(x + \delta x, y + \delta y, t + \delta t)$, which forms the basis of the *motion*

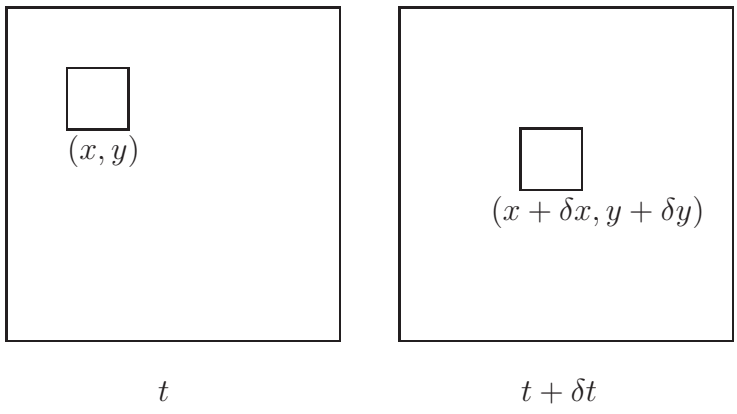

Figure 8.1: Image at time t and time $t + \delta$, where the part of the image at position (x, y, t) is the same as $(x + \delta x, y + \delta y, t + \delta t)$. Here δx is the motion along the x-axis and δy the motion along the y-axis between time t and $t + \delta t$.

constraint equation – see, for instance, Lucas and Kanade (1981).

How do we know that a part of an image has moved to a new position between two frames? One assumption is that all temporal intensity changes in the whole image are due to motion only. It is also assumed that all objects in the images are rigid and that no changes of shape occur. Optical flow is also based on the idea that for most points in the image, neighbouring points have approximately the same brightness. In other words, the world is made up of rigid, continuous objects over which brightness varies smoothly.

Even though these assumptions might seem very restricting and limiting, optical flow analysis is quite often very effective in real world applications, as seen in many computer vision and robotics applications. A typical application is to determine the speed and direction of a moving camera or a robot detecting moving objects in front of itself.

The next sections describe how motion flow can be computed in visual and other sensory fields of different modalities and non-rectangular sensory fields. Finally it will also be shown how sensors of different modalities can be adapted to use the traditional optical flow algorithm.

8.2 Motion Flow by Temporal-Informational Correlations

In the previous section we saw that traditional optical flow analysis is based on the idea that neighbouring points have approximately the same brightness, where the sensors in the visual field respond similarly to similar stimulis. This might not be the case if the sensors of the visual field are of different visual modalities such as red, green, and blue, as in the visual fields in figure 4.9, or of different modalities such as visual and infra-red.

The assumption of brightness varying smoothly over the image can be significantly relaxed and generalized by assuming that neighbouring sensors only are more highly *informationally* correlated, which does not necessarily entail that they have similar brightness values. Then, similarly to the optical flow method, we find sensors that are the same between t and $t + \delta t$, but that in this case are informationally the same instead of having the same brightness.

This can be illustrated by an example. Consider that the visual field with the layout shown in figure 8.2(a) has been reconstructed as shown in figure 8.2(b). Now the motion flow in a sensor S_x, for ex-

1	2	3	4	5	6	7	8
9	10	11	12	13	14	15	16
17	18	19	20	21	22	23	24
25	26	27	28	29	30	31	32
33	34	35	36	37	38	39	40
41	42	43	44	45	46	47	48
49	50	51	52	53	54	55	56
57	58	59	60	61	62	63	64

(a) Discrete map

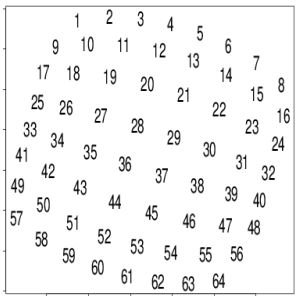

(b) Reconstructed map

Figure 8.2: Figure 8.2(b) shows the reconstructed visual field and 8.2(a) the discretized version used for the motion flow detection.

ample sensor 29 in the map of figure 8.2, can be computed by finding the sensor which is informationally closest to S_x in the temporal domain. Let S_x^t be the sensor we are interested in, in this case sensor 29, at time t and, $S_y^{t+\delta t}$ another sensor with all its values time-shifted δt time steps. Now sensoritopic maps can be created where the input is the time-series of the selected sensor S_x^t (in this case 29) and all the other sensors, $\{1, 2, \ldots, 28, 30, 31, \ldots, 64\}$ time-shifted by different δts in the range $\{1, 2, \ldots, \max\delta\}$. If the distance between two sensors S_x^t and $S_y^{t+\delta t}$ is zero or close to zero in one of the maps, the spatial relation between these two sensors describes the direction of the flow and δt can be used to estimate the relative speed.

A basic exploratory experiment was performed with the AIBO to test whether this actually works. The AIBO was placed in a sitting position in the lab capturing 20 frames of visual data per second. To simplify the experiment and results only four possible movements were allowed by the head: up, down, left, and right, using only one speed. Each possible movement was performed 30 times and all the data from each

movement saved to one file per movement. Then sensoritopic maps for each movement were created where all sensors, apart from sensor 36, were shifted in time one or two time steps to find the motion flow in the sensors that each movement induced.

Figure 8.3 shows examples of the created maps for all four movements. In each of these figures we find that sensor 1 is located in different corners of the sensor layout, while the ordering of the sensors is the same. This is due to the fact that the sensory reconstruction method does not find the real physical order of sensors, just their spatial positional relations[1]. We also find that for each map, the non-shifted sensor, 36, is in a very similar position as another sensor, which means that these two sensors are highly correlated. For example, in figure 8.3(c) we find that sensor 36 is closely correlated with 35. Looking at figure 8.2(a) sensor 35 is positioned to the left of sensor 36, which means the flow is from the right to the left. Similarly, if we look at for example figure 8.3(b), sensor 36 is completely correlated with sensor 44, which indicates a downward flow, which is the case since this flow was in fact induced by upward movements by the robot.

This method, of course, also has several serious drawbacks. One is undersampling. While ordinary optical flow computation can be done using only two frames of data, much more data is needed for this information theoretical method. It is also computationally expensive to compute the entropies for a large number of sensors with different time-shifts. One

[1]This could be corrected by assuming a fixed layout of the sensory field – see next section.

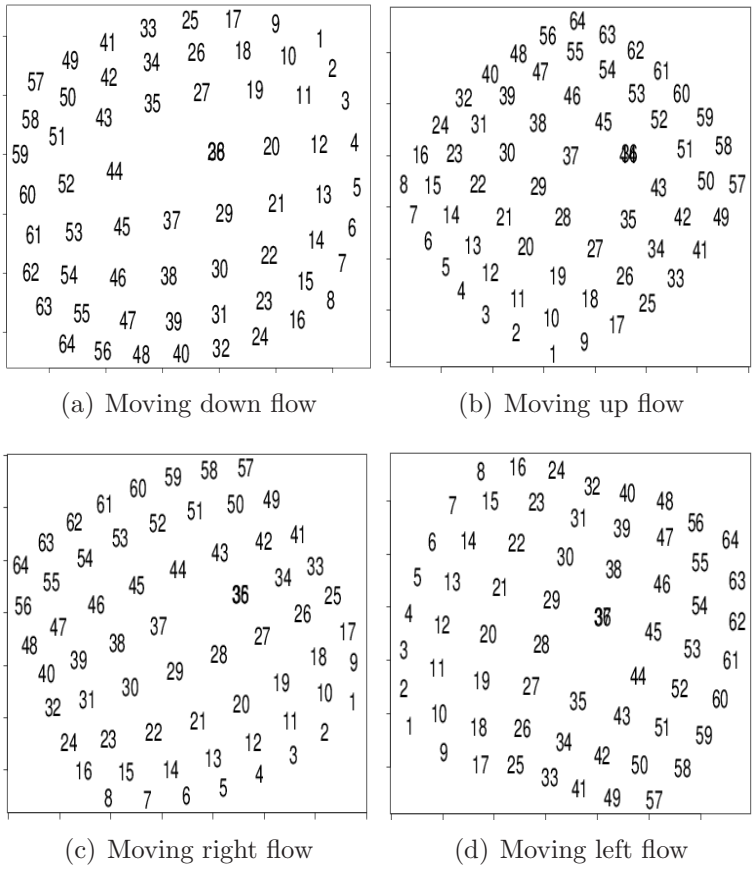

(a) Moving down flow (b) Moving up flow

(c) Moving right flow (d) Moving left flow

Figure 8.3: Figure 8.3(a) to 8.3(d) shows the sensoritopic maps with a time-shift of one for all sensors but sensor 36. The direction is found by finding what sensor the center sensor 36 is most closely correlated with. For example, in 8.3(b) sensor 36 is very close to sensor 44. Looking at the discretized map in 8.2(a) we find that this corresponds to a downward flow, which corresponds to an upward movement by the robot. In figure 8.3(a) the closest sensor is 28, in figure 8.3(c) the closest is sensor 35, and in figure 8.3(d) sensor 37. This corresponds to movements by the robot of down, right, and left.

advantage, though, is the fact this method does not assume a discrete and rectangular visual field, something that is often taken for granted in normal optical flow algorithms.

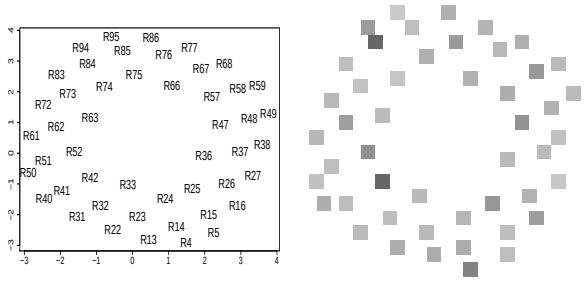

(a) Circular Visual Field (b) Image for optical flow calculation

Figure 8.4: Figure 8.4(a) shows the reconstructed visual field and 8.4(b) the corresponding image used in the optical flow calculation.

8.3 Motion Flow in Reconstructed Visual Fields

In previous chapters we have showed how visual fields can be reconstructed from raw sensor data in sensoritopic maps. How can these maps be used to compute optical flow using classical optical flow algorithms, which usually require rectangular visual fields?

This can be implemented as follows and will be exemplified in the next chapter where it is used for a robot to ground its actions in its own sensorimotor perceptions. Consider that the sensory reconstruction method has found that the visual field of a robot is two-dimensional and that the sensors are placed in a circle in the sensoritopic map, see figure 8.4(a). For each frame of data an image is created which is initially of uniform colour, for example all white. By discretizing the continuous coordinates of the sensors in the sensoritopic map of 8.4(a), the value of

each particular sensor in that time step can placed in its corresponding position in the image, resulting in an image such as figure 8.4(b). Now the optical flow can be computed between two images[2], and the motion vectors in the pixels corresponding to sensors can be saved.

8.4 Sensor Adaptation for Motion Flow

How can the classical optical flow algorithm be applied to sensor fields with sensors of different modalities, for example the red, green, and blue channels of camera pixels? Instead of the actual values varying smoothly over the sensors, just the correlatedness between the sensors will vary smoothly, and the closer two sensors are in the visual field, the smaller the informational distance will be. This may result in a lack of smooth change in sensory values as one moves over the sensoritopic map of the visual field. There are several possible solutions to this problem. One possibility is to partition the sensors based on value similarity and calculate the optical flow separately for each found partition. Another possible solution is to find a remapping of the sensor data to a mapping where the sensor values vary smoothly, while keeping the same information distance between all pairs of sensors as before. Here we will describe the second solution since that allows us to compute the optical flow using all sensors in one visual field rather than separate partitions.

The first problem to consider is how to find the greatest subset of sensors of the whole visual field where the sensor value as well as the

[2]We used the Lucas-Kanade algorithm (Lucas and Kanade, 1981) implemented in OpenCV: http://www.intel.com/research/mrl/research/opencv/

informational correlation varies smoothly over the sensors of the subset. This can be achieved by creating sensoritopic maps of the sensors using both the information metric, which measures the information correlatedness, and the 1-norm distance, which compares the values (in the case of visual sensors brightness) of the sensors. If a set of sensors is a visual field consisting of sensors of different modalities, say red and green sensors, the visual field will be reconstructed as one visual field in a sensoritopic map created using the information metric. This verifies that the all the sensors belong to a visual field, or sensors of other modalities with properties similar to visual sensors. Now, using the 1-norm distance, there will most probably be, depending on the data, one or more clusters per modality. This is exemplified in figure 8.5, where all the sensors are reconstructed to one sensor field in the information metric map, but where five sensors are separated from the rest in the 1-norm map. In this case, these are the five sensors that are of a different modality from the 95 other sensors.

The different subsets of the sensors in the 1-norm sensoritopic map can be found using the grouping algorithm described in section 3.5. Now all the subsets but the biggest can be combined into one subset of sensors, $\mathcal{S}_{adapt}$, which are the sensors that remain to be adapted. The biggest subset of sensors, $\mathcal{S}_f$, is the subset of sensors to which the subset $\mathcal{S}_{adapt}$ should be adapted. In our example above, $\mathcal{S}_{adapt} = \{G13, G27, G45, G63, G81\}$, and $\mathcal{S}_f$ the rest of the sensors ($R1, R2$, etc).

Let each sensor $S_a \in \mathcal{S}_{adapt}$, be a sensor that should be adapted to the sensors in $\mathcal{S}_f$ in such a way as to make the sensor value distances to

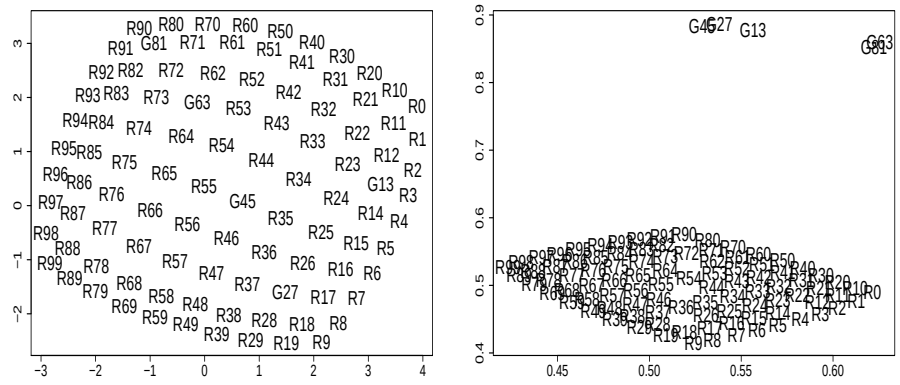

(a) Information metric (b) 1-norm

Figure 8.5: Sensoritopic maps using information metric and 1-norm. Sensors $\{13, 27, 45, 63, 81\}$ are green sensors, the rest are red. In figure 8.5(a) all the sensors are integrated in to one visual field. In the sensoritopic map created using the 1-norm distance of figure 8.5(b) the green sensors are in a separate cluster in the upper right corner.

the different sensors in $\mathcal{S}_f$ correspond to their informational distances. Here "adapted" means remapping the set of values taken by the sensor S_a so that it determines a formally new sensor S'_a. To achieve this, the adapted sensor should have the following properties:

1. The entropy of the adapted sensor should be the same as the original sensor.

2. The information distances between the adapted sensor and the fixed sensors should be the same as between the original sensor and the fixed sensors.

3. The 1-norm distances between the adapted sensor and the fixed

sensors should be the same as the informational distances between the original sensor and the fixed sensors.

Formally, the following three expressions should simultaneously be minimized, where $S_a^{'}$ is the adapted sensor:

$$\left| H(S_a) - H(S_a^{'}) \right|, \tag{8.1}$$

$$\frac{1}{|\mathcal{S}_f|} \sum_{X \in \mathcal{S}_f} \left| d_{IM}(X, S_a) - d_{IM}(X, S_a^{'}) \right|, \tag{8.2}$$

and

$$\frac{1}{|\mathcal{S}_f|} \sum_{X \in \mathcal{S}_f} \left| \frac{d_{IM}(X, S_a)}{d_{IM}(X, S_a)_{max}} - K(d_{1n}(X, S_a^{'})) \right|. \tag{8.3}$$

Here $d_{IM}(\cdot,\cdot)$ is the information metric (equation 3.2), $d_{1n}(\cdot,\cdot)$ is the 1-norm distance (equation 3.1), and $|\cdot|$ the absolute value or the cardinality of a set. In equation 8.3 $d_{IM}(X, S_a)_{max}$ is the maximum possible value of $d_{IM}(X, S_a)$, used to normalize $d_{IM}(\cdot,\cdot)$ in the range $[0, 1]$. Here $d_{IM}(X, S_a)_{max} = \log_2 |\mathcal{X}| + \log_2 |\mathcal{S}_a|$. The function $K(\cdot)$, $K : [0, 1] \rightarrow [0, 1]$, is used to scale the normalized 1-norm distance. This function is needed to compare the 1-norm and information metric distances since the spatial scaling of the information distances often is different from the scaling of the sensor (1-norm) values – see section 4.4 and later description of how $K(\cdot)$ can be estimated.

How can this minimization be computed? Following section 3.1 and 3.2, the value of a sensor for each time step t, S_a^t, is one symbol of the alphabet of the sensors, $\mathcal{X}$. If we, for example, assume that we use 10 bins, the alphabet is $\mathcal{X} = \{0, 1, \ldots, 9\}$. A remapping of S_a^t to $S_a^{t'}$ can

here be seen as a pairing of each possible value of S_a^t to a potentially different value of $S_a^{t'} = f(S_a^t)$, where $f : \mathcal{X} \rightarrow \mathcal{X}$. The function f is bijective which means that each possible value of S_a^t is mapped to a unique value. This can simply be implemented as an array of values, containing all the elements of $\mathcal{X}$ in some order, where the value of S_a^t used as an index can be used to compute $S_a t'$. For example, if the mapping is defined as $(2, 4, 6, 8, 0, 1, 3, 5, 7, 9)$, $S_a^t = 5$ will result in $S_a^{t'} = 1$ (index starts at 0). Now a particular remapping of a sensor can be evaluated by computing all three equations above for the collected sensor data and adding the three values together. To find the remapping that minimizes the equations given a particular set of data, all possible configurations can be enumerated and evaluated, or some kind of heuristic can be used to guide the search. The size of the search space depends on the size of the alphabet of the sensors. If $N = |\mathcal{X}|$ is the size of the alphabet, then $N!$ is the number of possible remappings. For instance, in most examples in this thesis 10 bins were used, which means that the search space has $10! = 3,628,800$ different possible mappings for each sensor to be adapted.

The scaling function in equation 8.3, $K(\cdot)$, can be found by comparing the information distances of pairs of sensors in $\mathcal{S}_f$ with the 1-norm distances of the same sensors to find the scaling relations for all possible values of $d_{1n}(X, S_a'), d_{IM}(X, S_a') \in [0, 1]$. In our implementation we approximated this by using an array of 100 values for the scaling constant indexed by multiplying $d_{1n}(X, S_a')$ by 100 and ignoring the decimals. Elements of the array that were not found by comparing the existing sensors

of $\mathcal{S}_f$ were estimated by considering a straight line interpolation between the values of the closest lower and higher index in the array. An example of the relation between the information metric distance and 1-norm distance can be found in the next section.

Although the search space of possible remappings per sensor is not huge considering the speed and memory capacity of present day computers, these computations are quite costly in terms of time because of the entropy calculations. However, by noting that a remapping of the values by a permutation does not change the entropy – remember that there are no semantics in information theory – equation 8.1 and equation 8.2 are actually superfluous, since these entropies will never change by remapping the values. The left expression of equation 8.3 needs to be computed only once. Consequently the right term of equation 8.3 is the only term that needs to be computed for each remapping when finding the minimal solution. This greatly simplifies the needed computations.

8.4.1 Experiments

To verify that the algorithm presented above for adapting sensors actually works, basic experiments were performed. The red AIBO data used in chapter 4 was used for the fixed set of sensors $\mathcal{S}_f$. Three different sensors were used as sensors to be adapted: a red sensor with a random map applied from position 31 (labeled *RM*), a red sensor where each sensor reading was transformed by replacing S_a^t by $255 - S_a^t$ for all time steps from position 57 (labeled *RT*), and a green sensor (labeled *G82*) from position 82. These are the three sensors that the algorithm should group

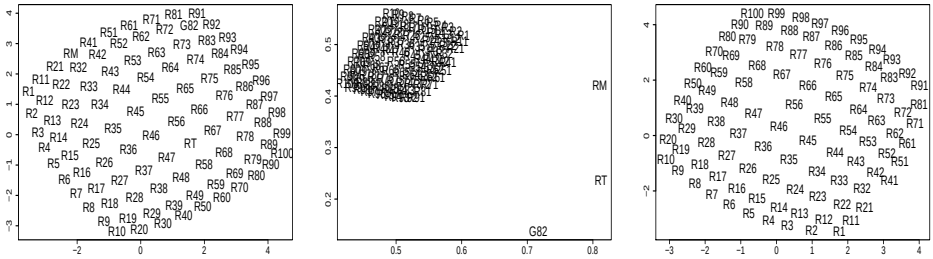

(a) Information metric - all sensors (b) 1-norm - all sensors (c) Information metric - only sensors in $\mathcal{S}_f$

Figure 8.6: Sensoritopic maps using information metric and 1-norm with three special sensors before adaptation. Figure 8.6(c) shows an information metric map with only the normal red sensors found by grouping - notice the missing sensors that should be in position 31, 57, and 82.

together as $\mathcal{S}_{adapt}$, and adapt to the normal red sensors in $\mathcal{S}_f$.

Figure 8.6 shows the information metric map and the 1-norm map before the adaptation. In the information metric map, figure 8.6(a), all the sensors including the three special sensors are already in their original layout. In figure 8.6(b), on the other hand, the three special sensors are far away from the cluster of the normal red sensors. Thus, the big group of 97 red sensors comprise the set of sensors that is fixed, $\mathcal{S}_f$, while the three sensors far away are grouped together as the sensors that should be adapted, $\mathcal{S}_{adapt}$. This was found by the grouping algorithm.

To evaluate the possible remappings the scaling function $K(\cdot)$ is first created by comparing the information metric and 1-norm distances between pairs of sensors of $\mathcal{S}_f$. Figure 8.7 shows the relation between the normalized information metric and the 1-norm distance between one sen-

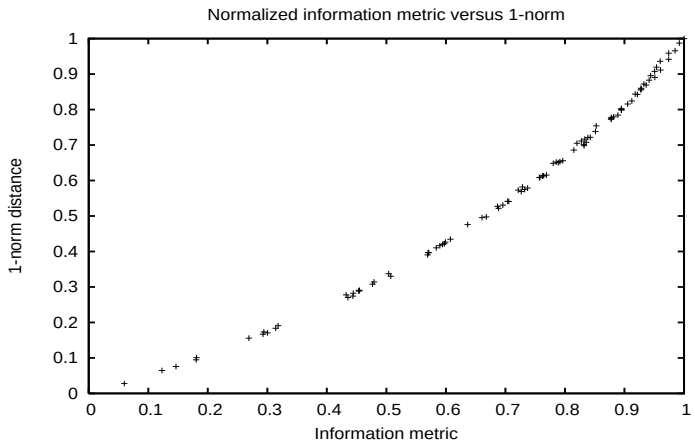

Figure 8.7: Example of normalized information metric and 1-norm distance used to estimate the scaling function $K(\cdot)$ in equation 8.3.

sor and all other sensors. As discussed before, this relation is related to the spatial scaling – see section 4.4. For each value of the 1-norm distance the scaling constant is found by dividing the information metric value of the corresponding point by the 1-norm value. For example, in figure 8.7, the scaling constant is approximately 1.5 when the 1-norm distance is 0.2, since the information metric for the same point is around 0.3. Missing points were approximated by assuming a straight line between the closest points higher and lower than the missing point.

The sensors in $\mathcal{S}_{adapt}$ were then adapted using the method described in the previous section, where hill-climbing was used to guide the search of possible remappings, starting with a random remapping. Figure 8.8(a), 8.8(b), and 8.8(c), show the sensoritopic maps after adaptation created using the 1-norm distance measure. Now the three sensors in $\mathcal{S}_{adapt}$ can be found in the same positions as in the information metric based map from

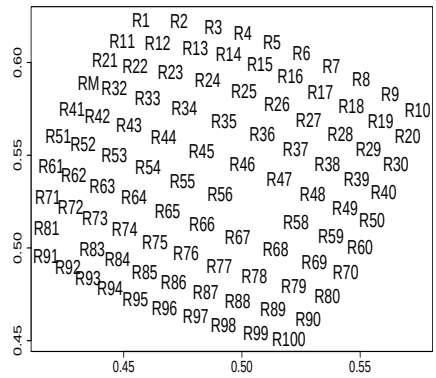

(a) 1-norm with RM adapted

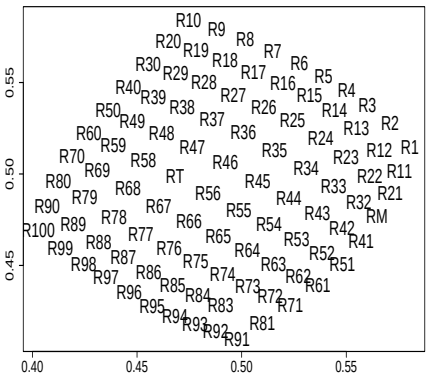

(b) 1-norm with RM and RT adapted

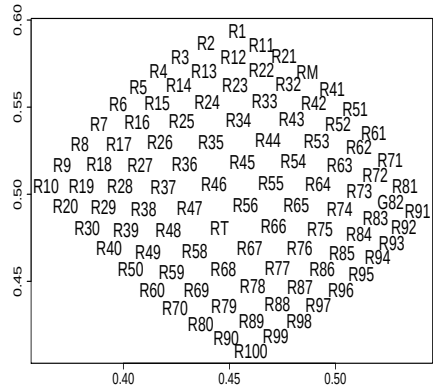

(c) 1-norm with RM, RT, and $G82$ adapted

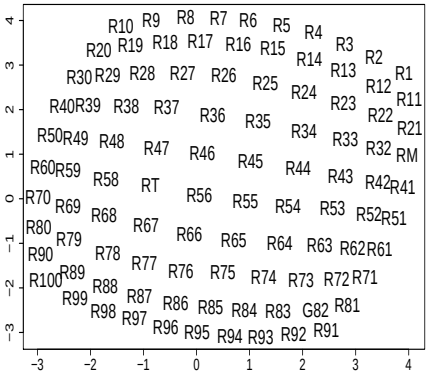

(d) Information metric with RM, RT, and $G82$ adapted

Figure 8.8: Maps using 1-norm distance and information metric after adaptation.

before the adaptation, figure 8.6(a). This means that the sensor values now vary smoothly over all the 100 sensors. Finally, figure 8.8(d) shows the information metric map after the adaptation with the three sensors *RM*, *RT*, and *G82* still in the same positions as before the adaptation.

This shows that the informational relations, as opposed to the values of the adapted sensors themselves, have not changed during the adaptation of the three sensors.

8.5 Conclusion

Optical flow analysis is a method for discovering and measuring local motion in images. One assumption in traditional optical flow analysis is that the sensor (brightness) values varies smoothly over the image, which in general means that all pixels (sensors) are of the same modality, e.g., all measuring the same intensity.

In chapter 4 we described how the sensory reconstruction method can reconstruct visual fields, or those consisting of other sensors with properties similar to those of visual sensors, but which consist of sensors of different modality (for instance, red, green, and blue sensors as showed in section 4.3.3). In section 8.2 the condition of values varying smoothly for computing optical, or, more generally, motion flow, was relaxed and generalized significantly by assuming that neighbouring sensors are only highly informationally correlated, which does not necessarily entail that they have similar sensor values. The motion flow in a certain sensor was computed by time-shifting the sensors around that sensor in the reconstructed sensory field and comparing the informational distance between this sensor and other sensors in different positions and times. This is loosely inspired by the way motion detection seems to work in the fly, where sensors are connected to correlators using temporal delays (Harris

et al., 1999). This method is relatively computationally expensive and needs much more data than normal optical flow techniques, which means that its introduction here is more a proof of concept than anything else.

In section 8.4 we described an algorithm for remapping the values of sensors while maintaining the same informational properties of the sensor itself as well as the informational relations with other sensors. This makes it possible to find a remapping in such a way as to keep the informational smoothness of a sensory field consisting of different modalities constant, and at the same time the sensor values vary smoothly over the image. This method and the optical flow method for reconstructed visual fields of section 8.3 make it possible to use traditional optical flow techniques on visual and other sensory fields of different modalities.

By reconstruction of its visual field and computation of motion flow using the methods of this chapter, a robot can develop to discriminate between motion of different directions in its sensors, where the discrimination is grounded in the experiences of the robot. How this can be done is the topic of the next chapter.

Chapter 9

Actions Grounded in Sensorimotor Perceptions

In the previous chapters we have studied various ways in which structure and organization can be found in sensor data of the robot without really taking in to account the movements performed by the robot. In this chapter we take the next step by presenting how the robot can learn actions that are grounded in its own sensorimotor perceptions. This is done by first learning the informational structure of the sensors as described in the earlier chapters of this thesis.

After learning the informational structure of the sensors, the effects that certain settings of the actuators have on the sensors are learned. This can be seen as learning a *forward model* (Jordan and Rumelhart, 1992) of the sensors and actuators, but via general means based on informational relations. Given a certain setting of the actuators (which constitute an action), what effect will this action have on the sensors?

For example, if the head is moved down, there will be a motion flow moving upwards in the visual sensors. This kind of learning is done autonomously by the robot, using the equivalent of body babbling in animals, here called *motor babbling*. The result of the motor babbling is a set of rules, or *sensorimotor laws*, describing the average effect actuator settings have on the sensors. These laws can then be used to perform movements that are guided by the sensors, e.g., by finding the sensorimotor law whose action corresponds the most to the perceived sensory input.

The rest of this chapter is structured as follows. The next section discusses how the space of possible actuator settings can be sampled when performing motor babbling. Section 9.2 describes the structure of sensorimotor laws and how they can be learned. How the appropriate sensorimotor law can be found for a certain effect in the sensors is described in section 9.3. Then the performed experiments and results are presented in section 9.4.

9.1 Sampling Actuator Space

The goal of motor babbling is to sample the space of possible actuator settings in as exhaustive a way as possible and to learn how to associate actions with sensory perceptions. While the methods presented in chapter 3 of the sensory reconstruction method were general and not dependent on a particular embodiment, sampling of actuator space is more dependent on the particular robot used. For example, some actuator

settings might physically harm the robot, or cause legs to get entangled in each other. Thus, some constraints might be necessary when sampling the possible settings of a robot's actuators.

In general, the aim is to sample, in as much detail as possible, the set of possible actuator settings, to understand how all the different actuator settings affect the sensors. As a basic example, consider a robot with two actuators, a_1 and a_2, where $a_1, a_2 \in \{-1, 0, 1\}$. This means that the whole actuator space consists of only 9 possible settings. In most robots this space is much larger, with more actuators, and more possible values (maybe continuous) for each actuator. There might also be a many-to-one mapping between the actuator vectors and the actual values sent to the motor, which means that more than one actuator vector might give the same effect in the motors.

Also, for more robust learning, each movement needs to be performed several times, resulting in a number of samples of sensor data for each possible movement. This is necessary since many sensors are sensitive to noise and the structure of the environment. There might also be moving objects in front of the robot, something that will seriously affect, for example, motion flow calculations.

9.2 Learning Sensorimotor Laws

The result from motor babbling as described above is a collection of sensor data associated with each possible actuator setting. This data can be used to compute the *sensorimotor laws*. Here a sensorimotor law

is defined as the average affect a certain actuator setting will have on a set of sensors.

Let the sensor S_n at position (x, y) in the two-dimensional visual field of section 8.3 be associated with its average effect for a certain actuator setting a as $\langle \vec{v}_{x,y,a} \rangle$. Here the effect of a certain actuator setting is defined as the optical flow in this sensor computed using the method of 8.3. The average effect is defined as the average optical flow in this sensor over all frames of data T for that particular setting a,

$$\langle \vec{v}_{x,y,a} \rangle = \frac{1}{T} \sum_{t=1}^{T} \vec{v}_{x,y,a,t}, \tag{9.1}$$

where $\vec{v}_{x,y,a,t}$ is the optical flow in $\vec{v}_{x,y,a}$ between time t and $t+1$.

A sensorimotor law for actuator setting a, SM_a, is defined as a matrix consisting of the average motion flow vectors for all the sensors in the two-dimensional grid with width w and height h:

$$SM_a = \begin{pmatrix} \langle \vec{v}_{1,1,a} \rangle & \langle \vec{v}_{2,1,a} \rangle & \cdots & \langle \vec{v}_{w,1,a} \rangle \\ \langle \vec{v}_{1,2,a} \rangle & \langle \vec{v}_{2,2,a} \rangle & \cdots & \langle \vec{v}_{w,2,a} \rangle \\ \vdots & \vdots & \ddots & \vdots \\ \langle \vec{v}_{1,h,a} \rangle & \langle \vec{v}_{2,h,a} \rangle & \cdots & \langle \vec{v}_{w,h,a} \rangle \end{pmatrix} \tag{9.2}$$

Since the actual field of the robot might not be rectangular, see section 8.3, some motion vectors will be of zero length since they are not associated with a sensor. This is not a problem since the layout of the visual field is the same for all sensorimotor laws SM. It might be the case that different actuator settings will have the same, or very close to the same,

effect on the sensors of the robot, even though they are different for an external observer. These two actuator settings should still be combined in to one sensorimotor law as the only information the robot has about itself and its environment is based on its own sensors.

For many movements if a rectangular visual field is used, for example pan and tilt motions, the vectors of the vector field will be of more or less uniform magnitude. If all possible actuator settings are of this kind in a certain experiment, sensorimotor laws can be simplified by computing the average over the whole matrix, excluding positions not corresponding to any sensor, and let the sensorimotor law SM_a be equal to the average of all motion vectors $\vec{v}_{x,y,a}$. This was done in (Olsson et al., 2005a).

9.3 Sensory Guided Movement

The set of sensorimotor laws can now be used to perform actions where a specific effect on the sensors is desired. For example, if the robot perceives a motion, the motion can be mimicked by performing an action from the set of sensorimotor laws that has as similar as possible an effect on the sensors as the observed motion.

To track a particular motion, the robot needs to find the sensorimotor law with effect closest to the perceived movement P, represented as a optical flow matrix like the sensorimotor law, equation 9.2. Given a set of learned sensorimotor laws, a law closest to the perceived visual movement can be found by minimizing some measure $D(SM, P)$ between the perceived flow P and sensorimotor law SM. Perhaps the most natural

is the one-norm:

$$D(SM, P) = \sum_{x,y} |SM_{x,y} - P_{x,y}| \tag{9.3}$$

If the perceived motion is caused by a moving object much smaller than the visual field, many of the vectors in P will be zero. Thus, vectors that are of zero magnitude in P are not compared.

An alternative to the one-norm is presented in (Lee and Seung, 2001), which is computed separately for the x and y component of the flow matrix. This distance is defined as

$$D(SM^c||P^c) = \sum_{x,y} \left(SM^c_{x,y} \log_2 \frac{SM^c_{x,y}}{P^c_{x,y}} - SM^c_{x,y} + P^c_{x,y} \right), \tag{9.4}$$

where c is either the x or y component of the flow. This distance measure reduces to the Kullback-Leibler divergence if $\sum_{x,y} SM_{x,y} = \sum_{x,y} P_{x,y} = 1$, and it can be made symmetric by $D(SM^c, P^c) = D(SM^c||P^c) + D(P^c||SM^c)$.[1] Finally, to compute the measured difference between the two matrices P and SM the distances of the two components x and y are added together. The methods of this section generalize in the obvious manner from sensory fields of two-dimensions to n-dimensional ones.

[1]It should be noted that strictly speaking, this is not a metric since the triangle inequality does not hold for the Kullback-Leibler divergence (Cover and Thomas, 1991).

9.4 Experiments

Here we present experiments performed with an AIBO learning sensorimotor laws starting with raw and unstructured sensors and actuators.

9.4.1 Experimental Setup

The experiments were performed in a laboratory with no windows that could seriously affect light conditions. The robot was placed in a sitting position overlooking the lab.

The AIBO has many degrees of freedom and to simplify the experiments we decided to only use the pan (horizontal movement) and tilt (vertical) motors of the head of the AIBO. To put less strain on the neck of the AIBO (which is the component that most often breaks down), we let the maximum pan and tilt be 0.5 and the minimum -0.5, where the possible values of the neck are in the range $[-0.6, 0.6]$. To move the neck the desired position of the pan and tilt motor were set 100 times per second, adding the value of the corresponding actuator setting each time step, until the maximum or minimum value of the pan or tilt had been reached. In our experiments the possible desired speed, s, for each of the two actuators was limited to three different values, $s \in \{-0.02, 0.0, 0.02\}$.

9.4.2 Results

The aim of this experiment was to have the robot develop from no knowledge of its sensors and actuators to a model of the relations between its sensory input and actions. As described above, 100 visual sensors were

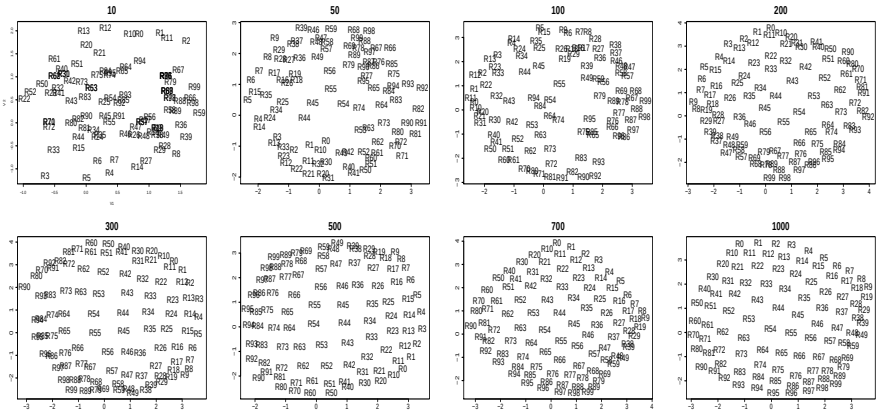

Figure 9.1: Development of sensoritopic map of visual field over time from 10 to 1000 time steps.

used and the robot had two actuators, pan and tilt. The first step was to reconstruct the visual field as described in chapter 4. Figure 9.1 shows the organization of the visual field used for learning the sensorimotor laws.

Using the reconstructed visual field in figure 9.1 optical flow can be computed as shown in section 8.3. Body babbling as described in section 9.1 was then used to sample the space of possible actuator settings. As mentioned above this particular experiment only used three possible settings per actuator, giving a total of eight possible non-zero settings. Each possible setting was executed 50 times, giving a total of roughly 1000 frames of data per setting.

Given this data the sensorimotor laws were computed as per section 9.2. Figure 9.2 shows the computed sensorimotor laws. The directions of the motions' vectors do not correspond exactly to an external observer's

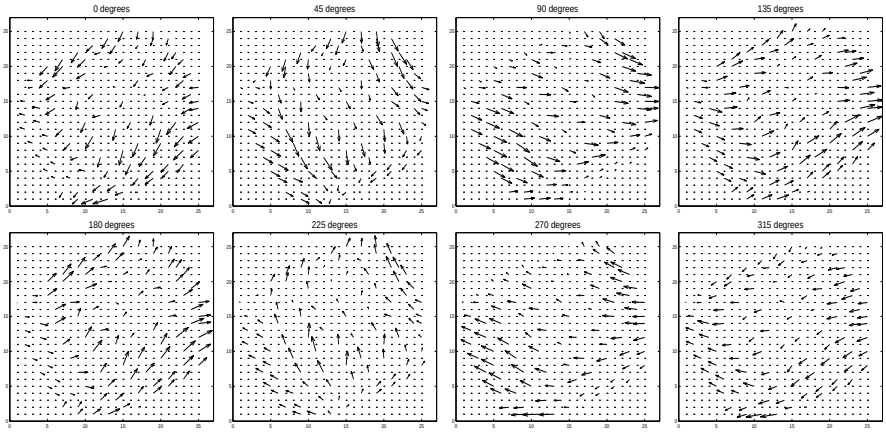

Figure 9.2: The discovered sensorimotor laws corresponding to motion of the head where 0 degrees is moving the head up, 180 degrees moving the head down, and 90 degrees to the right.

notion of direction of the movement. This is due to the reconstructed field being angled with respect to the x and y axes, which is unavoidable since the robot does not know anything about the real locations of the sensors, and grounds all actions and knowledge about its sensors and actuators in its own sensorimotor perceptions.

To verify that the method computed similar sensorimotor laws each time, the experiment was performed 10 times with each movement being executed 50 times as described above. Then the two distances functions of section 9.3 were used to compute the distance between the sensorimotor law computed for each time. The results showed that the learned laws were very similar, with an average distance of 1.2% for the one-norm distance and 0.9% for equation 9.4 averaged over all eight actuator settings and the 10 experiments.

When the sensorimotor laws have been autonomously found, the

Figure 9.3: Image displayed on wall in front of robot.

robot can now use these laws to detect motion and find which actuator setting corresponds to the perceived motion. To verify this step, two experiments were performed. In both experiments the AIBO was placed in front of a wall of uniform colour with a video projector displaying images on the wall. In the experiments the whole image on the wall moved in different directions. This was implemented by having an image, shown in figure 9.3, larger than the screen and only displaying a part of the image at any given time. The speed of the moving image was adjusted to be similar to the speed of the moving AIBO head. When the image was moved in front of the robot, 2 or 10 frames of data were used to compute the optical flow to find the sensorimotor law most similar to the experienced movement. In the case of ten frames the optical flow was averaged as in equation 9.2. The motion closest to the perceived motion could then be compared with the actual movement of the image on the wall.

$D(SM,P)$ / Action	O. 2	O. 10	K. 2	K. 10
0 degrees	75.5%	90.1%	79.2%	91.9%
45 degrees	77.0%	92.8%	78.7%	92.4%
90 degrees	76.6%	91.2%	79.7%	94.4%
135 degrees	75.1%	93.0%	77.7%	93.2%
180 degrees	74.8%	91.5%	75.3%	92.6%
225 degrees	77.1%	93.3%	77.2%	93.8%
270 degrees	76.1%	93.2%	78.8%	92.5%
315 degrees	74.8%	91.4%	76.6%	93.0%

Table 9.1: Percentage of correctly detected motion flows using the (o)ne-norm and (K)ullback-Leibler measure for two and 10 frames for the different directions out of eight possible flows.

Table 9.1 shows a comparison of the different distance measures and the performance of the motion detection for 200 examples of each movement. As expected the averaged motion flow over 10 frames was more often correctly classified than over only two frames. The one-norm and Kullback-Leibler distance measures performed similarly, with a slightly higher average performance for the latter for the optical flow computation between only two frames.

9.5 Conclusion

In the present chapter the robot developed a set of sensorimotor laws – rules describing the informational relations between actuator settings and effects in sensors – starting from uninterpreted sensor data. As in previous chapters the informational relationships between sensors were found and the visual field reconstructed. Then motor babbling – structured

exploration of the actuators – was used to find the relations between the actuator settings and the values of the sensors. These sensorimotor laws were then used to identify what action corresponded to a certain perceived effect in the sensors.

The learning was based on the robots own sensorimotor perceptions – there was no "built in" concepts of for example "up" or "down" – and the learned movements were solely grounded in the robot's own sensory experiences of performing the movements. In the presented experiments visual sensors were used but in general the method can be used with any sensors where movements have an informationally piecewise smooth effect on the sensors, for example tactile sensors.

Chapter 10

Summary and Future Directions

The central thesis of this dissertation is that information-theoretic methods can be used to ground the ontogeny of sensorimotor systems of embodied robots. We have presented and studied methods that will allow robots to develop and ground their perceptions and actions in their own sensor experiences – their Umwelt – rather than having these capabilities "built-in" by the designer of the robot. The idea is that by having a robot that can develop and adapt depending on its particular embodiment, environment, and tasks to perform, the robot's repertoire will be more open-ended and less susceptible to changing environmental conditions or faults in the robot itself. Central to the presented methods are the informational relations between sensors. To study these relationships we have used the framework of information theory, which is a general framework for analyzing communication and statistical relationships in

communication channels (Shannon, 1948).

In the next section we summarize our main results and contributions to knowledge. In section 10.2 we discuss possible applications of the presented methods and section 10.3 presents some directions for future research.

10.1 Summary of Contributions

One of our main contributions to knowledge is the introduction of the information metric (Crutchfield, 1990) as a distance measure to be used in the sensory reconstruction method, first introduced by Pierce and Kuipers (1997). The information metric generalizes the sensory reconstruction method by capturing all statistical relationships between sensors, instead of just linear correlations. This enables the sensory reconstruction method to find all informational relationships between sensors – something that, for instance, was used in chapter 4 for autonomous reconstruction of the spatial organization of visual fields of different shapes and modalities. Following our work, the sensory reconstruction method with the information metric has now also been used by other researchers. Hafner and Kaplan (2005), for instance, used it to study the body correspondence problem (Alissandrakis, 2003), and Kaplan and Hafner (2005) used it to compare different sensorimotor organizations.

The sensory reconstruction method can also be used for integration of sensors that share some informational properties into higher level sensor elements. This was shown in several chapters of thesis where the spatial

organization of the visual sensors was found, which allowed the sensors to be combined into a higher level visual field. This is also possible using the 1-norm distance, used by Pierce and Kuipers (1997), in the case when all the sensors are of the same modality and have similar sensor values. However, by using the information metric, it is enough that the sensors are informationally related, which does not necessarily entail that the sensor values themselves are linearly correlated.

In chapter 7 we asked why the information metric should be used in the sensory reconstruction method. Why not use the Kullback-Leibler divergence, Jensen-Shannon divergence, the correlation coefficient, the Hellinger distance, or any other measure? In chapter 7 we compared the information metric with these other measures, suggested by reviewers of our papers and colleagues, by using them as the distance measure between sensors in the sensory reconstruction method. Experiments with data collected from the AIBO robot from visual sensors of different modalities showed that the information metric was the only one of the tested distance measures to reconstruct the spatial organization of the real visual field of the robot. This is due to the information metric taking into account all informational relations between the sensors, by considering both the individual entropies as well as the joint entropies of the sensors.

The informational relations between sensors depend on the statistical structure of the incoming sensor data, and in chapter 4 we studied the scaling of spatial and temporal coherence in visual sensor data of the AIBO robot. The results confirmed previous studies in neuroscience

– see, for instance, Ruderman (1994) – where the spatial coherence in natural images was found to scale as a power law. We also found the temporal coherence in the collected AIBO visual data to scale as a power law. This is something that, to the best of our knowledge, has never before been studied in neuroscience or robotics. Similar structure has been found in sensor data of other modalities, such as acoustic signals (Rieke et al., 1999), and one possible avenue for future research is to study how power law scaling of spatial and temporal coherence can be exploited in robotics.

We have also presented methods for adapting individual sensors. One is entropy maximization, which optimizes – from an information-theoretic point of view – the representation of the incoming data. It was also shown in chapter 6 that entropy maximization enables the robot to find the spatial organization of some visual fields of different modalities with specific characteristics not found by uniform binning of the sensor data.

In chapter 8 we presented a novel algorithm for sensor adaptation of an individual sensor in relation to a set of other sensors. The goal of this algorithm was to adapt a set of sensors, for example a visual field consisting of sensors of different modalities, in such a way as to make the distances between the values of the sensors vary with the same smoothness as the informational distances. This makes it possible to apply classical optical flow algorithms to visual fields consisting of sensors of different modalities such as red, green and blue sensors. Experiments with a red visual field, one randomly remapped sensor, one inverted sensor, and one green sensor, showed that the hill-climbing algorithm found remappings

which made the value relations correspond to the informational relations. Sensoritopic maps created before and after the adaptation verified that the brightness values had been remapped in the desired fashion while the informational relations remained the same.

Finally, in chapter 9 we demonstrated that the robot, once the visual sensor organization has been found, can ground its actions in its sensorimotor perceptions. The relations between the actuators and sensors are found by body babbling, where the average effect that different actuators settings have on the sensors is computed by the information flow in the sensors. This enables the robot to develop, starting from no innate knowledge of its sensors and actuators, the abilities to select actions that have a predictable effect on the sensors, according to autonomously discovered sensorimotor laws. Or, conversely, to select an action that corresponds to a certain perceived effect in its sensors.

10.2 Possible Applications

Apart from the applications of our work to developmental robotics, the presented methods can possibly also be applied to related problems in some other areas as well. One example is in computer security, where the methods developed in our work can be applied to system call prediction and building models of executing processes, which can be used for anomaly and intrusion detection (Olsson, 2003). Another possible application is sensor networks (Akyildiz et al., 2002), where potentially thousands or millions of smart sensors are connected together. Here our

methods can be applied to find structure in the data, identify redundant sensors, and maybe also to help to understand the trade-offs of cost versus utility of using different sensor network configurations.

The presented methods can also find applications in space science and other fields where recovery, self-reconfiguration, sensor channel selection, and adaptive sensing are important. For instance, consider an autonomous robot on the surface of Mars that is hit by some space debris. Perhaps parts of the central processing unit are damaged and need to be reconfigured (Macias and Durbeck, 2002), or the camera and lens might be displaced or damaged. In both situations there is a need for the control system to learn a new model of the robot's sensors. Another example of the need to organize sensory channels arises from the fact that modern sensors provide high data rates, where not all of the information is relevant to solve a certain task, while storage and on-board processing capabilities are limited (Keymeulen et al., 2001). Also, in some situations, e.g., space exploration, not everything about the environment might be known and the conditions – for instance light and temperature, can change drastically over time – making adaptation of the sensor systems a crucial part of their specification.

10.3 Future Directions

There are also several future directions for research in the areas presented in this thesis. While most studies of the statistics and informational organization of sensor data in neuroscience as well as robotics have focused on

vision – see, for instance, Ruderman (1994) and Lungarella et al. (2005) – it would be interesting to study the statistical properties of other sensor modalities. One alternative would be to use a *Time-of-Flight* camera (Knoop et al., 2006), which produces depth images where the value of each pixel represents the distance to the nearest object from that particular pixel. Here the spatial and temporal scaling can be studied and compared with the spatial and temporal coherence in visual images of the same scenes. Does the temporal and spatial scaling follow a power law and is the spatial layout of the Time-of-Flight camera found by the sensory reconstruction method? It would also be interesting to study sensors organized in three dimensions. One option would be to study pressure sensors embedded in some fluid, or maybe distance sensors embedded in a rolling ball. As mentioned before it would also be fruitful to study if and how the power law scaling properties of certain sensor data can be exploited in robotics on a higher-level, and what general implications the statistics of natural environments have for robotic systems. Related to this is to study the statistical structure on higher level sensor data, far removed from the sensory periphery (Lungarella et al., 2005).

On a longer time scale are we interested in studying how a robot can be designed to optimally structure its sensor input and sensorimotor organizations, depending on the informational relations of its sensors, actions, the costs of sensing, and particular environment. For a recent attempt in this direction – see Lichtensteiger and Pfeifer (2002). One important issue to consider is how optimization, or specialization, to a particular environment might affect future adaptation – how can the

robot detect a non-optimal configuration in a new environment if its sensors and actuators are highly specialized and adapted for the previous environment?

To conclude, has this thesis presented methods based on information theory that could help robots, as well as the poor fellow of Franz Kafka's *Metamorphosis*, develop an understanding of their hitherto unknown bodies and the unstructured symphony of information available in their sensors.

Appendix A

Publications

The work presented in this thesis has been published in seven international peer-reviewed conference papers and one journal article. Here we list these publications and how they relate to the thesis.

1. Lars Olsson, Chrystopher L. Nehaniv, Daniel Polani, 2004, **Sensory Channel Grouping and Structure from Uninterpreted Sensor Data**, in *Procedings of the 2004 NASA/DoD Conference on Evolvable Hardware June 24-26, 2004 Seattle, Washington, USA*, IEEE Computer Society Press, 153–160.
   This paper introduced the idea of using the information metric in the sensory reconstruction method as described in **chapter 3**, and applied it to AIBO sensor data and descrambling of scrambled visual fields presented in **section 4.3.4**.

2. Lars Olsson, Chrystopher L. Nehaniv, Daniel Polani, 2004, **Information Trade-Offs and the Evolution of Sensory Layouts**,

in *Proceedings of the Ninth International Conference on the Simulation and Synthesis of Living Systems (ALIFE9) September 12-15th 2004 Boston, Massachusetts, USA*, MIT Press, 119–124.
Studied the evolution of sensory layouts in different environments and under different informational constraints. Introduced *informational coverage*, a measurement of redundancy and novelty similar to the concepts of integration and complexity of Tononi et al. (1998).

3. Lars Olsson, Chrystopher L. Nehaniv, Daniel Polani, 2004, **The Effects on Visual Information in a Robot in Environments with Oriented Contours**, in *Proceedings of the Fourth International Workshop on Epigenetic Robotics: Modeling Cognitive Development in Robotic Systems*, Lund University Cognitive Studies, 83–88.
Section 5.3 is based on this paper.

4. Lars Olsson, Chrystopher L. Nehaniv, Daniel Polani, 2005, **Sensor Adaptation and Development in Robots by Entropy Maximization of Sensory Data**, in *Proceedings of the Sixth IEEE International Symposium on Computational Intelligence in Robotics and Automation (CIRA-2005)*, IEEE Computer Society Press, 587–592.
Chapter 6 is based on this paper.

5. Lars Olsson, Chrystopher L. Nehaniv, Daniel Polani, 2005, **From Unknown Sensors and Actuators to Visually Guided Move-**

ment, in *Proceedings of the Fourth International Conference on Development and Learning (ICDL 2005)*, IEEE Computer Society Press, 1–6.

This is similar to **chapter 9** in this thesis but uses single vectors to represent sensorimotor laws, rather than the vector fields used in this thesis.

6. Lars Olsson, Chrystopher L. Nehaniv, Daniel Polani, 2005, **Discovering Motion Flow by Temporal-Informational Correlations in Sensors**, in *Proceedings of the Fifth International Workshop on Epigenetic Robotics: Modeling Cognitive Development in Robotic Systems*, Lund University Cognitive Studies, 117–120.

   Section 8.2 is based on this paper.

7. Lars Olsson, Chrystopher L. Nehaniv, Daniel Polani, 2006, **Measuring Informational Distances Between Sensors and Sensor Integration**, accepted for oral presentation at *the Tenth International Conference on the Simulation and Synthesis of Living Systems (ALIFEX)*, Bloomington, June 2006.

   Chapter 7 is based on this paper.

8. Lars Olsson, Chrystopher L. Nehaniv, Daniel Polani, 2006, **From Unknown Sensors and Actuators to Actions Grounded in Sensorimotor Perceptions**, in *Connection Science*, vol 18, issue 2, in press.

   Chapter 9 is based on this journal article. Also introduced the idea of finding motion flow in sensor fields of different modalities

described in **section 8.4** in this thesis but provided no algorithm. This paper introduced the method for computing optical flow in non-rectangular visual fields presented in **section 8.3** and some results of sensor reconstruction of visual field of different shapes and modalities presented here in **section 4.3.2** and **4.3.3**.

Bibliography

I. F. Akyildiz, W. Su, Y. Sankarasubramaniam, and E. Cayirci. A survey on sensor networks. *IEEE Communications Magazine*, 40:102–114, 2002.

A. Alissandrakis. *Imitation and Solving the Correspondence Problem for Dissimilar Embodiments - A Generic Framework*. PhD thesis, University of Hertfordshire, 2003.

P. Andry, P. Gaussier, J. Nadel, and B. Hirsbrunner. Learning invariant sensorimotor behaviors: A developmental approach to imitation mechanisms. *Adaptive Behavior*, 12(2):117–140, 2004.

D. Ballard. Animate vision. *Artificial Intelligence*, 48:57–86, 1991.

H. B. Barlow. Possible principles underlying the transformation of sensory messages. *Journal of Sensory Communication*, pages 217–234, 1961.

H. B. Barlow. Redundancy reduction revisited. *Network: Computational Neural Systems*, 12:241–253, 2001.

A. Basu, I. R. Harris, and S. Basu. Minimum distance estimation: The approach using density-based distances. In G. S. Maddala and C. R. Rao, editors, *Handbook of Statistics*, volume 15, pages 21–48, 1997.

R. Beer, H. Chiel, R. Quinn, and R. Ritzmann. Biorobotics approaches to the study of motor systems. *Current Opinion in Neurobiology*, 8: 777–782, 1998.

N. Bernstein. *The Co-ordination and Regulation of Movements*. Pergamon Press, 1967.

L. Berthouze and Y. Kuniyoshi. Emergence and categorization of coordinated visual behavior through embodied interaction. *Machine Learning*, 31:187–200, 1998.

L. Berthouze, Y. Shigematsu, and Y. Kuniyoshi. Dynamic categorization of explorative behaviors for emergence of stable sensorimotor configurations. In *Proceedings of the International Conference on Simulation of Adaptive Behavior (SAB1998)*, pages 67–72, 1998.

B. Y. Betsch, W. Einhäuser, P. Körding, and P. König. The world from a cat's perspective – statistics of natural videos. *Biological Cybernetics*, 90:41–50, 2004.

W. Bialek and R. R. de Ruyter van Steveninck. Features and dimensions: Motion estimation in fly vision. *submitted*, 2004.

J. Bird and P. Layzell. The evolved radio and its implications for modelling the evolution of novel sensors. In *Proceedings of the 2002*

Congress on Evolutionary Computation (CEC2002), pages 1836–1841, 2002.

C. Blakemore and C. F. Cooper. Development of the brain depends on the visual environment. *Nature*, 228:477–478, 1970.

D. Blank, D. Kumar, L. Meeden, and J. Marshall. Bringing up a robot: fundamental mechanisms for creating self-motivated, self-organizing architecture. *Cybernetics and Systems*, 36(2), 2005.

N. Brenner, W. Bialek, and R. de Ruyter van Steveninck. Adaptive rescaling maximizes information transformation. *Neuron*, 26:695–702, 2000.

R. Brooks. Intelligence without representation. *Artificial Intelligence*, 47:139–160, 1991.

E. M. Callaway. Visual scenes and cortical neurons: What you see is what you get. *Proceedings of the National Academy of Sciences*, 95(7): 3344–3345, 1998.

Peter Cariani. To evolve an ear: Epistemological implications of Gordon Pask's electrochemical devices. *Systems Research*, 10(3):19–33, 1993.

R. B. Cattell. The scree test for the number of factors. *Multivariate Behavioral Research*, 1(1):629–637, 1966.

B. Chapman, M. P. Stryker, and T. Bonhoeffer. Development of orientation preference maps in ferret primary visual cortex. *Journal of Neuroscience*, 16(20):6443–6453, 1996.

D.M. Coppola, H. R. Purves, A. N. McCoy, and D. Purves. The distribution of oriented contours in the real world. *Proceedings of the National Academy of Sciences*, 95:4002–4006, 1998.

T. M. Cover and J. A. Thomas. *Elements of Information Theory*. John Wiley & Sons, Inc., 1991.

J. P. Crutchfield. Information and its Metric. In L. Lam and H. C. Morris, editors, *Nonlinear Structures in Physical Systems – Pattern Formation, Chaos and Waves*, pages 119–130. Springer Verlag, 1990.

K. Dautenhahn, D. Polani, and T. Uthmann. *Artificial Life (Special Issue on Sensor Evolution)*, 7(2), 2001.

D. B. Dusenbery. *Sensory Ecology*. WH Friedman & Co, first edition, 1992.

G. Edelman. *Neural Darwinism: the theory of neural group selection*. Basic Books, 1987.

D. M. Endres and J. E. Schindelin. A new metric for probability distributions. *IEEE Transactions on Information theory*, 49(7):1858–1860, 2003.

J. Ernst, G. J. Nau, and Z. Bar-Joseph. Clustering short time series gene expression data. In *Proceedings of ISMB*. to appear, 2005.

D. J. Field. What is the goal of sensory coding? *Neural Computation*, 6:559–601, 1994.

J. Fodor. *Representations*. Harvester Press, 1981.

W. Gibson. *Neuromancer*. Voyager, 1986.

G. Goodhill, S. Finch, and T. Sejnowski. Quantifying neighbourhood preservation in topographic mappings. *Institute for Neural Computation Technical Report Series, No. INC-9505*, 1995.

V. Hafner and F. Kaplan. Interpersonal maps and the body correspondance problem. In Y. Demiris, K. Dautenhahn, and C. L. Nehaniv, editors, *Proceedings of the AISB 2005 Third International Symposium on Imitation in Animals and Artifacts*, pages 48–53, 2005.

S. Harding and J. F. Miller. Evolution in materio: A tone discriminator in liquid crystal. In *Proceedings of the 2004 Congress on Evolutionary Computation 2004 (CEC2004)*, pages 1800–1807, 2004.

S. Harnad. The symbol grounding problem. *Physica D*, 42:335–346, 1990.

R. A. Harris, D. C. O'Caroll, and S. B. Laughlin. Adaptation and the temporal delay filter of fly motion detectors. *Vision Research*, 39(16): 2603–2613, 1999.

R. Held and A. Hein. Movement produced stimulation in the development of visually guided behavior. *Journal of Comparative Physiology and Psychology*, 56:872–876, 1963.

M. I. Jordan and D. E. Rumelhart. Forward models: Supervised learning with a distal teacher. *Cognitive Science*, 16:307–354, 1992.

Franz Kafka. *The Transformation (Metamorphosis) and Other Stories.* Penguin Books, 1992.

E.R. Kandel, J.H. Schwartz, and T.M Jessell. *Principles of Neuroscience.* McGraw-Hill, fourth edition, 2000.

F. Kaplan and V. Hafner. Mapping the space of skills: An approach for comparing embodied sensorimotor organizations. In *Proceedings of the 4th IEEE International Conference on Development and Learning (ICDL-05)*, pages 129–134, 2005.

D. Keymeulen, R. Zebulum, A. Stoica, and M. Buehler. Initial experiments of reconfigurable sensor adapted by evolution. In *International Conference on Evolvable Systems, October 2001*, pages 303–313. Springer-Verlag, 2001.

A. S. Klyubin, D. Polani, and C. L. Nehaniv. Tracking information flow through the environment: Simple cases of stigmergy. In *Artificial Life IX: Proceedings of the Ninth International Conference on the Simulation and Synthesis of Living Systems*, pages 563–568. Springer, 2004.

A. S. Klyubin, D. Polani, and C. L. Nehaniv. Empowerment: A universal agent-centric measure of control. In *Proceedings of the 2005 IEEE Congress on Evolutionary Computation*, pages 128–135. IEEE Press, 2005a.

A. S. Klyubin, D. Polani, and C. L. Nehaniv. All else being equal be empowered. In *Advances in Artificial Life: Proceedings of the 8th European Conference on Artificial Life*, pages 744–753. Springer, 2005b.

S. Knoop, S. Vacek, and R. Dillmann. Sensor fusion for 3d human body tracking with an articulated 3d body model. In *Proceedings of the IEEE International Conference on Robotics and Automation*, 2006.

T. Kohonen. *Self-organizing maps*. Springer-Verlag, Berlin, third edition, 2001.

A. Korner and H. Kraemer. Individual differences in spontaneous oral behavior in neonates. In J. Bosma, editor, *Proceedings of the 3rd Symposium on Oral Sensation and Perception*, pages 335–346, 1972.

W. J. Krzanowski. *Principles of Multivariate Analysis: A User's Perspective*. Clarendon Press, Oxford, 1988.

Y. Kuniyoshi, Y Yorozu, M. Inaba, and H. Inoue. From visuo-motor self learning to early imitation - a neural architecture for humanoid learning. In *International conference on robotics and Automation*, pages 67–72, 2003.

M. Kuperstein. Neural model of adaptive hand-eye coordination for single postures. *Science*, 259:1308–1311, 1988.

S. B. Laughlin. A simple coding procedure enhances a neuron's information capacity. *Z. Naturforsch.*, 36c:910–912, 1981.

D. D. Lee and H. S. Seung. Algorithms for non-negative matrix factorization. In *Advances in Neural Information Processing Systems 13*, pages 556–662. MIT Press, 2001.

L. Lichtensteiger and R. Pfeifer. An optimal sensor morphology improves adaptability of neural network controllers. 2415:850–860, 2002.

J. Lin. Divergence measures based on the Shannon entropy. *IEEE Transactions on Information Theory*, 37(1):145–151, 1991.

R. Linsker. Self–organization in a perceptual network. *IEEE Computer*, 21:105–117, 1988.

B. Lucas and T. Kanade. An iterative image registration technique with an application to stereo vision. In *Proceedings of 7th International Joint Conference on Artificial Intelligence (IJCAI)*, pages 674–679, 1981.

M. Lungarella and R. Pfeifer. Robots as cognitive tools: Information-theoretic analysis of sensory-motor sata. In *Proceedings of the 2nd International Conference on Humanoid Robotics*, pages 245–252, 2001.

M. Lungarella, G. Metta, R. Pfeifer, and G. Sandini. Developmental robotics: a survey. *Connection Science*, 15(4):151–190, 2004.

M. Lungarella, T. Pegors, D. Bulwinkle, and O. Sporns. Methods for quantifying the informational structure of sensory and motor data. *Neuroinformatics*, 3(3):243–262, 2005.

N. Macias and L. Durbeck. Self-assembling circuits with autonomous fault handling. *Proceedings of the Fourth NASA/DoD Workshop on Evolvable Hardware, July 2002*, 2002.

A. Meltzoff and M. Moore. Explaining facial imitation: a theoretical model. *Early Development and Parenting*, 6:179–192, 1997.

N. A. Mirza, C. L. Nehaniv, R. te Boekhorst, and K. Dautenhahn. Robot self-characterisation of experience using trajectories in sensory-motor phase space. In *Proceedings of the fifth international workshop Epigenetic Robotics*, pages 143–144, 2005a.

N. A. Mirza, C. L. Nehaniv, R. te Boekhorst, and K. Dautenhahn. Using sensory-motor phase-plots to characterise robot-environment interactions. In *Proceedings of the 6th IEEE International Symposium on Computational Intelligence in Robotics and Automation (CIRA-2005)*, pages 581–586, 2005b.

C. L. Nehaniv. Meaning for observers and agents. In *IEEE International Symposium on Intelligent Control / Intelligent Systems and Semiotics, ISIC/ISIS'99*, pages 435–440. IEEE Press, 1999.

C. L. Nehaniv, D. Polani, L. Olsson, and A. S. Klyubin. Evolutionary information-theoretic foundations of sensory ecology:channels of organism-specific meaningful information. In *Modeling Biology:Structures Behavior, Evolution*. MIT Press, in preparation, 2006.

A. Newell and H. Simon. Computer science as empirical study: symbols and search. *Communications of the ACM*, 19:113–126, 1976.

E. A. Newman and P. H. Hartline. Integration of visual and infrared information in bimodal neurons of the rattlesnake optic tectum. *Science*, 213:789–791, 1981.

L. Olsson. Anomaly detection using self/nonself discrimination for the Linux kernel. In *Proceedings of the NordU/Usenix Conference February 2003*, pages 14–26, 2003.

L. Olsson, C. L. Nehaniv, and D. Polani. Sensory channel grouping and structure from uninterpreted sensor data. In *Proceedings of the 2004 NASA/DoD Conference on Evolvable Hardware*, pages 153–160. IEEE Computer Society Press, 2004a.

L. Olsson, C. L. Nehaniv, and D. Polani. Information trade-offs and the evolution of sensory layouts. In *Proceedings of the Ninth International Conference on the Simulation and Synthesis of Living Systems (ALIFE9)*, pages 119–124. MIT Press, 2004b.

L. Olsson, C. L. Nehaniv, and D. Polani. The effects on visual information in a robot in environments with oriented contours. In *Proceedings of the Fourth International Workshop on Epigenetic Robotics*, pages 83–88. Lund University Cognitive Studies, 2004c.

L. Olsson, C. L. Nehaniv, and D. Polani. From unknown sensors and actuators to visually guided movement. In *Proceedings of the Fourth International Conference on Development and Learning (ICDL 2005)*, pages 1–6. IEEE Computer Society Press, 2005a.

L. Olsson, C. L. Nehaniv, and D. Polani. Sensor adaptation and development in robots by entropy maximization of sensory data. In *Proceedings of the Sixth IEEE International Symposium on Computational Intelli-*

gence in Robotics and Automation (CIRA-2005), pages 587–592. IEEE Computer Society Press, 2005b.

L. Olsson, C. L. Nehaniv, and D. Polani. Discovering motion flow by temporal-informational correlations in sensors. In *Proceedings of the Fifth International Workshop on Epigenetic Robotics*, pages 117–120. Lund University Cognitive Studies, 2005c.

L. Olsson, C. L. Nehaniv, and D. Polani. From unknown sensors and actuators to actions grounded in sensorimotor perceptions. *Connection Science*, 18(2), 2006a.

L. Olsson, C. L. Nehaniv, and D. Polani. Measuring informational distances between sensors and sensor integration. In *Proceedings of the Tenth International Conference on the Simulation and Synthesis of Living Systems (ALIFEX)*. MIT Press, 2006b.

J. K. O'Regan and A. Noe. A sensorimotor account of vision and visual consciousness. *Behavioral and Brain Sciences*, 24(5):1011–1031, 2001.

L. Paninski. Estimation of entropy and mutual information. *Neural Computation*, 15:1191–1254, 2003.

Gordon Pask. Physical analouges to the growth of a concept. *Mechanisation of Thought Processes: Proceedings of a Symposium held at the National Physical Laboratory*, 2(10):877–928, 1959.

R. Pfeifer and C. Scheier. *Understanding Intelligence*. MIT Press, 1999.

D. Philipona, J. K. O'Regan, and J. P. Nadal. Is there something out there? inferring space from sensorimotor dependencies. *Neural Computation*, 15(9), 2003.

D. Philipona, J. K. O'Regan, and J.P. Nadal. Perception of the structure of the physical world using multimodal unknown sensors and effectors. *Advances in Neural Information Processing Systems*, 17, 2004.

J. Piaget. *The Origins of Intelligence*. Routledge, 1953.

D. Pierce and B. Kuipers. Map learning with uninterpreted sensors and effectors. *Artificial Intelligence*, 92:169–229, 1997.

J. R. Pierce. *An Introduction to Information Theory: Symbols, Signals, and Noise*. Dover Publications, second edition, 1980.

D. Polani. Measures for the organization of self-organizing maps. *Self-Organizing Neural Networks: Recent Advances and Applications*, pages 13–44, 2002.

D. Polani, Thomas Martinetz, and Jan Kim. An information-theoretic approach for the quantification of relevance. In Jozef Kelemen and Petr Sosík, editors, *Advances in Artificial Life, 6th European Conference, ECAL 2001, Prague, Czech Republic, September 10-14, 2001, Proceedings*, Lecture Notes in Computer Science, pages 704–713. Springer Verlag, 2001.

T. Quick, K. Dautenhahn, C.L. Nehaniv, and G. Roberts. On bots and bacteria: Ontology independent embodiment. In *Proceedings of the*

Fifth European Conference on Artificial Life (ECAL99), pages 339–343, 1999.

F. Rieke, D. Warland, R. de Ruyter van Stevenick, and W. Bialek. *Spikes: Exploring the Neural Code*. MIT Press, first edition, 1999.

P. Rochat. Self-perception and action in infancy. *Experimental Brain Research*, 123:102–109, 1998.

D. L. Ruderman. The statistics of natural images. *Network: Computation in Natural Systems*, 5:517–548, 1994.

C. E. Shannon. A mathematical theory of communication. *Bell Systems Tech. J.*, 27:379–423, 623–656, 1948.

E. P. Simoncelli. Vision and the statistics of the visual environment. *Current Opinion in Neurobiology*, 13, 2003.

E. P. Simoncelli and B. A. Olshausen. Natural image statistics and neural representation. *Annual Review of Neuroscience*, 24:1193, 2001.

A. Slater and S. Johnson. Visual sensory and perceptual abilities of the newborn: beyond the blooming, buzzing confusion. In F. Simion and G. Butterworth, editors, *The Development of Sensory, Motor, and Cognitive Abilities in Early Infancy: From Sensation to Cognition*, pages 121–141. Hove:Psychology Press, 1997.

Sony. *OPEN-R SDK: Model Information for ERS-210*. 2002.

O. Sporns. Embodied cognition. *MIT Handbook of Brain Teory and Neural Networks*, 2003.

O. Sporns and T. K. Pegors. Generating structure in sensory data through coordinated motor activity. *Proceedings of the International conference Neural Networks*, page 2796, 2003.

O. Sporns and T. K. Pegors. Information-theoretic aspects of embodied artificial intelligence. *Embodied Artificial Intelligence, LNCS 3139*, pages 74–85, 2004.

O. Sporns, G. Tononi, and G. M. Edelman. Theoretical Neuroanatomy: Relating anatomical and functional connectivity in graphs and cortical connection matrices. *Cerebral Cortex*, 10:127–141, 2000.

R. Steuer, J. Kurths, C. O. Daub, Weise J., and J. Selbig. The mutual information: Detecting and evaluating dependencies between variables. *Bioinformatics*, 18:231–240, 2002.

M. Suzuki, D. Floreano, and E. A Di Paolo. The contributions of active body movement to visual development in evolutionary robots. *Neural Networks*, 18:657–666, 2005.

G. Tarapore, M. Lungarella, and G. Gómez. Fingerprinting agent-environment interaction via information theory. In F. Groen, N. Amato, A. Bonarini, E. Yoshida, and B. Kröse, editors, *Proceedings of the 8th International Conference on Intelligent Autonomous Systems, Amsterdam, The Netherlands*, pages 512–520, 2004.

E. Thelen and L. Smith. *A Dynamic Systems Approach to Development of Cognition and Action.* MIT Press, 1994.

N. Tishby, F. Pereira, and W. Bialek. The information bottleneck method. In *Proc. 37th Annual Allerton Conference on Communication, Control, and Computing, Illinois*, pages 368–377, 1999.

G. Tononi, G. M. Edelman, and O. Sporns. Complexity and coherence: integrating information in the brain. *Trends in Cognitive Science*, 2 (12):474–484, 1998.

Giulio Tononi and Olaf Sporns. Measuring information integration. *BMC Neuroscience*, 4(31), 2003.

C. von Hofsten. Prospective control: a basic aspect of action development. *Human Development*, pages 253–270, 1993.

J. von Uexküll. *Umwelt und Innenwelt der Tiere*. J. Springer, 1909.

J. Weng, J. McClelland, A. Pentland, and O. Sporns. Autonomous mental development by robots and animals. *Science*, 291:599–600, 2001.

T.N. Wiesel. Postnatal development of the visual cortex and the influence of environment. *Nature*, 299:583–591, 1982.